FACULTY OF TECHNOLOGY

Kalle Kälkäjä

Process Engineering

Master’s thesis

November 2022

FACULTY OF TECHNOLOGY

THE EFFECT OF ADMIXTURES ON THE MECHANICAL PROPERTIES AND DURABILITY OF Fe-RICH ALKALI-ACTIVATED MATERIALS

Kalle Kälkäjä

Supervisors: Juho Yliniemi, Vitalii Ponomar.

Process Engineering

Master's thesis

November 2022

ABSTRACT

University of Oulu Faculty of Technology

Degree Programme (Bachelor's Thesis, Master's Thesis) Process Engineering, Master's Thesis		Major Subject (Licentiate Thesis) Process Engineering	
Author Kalle Kälkäjä		Thesis Supervisor Juho Yliniemi, Vitalii Ponomar	
Title of Thesis The effect of additives on the mechanical properties and durability of Fe-rich alkali-activated materials			
Major Subject Bioproduct technology	Type of Thesis Master's Thesis	Submission Date 2.11.2022	Number of Pages 101p. 18 App.

Abstract

Alkali-activated materials (AAM) as a potential alternative to ordinary Portland cement (OPC) could decrease CO_2 emissions and increase valorization of various metallurgical wastes and side streams in the construction sector. Fe-rich precursors are potential materials to be utilized in AAM production. Unlike usual AAM precursor materials in which the constituents and the main reaction products are known the role of iron in AAMs is not fully understood. This limits the utilization of Fe-rich precursors in AAMs since the optimal activation parameters, such as activating solution composition or curing regimes, remains unclear.

The goal of this thesis is to study the effect of low molarity of NaOH solution as a sole activator and different additives on the mechanical and durability properties of alkali-activated Fe-rich slag. NaOH molarities used in this study were in a range of 1-9 M. To enhance the performance of the AAM, $Ca(OH)_2$, CaO, MgO, and silica fume additives were used in different dosages up to 20 wt.%. Mechanical properties of the produced mortars were determined with unconfined compressive strength (UCS) test at different curing periods of 7-28 days. The durability of selected mortars was studied with free-thaw and chemical resistance tests using 3 wt.% NaCl, $MgSO_4$, H_2SO_4, and HCl solutions and water as a reference medium with 14 and 28 days of treatment time. The composition and microstructure of the produced mortars and pastes were studied with XRD, FT-IR, and SEM. Environmental leaching tests were carried out to study the solubility and content of harmful substances.

The results indicate that the increasing molarity of NaOH solution from 3M to 9M did not significantly increase the UCS. $Ca(OH)_2$ and MgO additions did not enhance the mechanical performance of the AAM. In contrast, CaO and silica fume additions were found to be beneficial to the UCS development of the mortars. The addition of CaO affected the compressive strength even when using 1M NaOH, while higher molarity up to 3M was needed to incorporate silica fumed into the reaction product. The positive effect of using CaO at low molarities can be attributed to the formation of katoite observed by XRD. The higher compressive strength of the samples with silica fume is due to the more uniform microstructure observed by SEM and the higher degree of polymerization observed by FT-IR. Resistance to a salty environment was found to be good on average the UCS decreased only by 4%. Sulphate resistance of the mortars against $MgSO_4$ caused strength loss on all mortars on average UCS loss being 15%. Both acid treatments had a significant degradation effect on the mortars UCS loss on average was 18% and 39% with H_2SO_4 and HCl, respectively. All of the mortars retained rigidity and were not brittle.

With and without additives, regulatory leaching limits of some elements from mortars were exceeded in the environmental leaching tests. Interestingly salt and $MgSO_4$ treatments reduced Mo leaching and acid treatments reduced V leaching below the regulatory limits.

The results shed light on the alkali-activation of Fe-rich materials and the effect of mineral additives. The obtained durability results offer great insight into the possible utilization of Fe-rich materials in industrial applications. The results should help future research on this topic.

PREFACE

The goal of this master's thesis was to study the effects of low molarity NaOH activators and additives on the strength and durability of alkali-activated Fe-rich non-ferrous metallurgical slag. The study was carried out in cooperation with the University of Oulu and Boliden Harjavalta Oy.

I want to thank my supervisors Vitalii Ponomar and Juho Yliniemi from the University of Oulu and Justin Salminen from Boliden Kokkola Oy and Petri Latosenmaa from Boliden Harjavalta Oy for the possibility with this master's thesis.

Thanks to all of those who have supported me in every way imaginable during the entirety of my studies and this thesis. Without you all, my university studies would not have been the same. Thank you for all the good memories and good times. Special thanks to Maria and my family.

Not the fastest nor best, but we got there.

Oulu, 30.9.2022

Kalle Kälkäjä

TABLE OF CONTENTS

ABBREVIATIONS AND DEFINITIONS

AAM	Alkali-activated material
BFS	Blast furnace slag
C-(N)-A-S-H gel	Calcium-(sodium)-aluminum-hydrate gel
C-S-H gel	Calcium-silicate-hydrate gel
FMS	Ferrous metallurgical slags
GGBFS	Ground granulated blast furnace slag
OPC	Ordinary Portland cement
N-A-S-H gel	Sodium-aluminium-silicate-hydroxide gel
NFMS	Non-ferrous metallurgical slags
UCS	Unconfined compressive strength

1. INTRODUCTION

A significant amount of CO_2 is emitted from various sources. Power generation, transportation, industries, and buildings are the main sources of CO_2 emissions[1]. Urbanization of the world leads to a growing need for building materials all around the world. Ordinary Portland Cement is one of the most used building materials, due to its excellent properties. OPC production nevertheless is one of the main contributors to CO_2 emissions coming from the construction sector. Annual CO_2 emissions from OPC production are 5-8% of the total CO_2 emissions. This significant release of CO_2 indicates that there is a need for more sustainable materials to replace OPC. In addition to CO_2 emissions, OPC production uses natural raw materials, thus leading to environmental problems[2], [3]. Alkali-activated materials are one of the most promising replacements for OPC.

Alkali-activated materials are alternative binders that are obtained from the alkali-activation of aluminosilicate precursors with various alkaline solutions. The formed hardened binder is hydrous alkali-aluminosilicate phase[4]. The use of AAMs reduces CO_2 emissions by 40 to 90% compared to OPC. Various precursor materials can be utilized in AAM production: kaolinitic clays, fly ashes, and different slags. The utilization of waste and side streams in AAMs will reduce natural material consumption[5]. This also allows the utilization of circular economy ideology, where side and waste streams are utilized to bring additional value to the life cycle of raw materials. Activation solutions used in AAM production are usually alkaline hydroxides or silicates[6]. Depending on the activator solution different mechanical and durability properties are obtained. It should be noted that alkali silicate solutions have a greater environmental impact[7]. Several types of AAMs have been shown to perform better in mechanical and durability properties when compared to OPC[8].

In this master's thesis, the goal was to produce AAM from Fe-rich non-ferrous metallurgical slag and to study the effect of different additives on the mechanical and durability properties using different molarities of NaOH solution. The first part consists of a literature review, where the environmental impact of OPC, alkali-activated materials; their precursors, activators, and additives, and properties of alkali-activated materials are explored. The second part is the study about producing AAM from Fe-rich NFMS and

the effect of different molarity of NaOH activators and additives on the mechanical properties and durability of the Fe-rich AAM.

The motivation for this thesis is the scarce publications about alkali-activation of Fe-rich metallurgical slag using low molar activators. Also, the effect of different additives on the properties of NFMS AAMs is unclear. Lower molarity of activation solutions may offer a greener option due to lower CO_2 impact and lower production cost compared to the silicate-based or high molarity activating solutions. The main goal is to produce binder material using low molar NaOH solutions that have comparable properties to OPC, to lower the environmental impact of AAMs for future use in the construction sector.

2. LITERATURE REVIEW

2.1 Circular economy

Circular economy is a concept that is defined by the European Commission as ” An economic space where the value of products, materials, and resources is maintained in the economy for as long as possible, and the generation of waste minimized”[9]. Figure 1 presents the concept of circular economy as a flowchart.

Circular economy utilizes a variety of routes for raw materials, recycling, and utilization of waste/side streams. All raw materials to some extent can be recycled and reused in some way. This allows cascade streams to be used during the lifespan of the product. Some raw materials are becoming more and more scarce so their efficient utilization is becoming a must. Production processes produce side/waste streams that can be utilized as raw materials. Products that are being used can be shared and maintained for a longer lifecycle, thus reducing waste. This is linked with a collection of such products and their trading and distribution. When a product reaches the end of its lifespan it’s preferable to remanufacture or recycle it rather than landfill it. This allows longer lifespan for the raw materials and decreases their need. If the products cannot be reused or recycled, they are used for energy and electricity production. The produced CO_2 from energy production can be recycled and used as raw material as well in certain cases. If the products can’t be reused or recycled or used in energy production, only then they are landfilled. Energy inputs are preferably renewable, and the sustainability of the whole cycle is emphasized.[9]–[11]

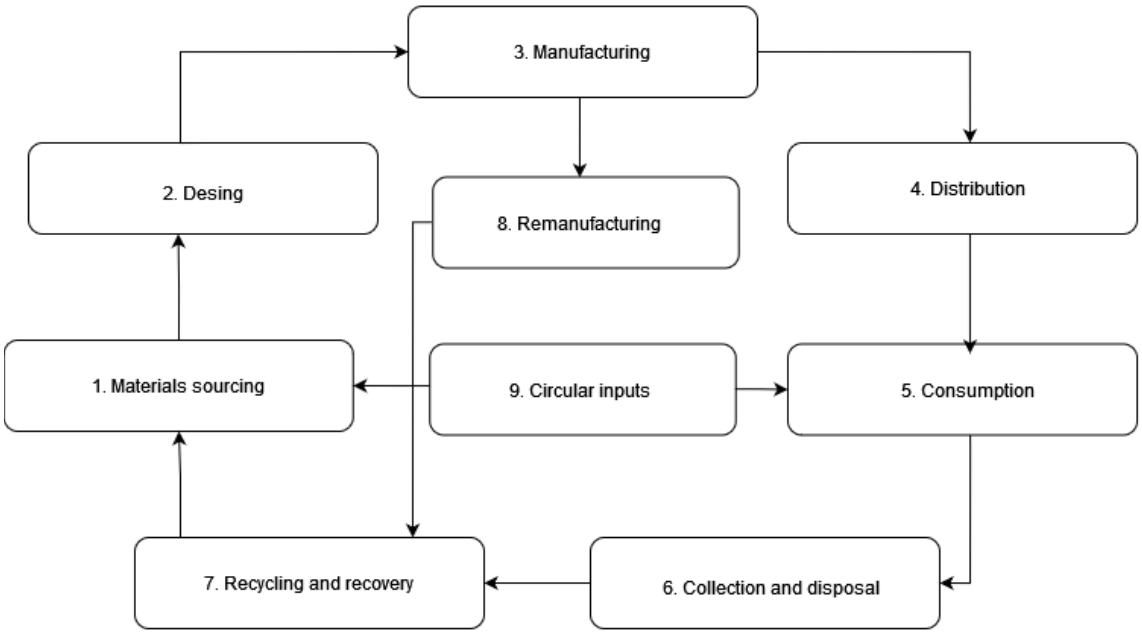

Figure 1. Concept chart of circular economy.[11]

Circular economy in the construction sector is not widely adapted and focuses on the reduction of waste. Sector-wide adaptation is needed as new projects or specific segments in construction apply these values. Design for circular economy in the construction sector should consider adaptability, standardization, modularity, and waste minimalization. Manufacturing should follow eco-design principles, optimization of materials, lower the consumption of materials and increase lifespan. The use of reused and recycled materials and waste minimization should be adapted in the actual construction phase. Repair and recycling should be adapted through the life cycle in the construction sector.[12]

2.2 Ordinary Portland Cement Concrete

Concrete is the most used construction material in the world. Concrete is made from aggregates such as sand or gravel and pastes that consist of cement and water[13]. Concrete has many reasons for its popularity such as excellent mechanical properties, affordability, and availability. Globally concrete production is estimated to be about 6 billion tonnes per year. The most used binder in concrete is Ordinary Portland Cement (OPC). China being the leading producer of OPC followed by India with an annual production of 22489 thousand tonnes and 20850 thousand tonnes, respectively. As urbanization increases so do the demand for reliable construction materials[2]. Properties such as compressive strength and water adsorption for normal strength concrete, high

strength concrete, and ultra-high strength concrete are 20-40MPa, 10-15%; 50-100MPa, 1-5% and 100-150MPa, <1%, respectively[14]. The minerals used in OPC clinker are tricalcium silicate $SiO_2 \cdot 3CaO$, dicalcium silicate $SiO_2 \cdot 2CaO$, tricalcium aluminate $Al_2O_3 \cdot 3CaO$, and tetracalcium ferroaluminate $4CaO \cdot Al_2O_3 \cdot Fe_2O_3$ [2], [15]. The hydration reactions that occur in concrete hardening can be classified as calcium-silicate-hydrate C-S-H gel[16].

Production of OPC clinker consumes materials such as limestone, clay, gypsum, and shale. These materials are quarried from open mining operations. OPC clinker demands sufficient amounts of calcium, silicon, aluminum, and iron, thus various additional raw materials are used. During the manufacturing process, the raw materials are dried, crushed, blended, and heated. As the materials are heated to 1200-1450 °C, considerable amounts of various fuels are burned[2]. The harvesting of raw materials leads to loss of biodiversity, global warming, climate change, ecosystem degradation, water pollution, and dust contamination. CaO formation in OPC production releases CO_2 with water vapor. Production of one tonne of OPC is estimated to release 0.8 tonnes of CO_2. Total CO_2 emissions from OPC production is 5-8% of the global CO_2 emissions[2], [3]. Other air pollutants such as particulate matter with a diameter of 10 or less microns (PM10), a diameter of 2.5 microns or less (PM2.5), nitrogen oxides (NO_x), SO_2, and volatile organic compounds (VOC) are released. Pollution of water sources is another impact of OPC production. Dust will contaminate water having a significant effect on the ecosystem. Wastewater runoff to the surrounding area will contaminate water sources, leading to soil degradation and erosion problems[2].

2.3 Alkali-activated materials

The increasing demand for sustainable construction materials has directed the attention of research on alternative greener options for OPC such as alkali-activated materials (AAMs). AAMs offer reduced binder costs, energy consumption, and lower CO_2 emissions compared to traditional concrete. Decreased usage of raw materials is also one prominent effect of AAMs as many industrial side and waste streams can be utilized[17]. AAMs are produced from solid aluminosilicate (precursor) and alkaline solutions (activator). The most commonly used activators are Na/K-OH and $Na/K_2O \cdot rSiO_2$ or their mixtures[4]. Activators are covered more extensively in the 1.3.4 Activators chapter. The

alkali-activation of the precursor results in a hardened binder that is typically based on the combination of hydrous alkali-aluminosilicate and/or alkali-alkali earth-aluminosilicate phases[4].

The common precursors for AAMs production are natural solid aluminosilicates, materials such as various slags, fly ash, calcined clays, kaolin, metakaolin, red mud, and natural pozzolans to provide a sufficient amount of dissolving and reactive silica (SiO_2) and alumina (Al_2O_3) that rearrange and harden. Their chemical and mineral compositions are variable from precursor to precursor[4]. This leads to different reaction products and properties of AAMs and thus they will not be universal replacements for OPC. The use of different precursors is based on availability, reactivity, cost, location, and value. Some AAM precursors have uses in current OPC blends so the competition from materials must be considered in viability for the production of AAMs. The transportation of precursor materials should be minimized as they have a significant contribution to the emissions of AAMs production. This also has advantages in areas where OPC is not readily available, but suitable AAM precursor materials are[4]. Depending on the composition of precursors, the alkali-activation forms Ca-Al-Si hydrate gels (C-A-S-H), Na-Al-Si hydrate gels (N-A-S-H), or zeolite-like nanostructures.[4], [6], [8], [14], [18]–[23] Precursor's compositions are covered more extensively in 2.3.1, 2.3.2, and 2.3.3 chapters.

There are two main routes in which AAMs are produced. These routes are a one-part mix and a two-part mix. The one-part mix system is based on mixing dry powder and water to form the binder. Co-calcination and inter-grinding of precursors and solid activators have been shown to be possible. Solid activators are usually alkali carbonates, silicates, or hydroxides. Similar to ones used in current mature cement systems. The two-part mix system uses separate liquid activator or activators, such as NaOH. Scalability issues in two-part systems are related to chemical handling and curing methods. This can be controlled more easily in precast products. Currently, the two-part mix is predominant. As the technology advances and becomes more readily available the one-part mix offers better scalability. Issues related to one-part mix systems are slow strength development. On the other hand, positive environmental effects are highlighted in one-part mix systems.[4]

2.3.1 High calcium precursors

Blast furnace slag (BFS) as well as ground granulated blast furnace slag (GGBFS) is a by-product of steel production that is already used in OPC replacement. BFS has four major chemical components CaO (30–50 wt.%), SiO_2 (28–38 wt.%), Al_2O_3 (8–24 wt.%), and MgO (1–18 wt.%)[24]. BFS has large variability in its constituents as production processes of steel vary greatly in raw materials and process conditions. Another significant factor affecting the reactivity of BFS is the cooling method. Different methods of cooling affect the amorphous content of the slag leading to higher reactivity[24], [25]. In AAMs, the alkali metal can participate in the gel formation, thus the formed gel is described as calcium-alkali metal (usually Na)-aluminum- hydrate (C-(N)-A-S-H) gel. The C-A-S-H gel is nanocrystalline and C-(N)-A-S-H gel is primarily amorphous[24].

Other slags such as ladle slag and basic oxygen furnace slag have been shown potential to act as a precursor in AAM production. But they are poorly studied in the literature[5].

2.3.2 Low calcium precursors

Metakaolin is derived from dehydroxylation of kaolin which is aluminosilicate clay. Kaolin can be mined as a pure mineral or obtained in a less pure form from mine tailings and paper industry wastes. The dehydroxylation of kaolin takes place at 500-800 °C. The heating breaks the ordering of kaolinite and bound hydroxyl groups. This makes aluminum available for alkali-activation reactions. The dissolution of aluminum also enhances the dissolution of silicon available for alkali-activation reactions. The different sources vary in properties like particle size, purity, and crystallinity, which affect the reactivity. AAM production from low-grade kaolin offers valorization possibilities. Crystallographically strained aluminum sites from an octahedrally coordinated layer of kaolinite provide the reactivity in alkaline activation. These factors make metakaolin a highly reactive precursor for AAM production. The binder gel formed by alkali-activation of metakaolin is structurally disordered and highly cross-linked sodium-aluminum-silicate-hydroxide (N-A-S-H) gel. The negative charge from silicon substitution with tetrahedral aluminum is balanced with the alkali cations in the gel framework of the AAM.[6]

Fly ash (FA) is non-combustible material that is formed as a by-product of coal-fired electricity production. FA is mainly composed of aluminosilicate remnants from coal combustion. Electrostatic precipitators collect fly ash from chimneys. FA particles are usually vitreous, spherical, and sufficiently reactive to be alkali-activated. Alkali-activated FA forms a similar highly crosslinked binder gel as metakaolin characterized as (N-A-S-H) gel. The content of Si, Al, Fe, and Ca in FA composition varies significantly from different sources.[6]

2.3.3 Iron-rich precursors: non-ferrous metallurgical slags

Non-ferrous metallurgical slags (NFMS) are typically highly amorphous slags that are rich in iron [5], [26]. The amorphous content of the slag depends on the cooling rate of the slag [5], [26]. An estimated 50 million tonnes of NFMSs are produced worldwide annually. In Finland, the annual production of NFMS is about 600 000 tonnes annually. NFMSs are a by-product of Fe–Ni, Cu–Ni, Cu, Cu–Ni, and Pb productions. The typical crystalline phases are iron oxides and silicates (wüstite FeO, magnetite $Fe^{2+}Fe^{3+}{}_2O_4$, and fayalite $Fe_2{}^{+2}SiO_4$) and other silicates (quartz [SiO_2] melilite group minerals $(Ca, Na)_2(Al, Mg, Fe^{2+})[(Al, Si)SiO_7]$, merwinite [$Ca_3Mg(SiO_4)_2$], forsterite [$Mg_2SiO_4$]). Iron's oxidation state in these minerals is +2 except +2 and +3 in magnetite. The compressive strength of NFMS AAMs is mainly affected by the amorphous content in the precursor. Although NFMSs have a high content of iron, many NMFS precursor AAMs demonstrate high and ultra-high compressive strength[5]. Different studies have demonstrated high compressive strength for NMFS Fe-Ni slag 120 MPa, Cu-Ni slag 119 MPa, fayalite slag 40 MPa, and Pb slag 64.9 MPa[5], [26]. However, NFMS as an AAM precursor is much less studied compared to BFS, for example, and thus studied further in this thesis.

Electric arc furnace slag (EAFS) is formed in steel production in the refining step in which iron oxide is formed. The iron oxide reacts with calcium and magnesium oxides that are fed to dephosphorize the steel[27]. The composition of EAFS is fairly amorphous with crystalline phases of FeO, Fe_3O_4, Ca_2SiO_4, and $Ca_2Al(AlSiO_7)$[5]. EAFSs need primary processes to be utilized as a precursor in concrete applications. These processes include sprinkling, turning, and crushing. Concrete applications require sufficient chemical, physical, and durability properties from the precursor. A compressive strength value of 41MPa [5] and flexural tensile strength of ~4MPa are reported in a previous study for AAM manufactured from EAFS activated with sodium hydroxide and sodium silicate

solution[27]. Other studies have reported compressive strengths for EAFS in the range of 145.02-31.3 MPa[5].

Bauxite residue, red mud (RM) is the non-soluble fraction of the Bayer process in which aluminum hydroxide is precipitated from sodium aluminum solution. RM composition is affected by the composition of the bauxite ore, processing, lime addition for digestion, and additives used. RMs chemical components consist of about 41 wt.% of Fe_2O_3, 16 wt.% Al_2O_3, 10 wt.% SiO_2, and other components, such as water and organics. Usage of RM has some legal issues for example when it's categorized as hazardous waste, due to alkalinity. RM is mainly crystalline, and the minor amorphous fraction generally consists of alumina and iron hydroxides, and oxides. The limited amount of silica in RM is another limiting factor for its usage in AAMs. AAMs produced solely from RM precursor has reached UCSs of 2.5-5 MPa[28]. The small particle size and large specific surface area offer possibilities for RM usage as filler in AAMs[28]. Studies have reported compressive strengths for RM mixtures with RM content in the range of 10-83.3 % in the range of 28-58.13 MPa[5].

2.3.4 Activators

Alkaline activating solutions are mainly alkali metal hydroxides or silicates, alkali metal carbonates and sulphates are also used but to a lesser extent. This is a distinct feature of AAM compared to OPC where hardening is induced with only water addition. The most commonly used alkali metals are sodium and potassium[6]. Activator solution plays a significant role in the polymerization reaction with soluble silica content as a major affecting variable. Silica modulus of 1-1.5 has been reported as optimum for many precursors[8]. Silicate activators are commonly used with iron-rich precursors, while hydroxide activators are much less studied, especially for iron-rich precursors[5].

Alkali silicate-based activators are usually produced from carbonate salts by melting to form a glass that is then dissolved in warm water. The resulting viscous and sticky solution is also known as waterglass. In contrast, alkali hydroxide-based activators are usually produced from chlorine salts electrolytically. Both processes lead to energy usage and CO_2 emissions affecting the emissions and energy consumption emissions and energy consumption of AAMs production. Silica polymerizes into a complex array of oligomeric species that contain 2-15 monomers. In alkali-activation, monomeric structures are

preferred as they offer the greatest reactivity due to their size. In alkaline activators, the silica is buffering the pH to a range of 11-13.5. This leads to higher alkalinity compared to hydroxide-based activators. Alkali hydroxide activators are usually used in molarity of 5 and above, especially when low calcium precursors are used. This leads to occupational safety issues as high concentrations are classified as corrosive. Thus, the production of AAM using lower molarities of the solution and lower content of chemical used is needed.[6]

Thermal stability is higher for hydroxide-activated AAMs. compared to sodium silicate activated. These thermal properties are due to the high degree of connectivity of silicate gels in the formed binder. Whereas silicate solution-activated AAMs lead to a low amount of silanol groups that lose water when heated and expand the material. The viscosity of hydroxide-based activators is lower leading to better workability[4], [6], [8]. Alkali-activation with hydroxide solution leads to higher permeability and inclination to efflorescence, when compared to silicate-activated AAMs. This is due to the low extent of reaction reached before hardening. Leading to open microstructure with mobile alkaline pore solution [4], [6], [8].

2.3.5 Admixtures

NFMSs with a high content of Fe decrease the relative amount of Al which is found to have the main effect on strength development[5]. Additional reactive materials can be used to enhance the properties of the formed binder in Fe-rich slag systems with low molar activating solutions, different co-binders and/or co-activators can be used, including metal oxides and hydroxides and more reactive silica sources.

Calcium hydroxide ($Ca(OH)_2$) is a mineral obtained from the hydrolysis of CaO. In natural mineral form, $Ca(OH)_2$ is called portlandite. Portlandite is a somewhat rare mineral, found in some volcanic, plutonic, and metamorphic rocks. $Ca(OH)_2$ is a weak base. It is used as a flocculant, paints, sealants, and mortars[29]. Alkali-activation of metakaolin was studied with 5 and 12 M NaOH solutions and $Ca(OH)_2$, which showed that 5M NaOH activated AAMs reaction product is C-S-H gel and 12M NaOH activated AAMs primary product is alkali-network structure and secondary C-S-H gel product, $Ca(OH)_2$ addition didn't affect the reaction product. Excess of OH^- from higher molarity NaOH inhibits $Ca(OH)_2$ dissolution making Ca not available for C-S-H formation. As the

reaction proceeds the hydrated aluminosilicate causes a pH increase which increases $Ca(OH)_2$ dissolution forming C-S-H gel as a secondary reaction product[30].

Calcium oxide (CaO), also known as quick lime, is inexpensive white, alkaline, caustic material that is widely used. CaO is a corrosive material that reacts intensely when combined with water. CaO hydrates to $Ca(OH)_2$ releasing heat. Powdered CaO has a high specific surface area, which enhances its properties as a mineral additive in binder formation. CaOs ability to react with silicates is also used in modern metal production industries to remove impurities in a slag form. CaO forms a solution with silicates[29]. When GGBFS and iron tailing mix with CaO addition hydrothermally activated in 5M NaOH solution, the produced AAMs after 28 days showed UCS of 13 and 9.5 MPa with 4.5 and 9 % CaO, respectively[31]. In another study, the effect of 10% CaO addition on three types of FA with sand aggregate activated with 5M NaOH solution was studied. After curing the samples for 28 days the UCS values obtained were 9 MPa, 6 MPa, and 10.8 MPa[32]. CaO addition was found to increase C(N)-A-S-H gel formation during alkali-activation thus increasing the UCS of the produced mortar. The increased C(N)-A-S-H gel formation was attributed to the increased pH of the pore solution[33].

Magnesium oxide (MgO) also known as magnesia is a white solid mineral that is found in nature as a periclase mineral. MgO is hygroscopic, meaning that it attracts and holds water, forming magnesium hydroxide. MgO is a stable molecule, that is readily available commercially. Because of its hygroscopic nature, MgO is an efficient moisture absorbent. And it is used in dry cement production. Excess of MgO in Portland cement causes expansion. In the construction sector, MgO usage has applications for materials requiring a fire rating, mold and mildew control, and sound insulation applications[29]. Another study used BFS and Cu slag with 3, 5, and 10% MgO and phosphogypsum additions. The resulting UCS values were low, reaching 1.5, 1.8, and 1.6 MPa with 3, 5, and 10% MgO, respectively. MgO addition in all dosages had an increasing effect on the UCS compared to the reference sample[34]. Alkali-activation of fly ash with different admixtures activated with sodium silicate solution was studied. The MgO content in the mix design was 1.5, 3.0, and 4.5 %. The UCS of the reference mortars was 38.5 MPa. 1.5 % MgO, 3.0 % MgO and 4.5 % MgO additions resulted in UCS of 35.5 MPa, 36 MPa and 40.5 MPa, respectively. Thus, MgO addition did not have a significant effect on UCS [35].

Silica Fume is a by-product of the elemental silicon or ferrosilicon industry[36]. The role of silica fume in AAMs is usually a filler, but it can provide available silica for the polymerization reactions and reduces the permeability of the hardened AAM. Silica fume is highly reactive pozzolan due to its properties, such as the small average particle diameter of 0.1 μm, high amorphous silica content, and very high surface area which all have positive effects on the mechanical and durability properties of the formed AAM [23], [37]. Silica fume addition is known to reduce workability in OPC systems; this is due to the high specific surface area. Silica fume addition of up to 20 % has been reported to enhance the mechanical properties of the alkali-activated binder[36]. However, the reactivity of silica fumed at different molarity of NaOH solutions is not well understood.

GGBFS and FA activated with sodium carbonate and silicate solutions were studied in the presence of 0-10 % of silica fume. After 28 days of curing, the mortars reached UCS of 31, 37.5, 34, 42.75, 29.5, 38 and 25 MPa with silica fume addition of 0-10 % in 2% intervals[38]. AAM suitable for structural applications was produced in a study where two silica sources were used as additives. Silica fume and rice husk ash were blended with GGBFS activated with NaOH to produce mortars with 35 MPa after 28 days of curing[39]. NaOH activator mixed with silica fume was used to activate GGBFS and MK mixture with SiO_2/Al_2O_3 molar ratios of 3.0 and 3.8. The resulting UCS values were 31 and 76 MPa, respectively, with a GGBFS:MK ratio of 0.8[40]. MK with 2, 6, and 10% silica fume activated with 10M NaOH solution resulted in mortars with UCS of 27.5, 35, and 14.5 MPa respectively[41]. Previous studies have shown the UCS values for GGBFS with silica fume addition of 5, 7.5 and 10 % activated with a mixture of NaOH and sodium silicate solution with a molarity of 6. The solution to precursor ratios of 0.9 and 1.0 was used. With s/p ratio of 0.9, the UCS values after 28 days were 40.3 MPa, 44.3 MPa, 44.7 MPa and 44.2 MPa with 0, 5, 7.5 and 10 % silica fume addition. Samples measured before 28 days of curing exhibited UCS values lower than the reference sample, suggesting that silica fume addition causes a delay in the final hardening of the AAM. With s/p ratio of 1.0, the UCS values after 28 days were 40.5 MPa, 42.7 MPa, 36.5 MPa and 41.7 MPa 0, 5, 7.5 and 10 % silica fume addition. Similar to the lower s/p ratio UCS of the samples was lower than the reference samples with shorter curing times. Overall higher s/p ratio produced mortars with lover UCS[36].

2.4 Mechanical properties and durability of AAMs

2.4.1 Compressive strength and reaction products

GGBS activated with NaOH, and desulphurization dust has been reported to reach UCS of 28 and 29 MPa with NaOH and desulphurization dust, respectively. The main reaction products are hydrotalcite ($Mg_6Al_2CO_3(OH)_{16} \cdot 4\ H_2O$) and C-(A-)S-H gel phase. The differences in UCS may be due to lower Ca content in the system decreasing the amount of reaction products.[39]

GGBFS activated with NaOH and sodium sulphate solutions with molarities of 5, 8, and 12 M for NaOH and 1.5 and 2.5M for sodium silicate showed differences in reaction kinetics and UCS formation. The NaOH-activated samples showed rapid reaction kinetics. The later age UCS was not dependent on the activator molarity. UCS values from 25 to 32 MPa are reported, after 28 days of curing, the lowest value was with 12 M and the highest with 8 M solution. Silicate-activated samples showed UCS of 40 to 70 MPa after 28 days.[42]

The study on alkali-activation of three different technical slags with NaOH, and sodium silicate reported higher initial UCS values for NaOH activated system (8-10 MPa). Long-term UCS development of 1 year reported UCS for NaOH and sodium silicate activated systems of 25-28 MPa and 69-105 MPa, respectively. Hydrate phases are formed during the first day in the NaOH activated system explaining the higher initial UCS. The C-(A-)S-H gel structure is denser but also more porous in the NaOH-activated system, explaining the lower long-term UCS although having a similar reaction degree.[43]

6 % Na_2O dosage of NaOH, Na_2CO_3, and Na_2SiO_3 was used to activate BFS to study the effect of UCS, porosity, and permeability. Na_2SiO_3 exhibited the highest and NaOH-activated samples lowest UCS values at all ages. The low UCS of NaOH-activated samples was explained by the highest porosity and coarse structure.[16]

Kaolin with NaOH additive activated with sodium silicate solution was studied. The NaOH addition was 0-20 % of the weight of the kaolin. Standard silica sand was used as aggregate. The samples without NaOH addition exhibited UCS of ~30 MPa and the highest UCS was reported with 5 % NaOH addition ~48 MPa after 7 days of curing.[44]

GGBFS was activated with MgO, CaO, and their mixtures to achieve UCS values of 8-43 MPa with a water/binder ratio of 0.35 and 4-35 MPa with a water/binder ratio of 0.38[45]. A study of activation of metakaolin with NaOH solution with concentrations of 1, 5, and 10 M showed that 1 M solution was not enough to sufficiently dissolute metakaolin. 5 and 10 M solutions led to the dissolution of the metakaolin and precipitation of N-A-S-H gel[46]. 70 wt.% GGBFS and 30 wt.% RM activated with sodium aluminate clinker, solid waterglass and water reached UCS of 56 MPa after 28 days of curing[28]. Cu-slag activated with 4, 6, and 8% NaOH and sodium silicate solutions provided mortars with UCS from 1.5 to 4.7 MPa with NaOH and from 2.0 to 30.3 MPa with silicate solutions respectively[47].

The compressive strength of BFS-based AAM mortars has exceeded 95 MPa with alkali silicate activation after 28 of curing, similarly, phosphorous slag AAM mortars have reached 120 MPa, and metakaolin mortars over 90 MPa. These results show that AAMs do not require extended curing times and high curing temperatures to reach excellent mechanical strength. BFS and FA AAMs have commonly reached UCSs over 50 MPa.[48]

2.4.2 Compressive strength and reaction products of Fe-rich AAMs

Synthetic slags emulating NFMS with varying compositions were alkali-activated. The FeO content by wt.% were 41-60 %. Sodium silicate solutions were used as activator solutions and standard sand was used as aggregate. After 28 days of curing UCS values over 25 MPa were reported. The highest UCS was obtained with the slag composition of FeO 49.9% reaching 53 MPa. Alkali-activation oxidized part of the Fe from 2+ to 3+. The Fe^{3+} is assumed to take place in the formed silicate network, leading to a decrease in non-bridging oxygens, and increasing the polymerization degree. Fe^{2+} acts as aggregate and participates in the trioctahedral layers.[49]

EAFS with aggregate activated with NaOH and sodium silicate mixture was studied. Previous studies with similar precursors and activators provided mortars with UCS of 16, 40.7, and 27 MPa after 28 days of curing[50]–[52]. The maximum UCS was obtained using the solution with a silica modulus of 2 and sodium concentration of 6% cured for 12 hours was 22.02 MPa. An increase in silica modulus increases the anion concentration in the activation solution. C-S-H gel is formed by the solution reacting with the Ca^{2+} from

EAFS. Excess amount of OH^- causes inhibition of Ca^{2+} from EAFS surface due to $Ca(OH)_2$ presence on the slag particles. This leads to insufficient C-S-H gel formation to gain UCS. $CaCO_3$ was revealed in XRD to be one of the hydration products. $CaCO_3$ is formed from $Ca(OH)_2$ reacting with CO_2. $CaCO_3$ is believed to fill micro pores in the AAM and thus increase its UCS[27].

EAFS with electric arc furnace dust (EAFD) as co-binder was activated with sodium silicate solution. The alkali-activation of EAFS produced mortars with 21.04 MPa. 1-5% replacement with EAFD as aggregate decreased the UCS up to 10 MPa. 7% replacement formed mortars with UCS of 8.4 MPa. The mechanical properties of AAMs are linked to the properties of the formed hydrate gel from the alkali-activation. In this study, the main influence on the decrease of UCS for the dust-containing samples was linked to cumulative pore volume. FT-IR results show that the reference mortar without EAFD formed C-A-S-H gel. The EAFD addition caused a shift in the band ascribed to C-A-S-H gel indicating that Zn was incorporated in the hydration product.[53]

EAFS activated with 5, 7, and 10 M NaOH and KOH solutions showed that initial activator concentration increased the dissolution of Al and Si from the EAFS. The most significant release of Al and Si occurred in the first 15 minutes. The increase in molar concentration of alkali leads to faster braking of the Al-O and Si-O bonds due to higher OH^- content. NaOH solution is more effective in Si dissolution and KOH in Al dissolution. At 5 M solution, Fe was found not to dissolve. Depending on the concentration of the NaOH and KOH, Fe was released in the range of 0.5-0.85% and 0.9-1.4%, respectively.[54]

Synthetic Fe-silicate glass with standard sand was activated with NaOH and sodium silicate solutions [55]. High Al content in the precursor requires more Na from the activation solution. The amount of NaOH affects the precursor dissolution through hydrolysis of Si–O–Si bonds to form Si–O–Na and Si–O–H. Excess NaOH will decrease the degree of polymerization. In Fe-rich precursors, it is harder to determine the optimal Na content as Fe can be incorporated into the formed gel. UCS values after 28 days of curing varied from 14 to 35 MPa. The highest UCS were obtained with an activation solution to Fe-silicate glass ratio of 0.45. Lower or higher ratios led to porosity development, thus decreasing the compressive strength [55].

Iron and aluminum-rich soil and rock called laterites activated with NaOH and sodium silicate mixed with calcinated laterite and sand admixtures were used to produce AAMs. The laterites contained 9.68 and 35.2 wt.% of FeO. The formed pastes were pressed using a uniaxial type hydraulic press at 40 MPa. XRD showed a significant decrease in kaolinite, goethite and hematite contents after the alkali-activation, suggesting a high degree of laterites geopolymerization. Otherwise, when enough soluble silica is present, zeolite formation could occur and lead to amorphous matrix formation. With the addition of 30 and 35 % of calcinated laterite, the bi-axial flexural strength reached 15 and 14 MPa, respectively. The degree of geopolymerization and development of mechanical properties are linked to the stability of iron phases and their incorporation into the formed structure after alkali-activation. The formed AAMs exhibited good stability in water, low water absorption, and mechanical properties that are comparable to those for OPC.[20]

NFMS plasma converter slag with a FeO content of 19.9 % was activated with sodium silicate solution. Fe is present across the formed binder and in local areas. The local areas suggest precipitation of Fe-rich phases such as hydroxide or oxo-hydroxide. From the total of 7 mortars tested, 5 of them reached UCS over 60 MPa after 28 days of curing at room temperature. The highest UCS value of 81.3 MPa was reached with a SiO_2/Na_2O ratio of 0.9. With a SiO_2/Na_2O ratio of 2, the resulting UCS values were below 3 MPa.[56]

Alkali-activation of Fe-Ni slag with sodium silicate solution with NaOH molarity of 7, SiO_2 molarity of 4, and solid/liquid ratio of 5.4 mg/mL resulted in a mortar with UCS of 120 MPa. This shows the major role of silica in the activation solution as 0.7 M SiO_2 showed UCS of 48 MPa, which is 2.5 times lower compared to the 4 M solution. The effect of NaOH molarity was also studied. Fixed SiO_2 molarity of 1.3 M and s/l of 5.4 mg/mL resulted in UCS values of 3, 34, 62, and 47 MPa with 1, 4, 7, and 10 M NaOH, respectively. An excess of NaOH decreases the SiO_2/ Na_2O ratio and thus inhibition of polycondensation. The formed AAM was compact, cohesive, and almost non-porous material.[21]

Fe-Ni slag with Fe_2O_3 content of 43.83 % was alkali-activated with NaOH/KOH and sodium silicate solution. The study found that curing temperature does not play important role in NaOH/sodium silicate systems as a temperature increase from 40 to 80 ºC results in UCS between 20-24 MPa. Using KOH/sodium silicate systems, the same increase in

curing temperature increased the UCS from 20 to 40 MPa. With both alkali hydroxide the optimal molarity is between 6 and 8 M. Solely NaOH or KOH activation led to UCS of 22.5 and 18.5 MPa respectively. An excessive amount of the formed calcite is degrading the UCS by the formation of $Ca(OH)_2$.

Fe-Ni slag (Fe 34.74 wt.%) activated with sodium silicate solution was studied for usage in fire-resistant materials. The formed AAMs exhibited UCS values of 48 and 120 MPa and water absorption of 3.2 and 0.7 % after 28 days of curing, with lower and higher silicate solution molarity. The higher UCS was obtained with higher silica content. These strengths are comparable to normal (20-40 MPa) and ultra-high-strength concretes (100-150 MPa).[14]

Two volcanic ashes activated with 8.3 to 19.1 M NaOH solutions produced mortars with UCSs over 15 MPa with all solutions. The highest UCS values obtained were 35 MPa (19.1 M) and 62 MPa (12.9 M). The results are interesting as the two volcanic ashes were almost identical as the chemical compositions in oxides vary less than 1 percent point. The better performance is thus linked to particle size distribution.[57]

Cu-Ni slag with Fe content of 33.55 wt.% was activated with sodium silicate solution. Milling the slag in CO_2 atmosphere compared to the milling in air was shown to give better results as it increased the UCS of the mortars produced. XRD and FT-IR analysis did not show a difference between air and CO_2-milled AAMs. Air-milled slag-based AAMs produced mortars with UCS of 81.1 MPa and CO_2-milled precursor provided a UCS of 94.4 MPa.[22]

Fayalitic slag with the FeO content of 57.4 wt.% was used as a precursor to produce AAM. The mix of NaOH and sodium silicate was used as an activator to produce the AAM mortars. Curing was carried out at different temperatures and humidity. 20 ºC/50%, 20 ºC/90% and 60 ºC/20% cured mortars provided the UCS of 19.3, 31.0, and 20.6 MPa, respectively.[58]

2.4.3 Freeze-thaw resistance of AAMs

Freeze-thaw resistance depends on the critical saturation point and the pore structure of the AAM. After the critical saturation point unbound free water in the pores freezes,

leading to cracking. The freezing temperature of the pore solution also plays a significant role in freeze-thaw resistance. Sodium silicate-activated AAMs offer the greatest freeze-thaw resistance, due to lower porosity. $NaSiO_3$ activated slag mortars exhibited resistance to 300-1300 freeze-thaw cycles whereas OPC resisted less than 300 cycles. FA-based AAM mortars did not exhibit loss of mechanical properties after 150 freeze-thaw cycles submerged in water. Relatively poor performance of AAMs compared to OPC has been reported and the performance was linked to a higher amount of free water in AAM[59]. However, the mortar with 70 wt.% GGBFS and 30 wt.% RM activated with sodium aluminate clinker, solid water glass and water resulted in low porosity that provided a better resistance of AAM to freeze-thaw cycles than reference OPC mortar[28].

AAMs have shown better freeze-thaw resistance compared to OPC under the same conditions in some cases. The excellent frost resistance of BFS AAMs is explained with low porosity and small pore diameter. Some flexural strength increases have been reported with 100 freeze-thaw cycles (+20/-20 ºC). Residual UCS after 700 freeze-thaw cycles were 87-97 %. Alkali silicate activation provides significantly better performance in freeze-thaw resistance than NaOH-activated AAMs[48]. Silicate-activated BFS AAM resisted 1000 freeze-thaw cycles (+20/-15ºC) and NaOH-activated samples failed between 200 and 700 cycles of -15°C for 16 hours and thawing at 20°C[60]. However, the NaOH-activated BFS AAM performed worse than OPC with similar mechanical strength. FA AAMs have been reported retaining 70 % of their initial UCS after 150 freeze-thaw cycles. Another study noted that AAMs have higher free water content than OPC in which the water is chemically bound. The free water content in some AAMs decreases the freeze-thaw resistance[48].

2.4.4 Freeze-thaw resistance of Fe-rich AAMs

Two different RMs (Fe_2O_3 content 18.44 and 46.61%) and iron tailing (Fe_2O_3 content 8.27%) as admixture and/or aggregate were alkali-activated to study its freeze-thaw resistance. The freeze-thaw cycle used was from -17 ºC to 5 ºC with a duration of 2.5 hours. The mortars were submerged in water during the cycles. UCS of all 4 mortars increased after 50, 100, and 150 cycles when compared to the reference sample. The best performing mortar in the freeze-thaw test was composed of RM with a higher Fe content and iron tailing as an aggregate. The UCS of the sample increased from 32.5 MPa to 34, 42.5, and 40 MPa after 50, 100, and 150 freeze-thaw cycles. Good freeze-thaw resistance

was attributed to C-A-S-H gel formation as the main product resulting in the dense microstructure.[61]

Freeze-thaw resistance of AAM produced from Fe-Ni slag with kaolinite filler activated with sodium silicate solution was studied. The FeO content of the slag was determined to be 38.8 wt.%. The AAM mortars were subjected to weekly freeze-thaw cycles with temperatures between -15 ºC and 60 ºC for 4 months. Effects of the freeze-thaw cycles on the UCS of the AAM mortars were extremely minor. The UCS decreased from 14.5 MPa to 14.4, 14.3, 14.2, and 14.12 MPa after 1, 2, 3, and 4 months, respectively. For the reference mortars, the UCS increased during the 4 months in the air from 14.8 to 17 MPa.[62]

The freeze-thaw resistance of AAMs obtained from Fe-Ni and ladle slags showed better performance than OPC. The freeze-thaw cycles were run for 7 and 30 days. The temperature extremes in the cycles were -18 ºC for 4h and 20 ºC for 12h. UCS dropped after 30 days of freeze-thaw cycles to 67 and 50 MPa, which are 14 and 12 % decreases, respectively.[63]

AAM obtained from Cu-slag precursor exhibits low freeze-thaw resistance. Study shows that a mass loss of 90 % occurred after the freeze-thaw experiment. This is due to a high amount of free water in the pore structure of the AAM.[64]

Freeze-thaw resistance of OPC, 50/50% OPC/GGBFS, and 50/30/20% OPC/GGBFS/Fe-Ni slag mixtures have been studied. Reference values of UCS before freeze-thawing of the mixes were 39.5, 34.0, and 37.7 MPa, respectively. The mixes were subjected to 300 cycles with temperature extremes of 4 °C for 5h to -18 °C for 1.5h with the rate of 10°C/h. The mixture with Fe-Ni slag was the only sample that was measurable after 300 cycles with a UCS of 10 MPa. The OPC and 50/50 mix was measurable till 180 cycles with 13 MPa and 210 cycles with 12 MPa. At 150 cycles, the UCS of OPC, 50/50 and 50/30/20 was recorded to be 24, 26, and 26 MPa respectively. C-S-H gel content was highest with OPC/GGBS/Fe-Ni slag mixture followed by 50/50 and OPC samples. This leads to the best performance of the OPC/GGBS/Fe-Ni slag mixture as density increase is observed along with the most significant gel formation.[65]

2.4.5 Chemical resistance of AAMs

Building materials are not usually subject to highly acidic conditions, long exposure to acid rain or contact with seawater, or de-icing salts may degrade the properties of AAMs. Ion exchange reactions are the main mode of acid attack on a binder material. Acid resistance is mainly studied by mass loss and strength loss studies are less employed.[36]

Acid attacks can cause significant damage to AAMs. When comparing the acid resistance of AAMs and OPC, the AAMs usually perform better. The raw materials and activation solution used and curing conditions affect the chemical resistance of the produced AAM greatly. This is attributed to the difference in hydration products. For example, an acetic acid attack for 150 days decreased the UCS of alkali-activated slags by 25% [37]. This is attributed to the low initial permeability, higher alkalinity of the pore solution, and CaO/SiO_2 ratio of the AAM compared to OPC. The decalcification from the formation of calcium acetate leaves aluminosilicate gel in the affected area. The gel is less soluble and has higher mechanical properties when compared to the silicate gel formed in OPC systems. The pore diameter is a more significant factor than porosity leading to better acid resistance. FA, FA+OPC, and OPC with similar porosities 17.5%, 18%, and 16.6%, respectively led to significantly different acid resistances. The pore diameter of FA AAMs was reported as ~45Å and OPCs ~100Å, providing the AAM with better acid resistance.[37]

Sulphate attack can occur from exposure to excess internal or external sulphate. Degradation happens from sulphate transport through the pore structure of the AAM. Due to expansive reaction products and mechanical response, spalling and cracking occur. The cation plays a significant role in the sulphate attack. Na_2SO_4 immersion has been shown not to degrade the AAM. This is due to continued stabilization and development of the binder as Na acts as an activator. $MgSO_4$ causes severe degradation of the AAM. Decalcification, gypsum formation, and loss of mechanical properties occur when AAM is immersed in $MgSO_4$. It should be noted that both Mg^{2+} and SO_4^{2-} both are participating in the structure degradation. Alkali-activated slags have higher resistance to sulphate attack due to the absence of portlandite and the unavailability of Al species as they are incorporated in C-S-H gel or hydrotalcite. When submerged in 5% Na_2SO_4 and 5% $MgSO_4$ for 1 year the decrease of UCS with OPC was ~25-37% for OPC and ~17-23% for alkali-activated slag. Activator selection affects the sulphate resistance of the AAM

in FA-based systems. When comparing NaOH, $NaSiO_3$, and NaOH +KOH mixture. The NaOH activated performed best in sulphate attack with 5% Na_2SO_4 and 5% $MgSO_4$. With NaOH solution after the immersion, the UCS increased by 4-12%.[59]

In general, the sulphate resistance of AAMs is equivalent to OPC, but the wide variety of materials used in AAMs (precursors and activators) showed different performances. A small change in the properties of AAM obtained from BFS by alkali-activation with sodium silicate solution was observed during exposure to $MgSO_4$ and Na_2SO_4 over a period of 4-6 months. Resonance frequency analysis, compressive or tensile strength, dimensional stability, and elastic modulus were measured. 12 months exposure to 10 wt.% $MgSO_4$ led to the disintegration of BFS AAM, OPC, and the blended samples. Up to 25 months of exposure to 1 wt.% $MgSO_4$ and 1 or 10 wt.% Na_2SO_4, on the other hand, kept or increased the UCS of the samples. BFS mortars were immersed in 50 g/L $MgSO_4$ and Na_2SO_4 solutions for up to 12 months. In the Na_2SO_4, the AAM performed better than OPC. The $MgSO_4$ immersion caused gypsum formation and deterioration of the C-S-H gel. NaOH-activated BFS AAMs exhibit lower resistance to sulphide attack. In FA-based AAMs, no loss of mechanical properties was observed when immersed in 44 g/L Na_2SO_4 or 5 g/L $MgSO_4$.[48]

Mortar with 70 wt.% GGBFS and 30 wt.% RM activated with sodium aluminate clinker, solid waterglass, and water provided low porosity AAM mortar that had comparable resistance to a variety of acid and salt attacks. RM and FA mortars immersed in sulphuric acid reported acid resistance to be similar to OPC references. The partial dissolution of the AAM decreased the UCS by about 30 % from 10 to 7 MPa. Acid and sulphate resistance of GGBFS-RM AAM with 70-80 wt.% of aggregate were immersed in 5 % sulphuric acid and sodium sulphate for 28 days. The increases in UCS were by 23% up to 40 MPa for the acid and by 17% up to 38 MPa for the sulphate immersed sample. NaOH-activated mortar consisting of 30 wt.% RM, 60 wt.% FA and 10 wt.% silica fume were immersed in 5% sulphuric and 5% acetic acid. This led to the increased UCS up to 38 MPa from 32 MPa. This mixture formed AAM that was less affected by the acids than the OPC reference.[28]

BFS-based AAMs show good resistance to seawater. UCS increases have been reported after 1 year of exposure. Pore structure changes are reduced in silicate-activated BFS

AAMs compared to NaOH activated, both still proved to be resistant to 180 days of saltwater exposure.[48]

2.4.6 Chemical resistance of Fe-rich AAMs

Two different RMs (Fe_2O_3 content 18.44 and 46.61 %) and iron tailing (Fe_2O_3 content 8.27 %) as aggregate were alkali-activated and the formed mortars were tested for resistance to 5 % NaOH, 5% Na_2SO_4, and 2% HCl. The 28-day UCS values of the mortars were 31-37.5 MPa. The chemical resistance was tested after 7 days of curing and 21 days of submersion in the solutions. Only one mortar exhibited a decrease in UCS from 37 MPa to 35 MPa after submersion in 2% HCl. UCS of all other samples increased after the submersion period. After immersion in 5 % NaOH, 5% Na_2SO_4, and 2% HCl, the UCS values measured were 41-50 MPa, 35-46 MPa and 35 MPa, respectively. Good chemical resistance was attributed to C-A-S-H gel formation as the main product resulting in dense microstructure.[61]

Fe-Ni slag with kaolinite filler activated with sodium silicate solution was studied. The FeO content of the slag was determined to be 38.8 %. The resistance to chemical attacks was studied using seawater, 1 M (8.3%) HCl, and H_2SO_4:HNO_3, 60:40 wt.% with pH 3 to simulate acid rain. The 28-day UCS before immersion was measured to be 14.8 MPa. The chemical attack was carried out for 4 months. Sea water had minor effects on the UCS of the mortars. After 1, 2, 3, and 4 months the UCS was 14.4, 14.1, 14.95, and 13.5 MPa, respectively. With simulated acid rain, the loss of strength was more severe. After 1, 2, 3, and 4 months of exposure, the UCS dropped to 14, 13, 12, and 11.9 MPa, respectively. Similarly, as the acid rain, the 1 M HCl had a severe degrading effect on the AAM. After 1, 2, 3, and 4 months of exposure, the UCS dropped to 13, 12.5, 11.9, and 11.59 MPa, respectively. The UCS of the mortars reached 17 MPa when they were air cured for 4 months. The loss of UCS in acidic solutions is due to depolymerization and the formation of zeolites. Acid attacks break the Si-O-Al bonds in the AAM matrix.[62]

Immersion of Fe-Ni and ladle slag AAMs in 1 M HCl and distilled water for 7 and 30 days did not break the structure. Distilled water caused a marginal drop in UCS whereas immersion in HCl reduces the UCS to 65 and 45 MPa after 7 and 30 days respectively, compared to the UCS of the reference sample of 78 MPa.[63]

The resistance of Cu-slag-based AAMs to sulphide and acid attacks has been reported in previous studies. The produced AAMs [64] treated with 10% $MgSO_4$ and 10% Na_2SO_4 resulted in an increase in UCS by 8.2 % and 7.9%, respectively. Acid attack with H_2SO_4 to Cu-slag AAM resulted in a UCS decrease of 16.7%. The weak resistance of Cu-slag AAM to acid attacks is attributed to ferrous salt formation[64]. Another study reported decreases in UCS after 5% $MgSO_4$ submersion. 1- and 3-month submersion decreased UCS by about 10 and 15%, respectively. After 1 year, the decrease in strength was 23%. The AAM exhibited significantly better chemical resistance than OPC[66].

Chemical resistance of low purity kaolin AAM against sulphate and acid attacks has shown good results. Fe content was determined with XRF to be 25.21 wt. %. Silicate solution was used as an activator and sand as an aggregate. Lower and higher strength mortars were prepared. The compressive strength of the prepared mortars were 37.5 and 60 MPa. The sulphates used in the study were 5% Na_2SO_4 and 4.24% $MgSO_4$. The mortars were kept submerged in the solutions for 52 weeks. During the first 28 days, the mass of the mortars increased slightly with both solutions. The maximum mass increase was 0.12%. Longer exposure led to a mass loss of 0.3 % and 0.17 % with Na_2SO_4 and $MgSO_4$ solutions, respectively. The mass loss was attributed to the leaching of alkalis. The UCS of the mortars had no correlation with the mass losses. 1%, 3%, and 5% H_2SO_4 and 0.37%, 1.12%, and 1.86% HCl solutions were used to study the resistance against acid attack. The mortars were submerged for 8 weeks. The lower strength mortars resulted in mass losses of 2.4, 5.5, and 7.9% after 8 weeks of exposure to 1%, 3%, and 5% H_2SO_4 solutions respectively and with 0.37%, 1.12%, and 1.86% HCl 1.6, 3.6 and 5.5%, respectively. The mortars with a higher strength performed better, and the cumulative difference was 0.9 % compared to the mortars having a lower strength. The better performance is attributed to lower porosity. It was shown that H_2SO_4 causes more degradation of the mortars compared to HCl solutions.[67]

In general, increasing the Ca content makes AAMs more vulnerable to acid attacks. Ca-hydrated reaction products are converted to Ca-sulphates and calcium-sulpho-aluminates. $CaSO_4$ reacts forming gypsum that is deposited on the mortar surface, where it is easily dissolved. Sodium silicate-activated FA was exposed to 2% H_2SO_4 for one year period. During the first 28 days, the solution absorption caused a mass increase. One year of exposure decreased the mass by 13%. The Ca content was increased by OPC addition and

more severe mass loss was reported. Pure FA AAM lost its strength by 18, 33, and 52% during the submersion for 28, 90, and 365 days, respectively. The formation of strong alumina-silicate bonds makes AAMs stronger to acid attack compared to OPC. 10% replacement of FA with OPC gave the best resistance to H_2SO_4. The loss of UCS was 16, 30, and 48% by submersion of the mortars for 28, 90, and 365 days. The UCS values were compared to air-stored reference mortars. The increased Ca content increases the share of C-S-H gel in coexistence with C-A-S-H and N-A-S-H gels, thus resulting in a more compact structure reducing porosity, and thus offering better resistance to H_2SO_4. Increasing Ca content provides more nucleation sites for an acid attack.[68]

3. RESEARCH REALISATION

To minimize natural resource consumption and decrease CO_2 emissions, a more sustainable binder for the construction sector is needed. For this reason, AAMs have been studied extensively. But there is insufficient data on studying the possibility of producing AAMs from Fe-rich NFMS without the usage of high molarity solutions and commercial alkali silicate solutions. In this study, the goal is to study the alkali-activation of NFMS with NaOH solutions with different molarities. Also, the effect of admixtures is studied. The first section of this study focuses on the compressive strength of the mortars produces with and without additives. Based on the results the most promising mix designs are selected and used in the second part of this study. The second part focuses on the durability properties of the produced AAMs. The durability of Fe-rich AAMs is insufficiently studied in the previous literature. Thus, the effect of non-silicate activator with low molarity and admixtures on the mechanical and durability properties was studied.

4. EXPERIMENTAL

4.1 Materials and methods

4.1.1 Materials

The sample was modified jarosite industrial slag from zinc production with wüstite as the main mineral component. To remove moisture the received slag was dried in the oven at 60 ºC. The dried slag was ball-milled for 3 hours in a laboratory tumbling ball mill (Germatec, Germany) to achieve particle sizes below 100 μm. Standard sand in compliance with European standard EN 196-1 (EN 196-1, 2016) with a particle size distribution (PSD) between 0.08 and 2 mm and a maximum moisture content of 0.2 wt.%, was used as an aggregate.

Sodium hydroxide pellets (>98 % purity; VWR Chemicals) were used in NaOH solutions. Additives used were calcium hydroxide (Merck KGaA), calcium oxide (Sigma-Aldrich), magnesium oxide (98% purity, 99%< 150 μm Acrös), and silica fume (0.2-0.3 μm, Sigma). Deionized water was used throughout the experiments.

4.1.2 Initial material characterization

X-ray fluorescence results as oxides in wt.% are presented in Table 1. The three major components are Fe_2O_3, SiO_2, and CaO with wt.% of 49.3 wt.%, 20.6 wt.%, and 12.2 wt.%, respectively. Some trace elements are also present. The crystalline and amorphous content of the slag from X-ray diffraction showed that the amorphous phase was dominant at 73.8 wt.% and the crystalline phase was 26.2 wt.%. Figure 2 presents the particle size distribution of the slag after 3 h of milling in a ball mill. The particle size is mainly below 100 μm and the mean particle size of 10 μm.

Table 1. The bulk chemical components of initial slag as wt.% as oxides.

Fe_2O_3	SiO_2	CaO	Al_2O_3	Na_2O	MgO	SO_3	MnO	P_2O_5	Fe_2O_3	K_2O	SrO	TiO_2	Cr_2O_3
49.3	20.6	12.2	6.8	4.8	1.5	0.7	0.6	0.6	0.5	0.4	0.3	0.2	0.1

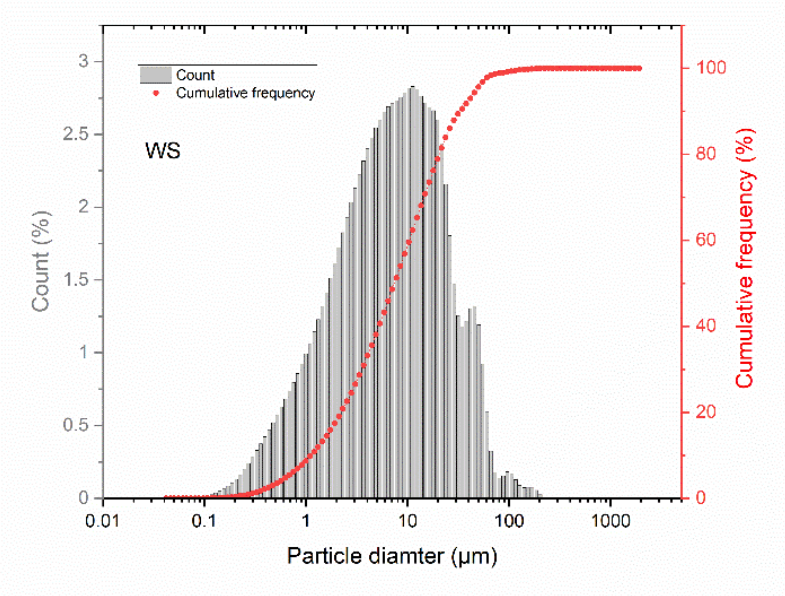

Figure 2. Particle size distribution of initial slag after 3 h of ball milling.

4.1.3 Sample preparation

The activation solutions were prepared in a 1000 ml plastic measuring flask. The sodium hydroxide solutions (1M, 3M, 6M, and 9M) were prepared by weighing 40 g, 120 g, 240 g, and 360 g of NaOH pellets and dissolved in 500 ml of water. After the pellets were dissolved the measuring flask was filled to the 1000 ml mark. The solutions were then left to reach equilibrium for 24 h.

Sample codes are denoted with XM-Yz, where X is the molarity of NaOH, Y is the % replaced slag, and z is the additive used (CH-$Ca(OH)_2$, CO-CaO, MG-MgO, and SF-silica fume). A full list of all mix designs of prepared samples is presented in APPENDIX 1-5.

The mixing of the materials was made mechanically in accordance with EN 196-1 standard (SFS-EN 196-1, 2011). The additives, if used, were mechanically mixed for 1 minute. The activator solution was then added and mixed for 1 minute. Standard sand in the sand to binder ratio of 0.5 in all samples was gradually added during 1 minute of continuous mixing. Final mixing was carried out for 1 minute. The mixture was cast into a 20 × 20 × 80 mm^3 oiled rectangular prism mould. A jolting machine was used for compacting the cast samples (60 shocks, 1/s). All the samples were sealed in a plastic bag and cured at 60 ºC for 24 h. The samples were demoulded and sealed in a plastic bag and stored at room temperature (approximately 23 ºC) until testing the compressive strength

after 7-, 14-, 21- and 28-days curing. Photos of the produced mortars are presented in provided APPENDIX 6.

Some of the samples had lower workability, mainly the ones with silica fume. The procedure described previously caused gel formation that prevented thorough mixing. Due to this problem, the solution to binder ratio was higher. And the procedure was altered to improve workability, rather than dry mixing of slag and silica fume the silica fume was added last. The 0.4 solution to binder ratio was not sufficient with a 10 % silica fume addition and the sample was dry and did not mix appropriately.

Pastes were prepared from 1M, 6M, 1M-1SF, 1M-10SF, 6M-1SF, 6M-10SF, 1M-1CO, 1M-10CO, 6M-1CO, and 6M-10CO. Binder (slag and additive) mass was 15g and solution mass was 4.5 g for all additives except for the silica fume (SF) ones in which the solution mass was 6 g. The pastes were moulded in plastic moulds and sealed in a bag and cured for 24h at 60 ºC and after that at room temperature for a total of 14 days. The pastes were milled with a disk mill (Retsch GmbH, Germany). 1 g mixture of the milled AAM pastes and ZnO (10 wt.%) standard were prepared for XRD analysis of the pastes.

4.1.4 Test procedures

The chemical composition of initial slags was determined by using X-ray fluorescence (PANalytical Omnian Axiosmax) from a melt-fused tablet and a loss on ignition (LOI) was measured with PrepAsh (Precisa). Particle size distribution was determined with Beckman Coulter LS 13320 laser diffraction particle size analyzer with water used as dispersion medium during measurement.

The unconfined compressive strength (UCS) of mortars was measured using a Zwick testing machine (Zwick Roell Group, Ulm, Germany) with a maximum load of 100 kN and a loading force of 2.4 kN/s. Each sample was tested twice, and the average was regarded as the representative value of the strength measurement. The error bar in the strength measurement graph indicates the standard deviation for each sample. Limited access to UCS measurement caused deviations in desired curing times. This resulted in limited comparability of the UCS results. The results are comprised in the best way possible with the data available.

The microstructure and composition of prepared mortars were studied with SEM-WDS analysis. Mortars selected for SEM analysis were 3M, 6M, 3M-5SF and 1M-10CO cured in air and after 28-day treatment in NaCl and HCl, to study the effect of the chemical treatment. The mortars were cut into smaller pieces and cast in epoxy resin. Then ground and polished using ethanol as a lubricant to prevent additional hydration and dissolution. The mortars cast in epoxy were then coated with carbon and analyzed using a field emission electron probe microanalyzer (FE-EPMA) (JEOL JXA-8530FPlus) and the elemental mapping was performed using an EDS (Energy-Dispersive X-ray Spectroscopy) detector.

X-ray diffraction (XRD) pattern of the alkali-activated slag with and without additives was determined by using a Rigaku Smartlab diffractometer, with a Cu K-beta radiation and a scanning rate of 0.02 θ/step from 5–130º, operated at 135 mA and 40 kV. The quantification of the amorphous phases was done with 10 wt.% zincite (ZnO) as the internal standard. The Rietveld refinement method was used for qualitative and quantitative analysis of crystalline phases.

FT-IR was used to analyze the structural changes of the initial slag and AAM pastes. The spectra were collected using a Bruker VERTEX 80v spectrometer (Bruker, Billerica, MA, USA) in the 500–4000 cm−1 range and 40 scans at a resolution of 2 cm−1 for each sample. The samples were prepared in same the way as for the XRD but without the ZnO.

4.1.5 Durability tests

Freeze-thaw resistance was studied based on the ASTM C666 recommendation[69]. The mortars were half immersed in water. Then the mortars were subjected to 60/120 freeze-thaw cycles. The cycles involved lowering the temperature in the chamber from +15 ºC to -20 ºC in 2 hours, maintaining the -20 ºC temperature for 2 hours, increasing the temperature back to +15 ºC in 2 hours, and maintaining the +15 ºC temperature for 2 hours. The UCS is measured after 60/120 cycles.

Mortars cured for 14 and 28 days were used to study chemical resistance of the AAM. Resistance to salt water was analyzed with 3 wt.% NaCl solution. The concentration of the solution was emulating the salt content of natural seawater. Sulphate attack resistance was analyzed with 3 wt.% $MgSO_4$ solution. Acid resistance was analyzed by submerging

the mortars in 3 wt.% H_2SO_4 and 3 wt.% HCl. H_2SO_4 solution has a dual mechanism of acid and sulphate attack on the AAM mortar. Acid attack causes scaling and sulphate attack degradation of the binder phase. 3 wt.% concentration of H_2SO_4 was considered by referring to previous studies. Mortars were submerged in H_2SO_4 solution for 28 days[70]. The mortars were submerged for 14 and 28 days in the solutions.

5. RESULTS AND DISCUSSION

6.1 Compressive strength

6.1.1 Compressive strength without additives

The UCS of reference samples 1M, 3M, 6M, and 9M are presented in Figure 3 after 28 days of curing. Increasing the molarity of the activator solution seems to increase the UCS at 7 days of curing. However, the compressive strengths of the mortars activated with 3M and 6M NaOH solutions were close, thus suggesting that the 3M solution has enough alkalinity to dissolve the slag and form the binding phases. All the samples except the one with 1M activator solution exhibit a significant UCS increase after 14 days of curing. The UCS of 1M samples increased by 1 MPa from 7 to 14 days. The UCS of 3 and 6 M samples increased about three-fold from 7 to 14 days. The lowest UCS was observed with 1M at 5.4 MPa and the highest with 9M at 20.28 MPa. The UCS did not increase significantly from 3 M to 9 M. Interestingly, a slight drop in UCS was observed from 3 M to 6 M, from 17.17 MPa to 15.06 MPa.

Usually, increasing the activator concentration leads to higher reaction rates. The formation of hydrate gel on the surface of precursor particles prevents efficient silica and aluminum dissolution. This leads to lower UCS with NaOH molarities over the optimum value. In the present study, the optimum is between 3 and 6 M NaOH. This is a lower value compared to the previous works on alkali-activation of the slags and other Fe-rich materials. For example, the authors used the initial NaOH solution concentrations from 8.3 to 19.1 M to activate volcanic ash from Cameron[57]. The low molarity in the present study can be explained by the high Na_2O content in the initial slag, that is, probably, in the glassy part. This suggests the saturation of the system with alkalis at a lower concentration of Na_2O in the solution and better solubility of Na-rich glass at lower molarities. The next results also showed the minor participation of Na in the reaction products due to the high content of Ca. Thus, the role of Na in the activating solution can be limited to the dissolution process. On the other hand, the dissolution of the Na-rich glassy part of the slag is easier due to the high content of Na_2O.

The literature review suggests that increasing the molarity of the activation solution should increase the UCS. A study was carried out with NaOH activator solution molarities

of 5, 10, 15, 20, and 25 M. The UCS of the samples after 7 days of curing showed values between 26 MPa to 40 MPa. The lowest UCS was recorded with a 5 M activator solution and the highest with a 15 M activator solution. An increase above 15 M NaOH decreased the UCS. The increase of UCS with molarity is due to increased silica and aluminum leaching.[71]

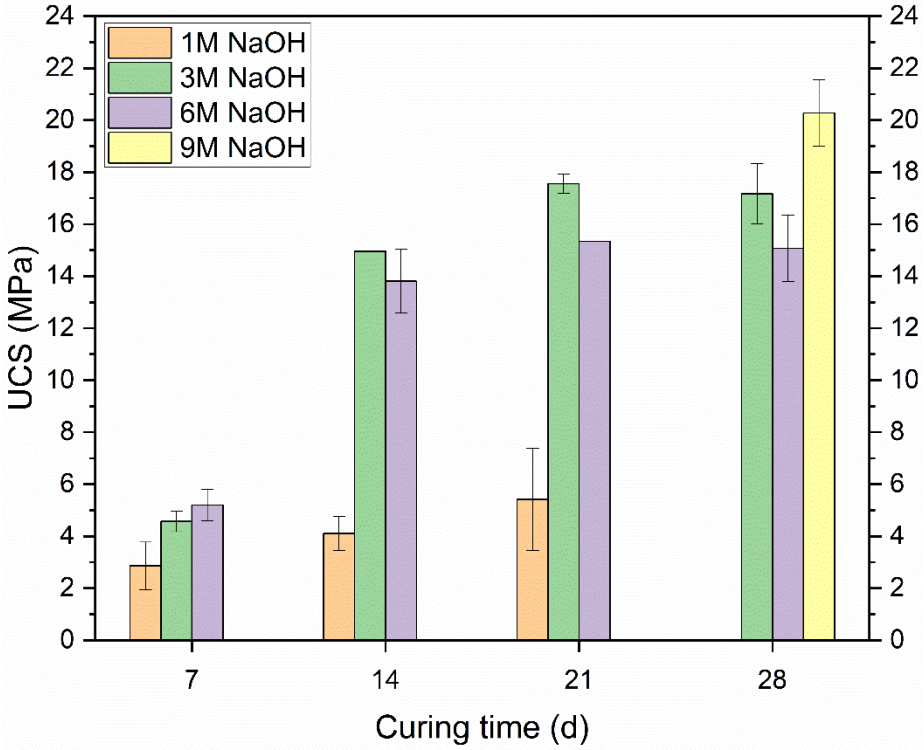

Figure 3. UCS of the reference samples at 7, 14, 21, and 28 days of curing with 1 M, 3 M, and 6 M NaOH solutions. Due to 1M mortars being brittle no data for 28-day curing time was obtained. Mortars were cured for 24 h at 60 ºC and after that at room temperature.

Another study [42] reports that UCS development was rapid with NaOH-activated GGBFS systems, showing that most of the UCS was achieved during the first 24 h of curing. The increase of UCS was lower with 12 M than with 5 or 8 M. The formation of reaction product on the surface of the slag is suggested to limit the later UCS development. UCS values reported for 5, 8 and 12 M activated samples were 27.5, 32, and 25 MPa, respectively.

In contrast to the study [42], the UCS of the mortars produced in this work increased significantly with longer curing times, most notably with 3 and 6 M solutions. This might

be the result of different precursor materials. The GGBS has higher aluminum content than the Fe-rich slag used in the present study. The higher aluminum content in GGBFS might accelerate the kinetics and thus allow significant product formation during the first 24 h.

6.1.2 Calcium hydroxide addition

Figure 4 presents the effect of the slag replacement with $Ca(OH)_2$ at different curing times and molarities of the activating solution. Using molarities of 1 and 3, the $Ca(OH)_2$ addition did not have any significant effect on the UCS. At 6 M the UCS increased most notably at 10 % replacement. The 10 % replacement increased the UCS from 15.06 MPa to 20.96 MPa which is a 32.8 % increase. The replacement of slag with 20 % of $Ca(OH)_2$ decreased the UCS to 17.33 MPa compared to the 10 % replacement.

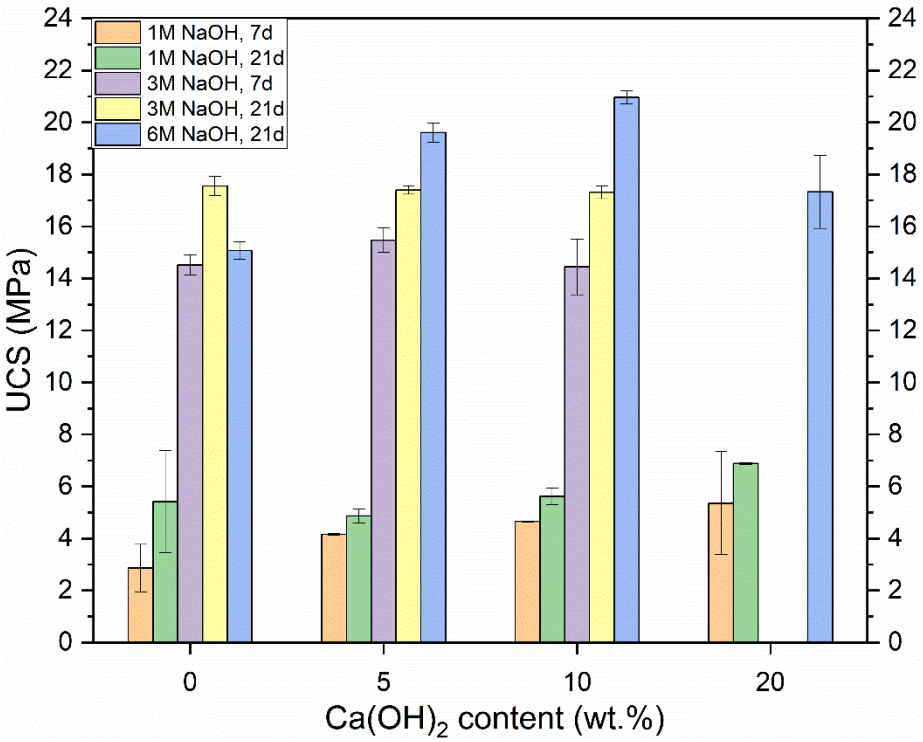

Figure 4. Effect of $Ca(OH)_2$ addition on the UCS of the non-ferrous slag activated with 1 M, 3 M, and 6 M NaOH solutions.

Another study where metakaolin with $Ca(OH)_2$ ($Ca(OH)_2$/MK ratio of 0.4) addition reported the UCS of the mortars of 19.0, 18.0, 12.0, 13.0, 17, and 7 MPa using 0.01, 0.1, 1, 3, 5, and 10 M NaOH solution activator, respectively. 1M NaOH activated samples achieved the UCS value of 13 MPa after 28 days of curing [72] and the value in the

present study for the sample with 20% $Ca(OH)_2$ was 6.9 MPa. The values obtained in the present study with 10% $Ca(OH)_2$ after 7 and 21 days of curing were 14.4 and 17.3 MPa, respectively. The 5M [72] and 6M NaOH with 20% $Ca(OH)_2$ in the present study after 21 days of curing showed similar UCS of 17 and 17.3 MPa, respectively. It can be concluded that calcium hydroxide is not suitable as an additive for NFMS used in this work, a similar effect was detected for metakaolin precursors.

The use of 1 and 3 M NaOH activators (Figure 4) did not have any prominent effect on the UCS development of the slag-$Ca(OH)_2$ mix i.e., no significant increase in UCS occurred with $Ca(OH)_2$ addition. This might be due to a lower amount of silica from the dissolution of the precursor. With sodium silicate activators, the low molarity of the activator reduces the degree of the precursor dissolution lowering the amount of dissolved aluminium[8]. In the present study, the NaOH activator with low molarity does not maintain the good dissolution rate of aluminosilicates to provide silica for intensive C-S-H formation. A previous study showed that the effect of $Ca(OH)_2$ was minimal with NaOH activated systems but with sodium silicate activated systems showed better results, thus suggesting the need for liquid silica in the first stages of the alkali-activation to enhance reaction kinetics[46].

Another reason for the loss of strength can be an excess $Ca(OH)_2$ in the AAM that causes carbonation (the formation of $CaCO_3$), thus lowering the UCS[73]. In the present study, a significant UCS decrease was not observed, although no formed carbonates were observed.

6.1.3 Calcium oxide addition

UCS results for the slag activated in the presence of CaO are presented in Figure 5. A decreasing trend with increasing CaO content can be seen with the 3 M solution. UCS decreased from 14.52 MPa to 11.63 MPa as the content of CaO was increased to 10 %. Compared to the reference sample (1M), the 10 % addition of CaO led to the increase in UCS from 6.69 MPa to 12.87 MPa after 7 days of curing, thus the strength of the 1M sample increased almost twice. Also, the addition of 5 wt.% of CaO with 6 M NaOH resulted in an increase in UCS from 15.06 MPa to 21.18 MPa after 21 days of curing, providing a 40.63 % increase in strength.

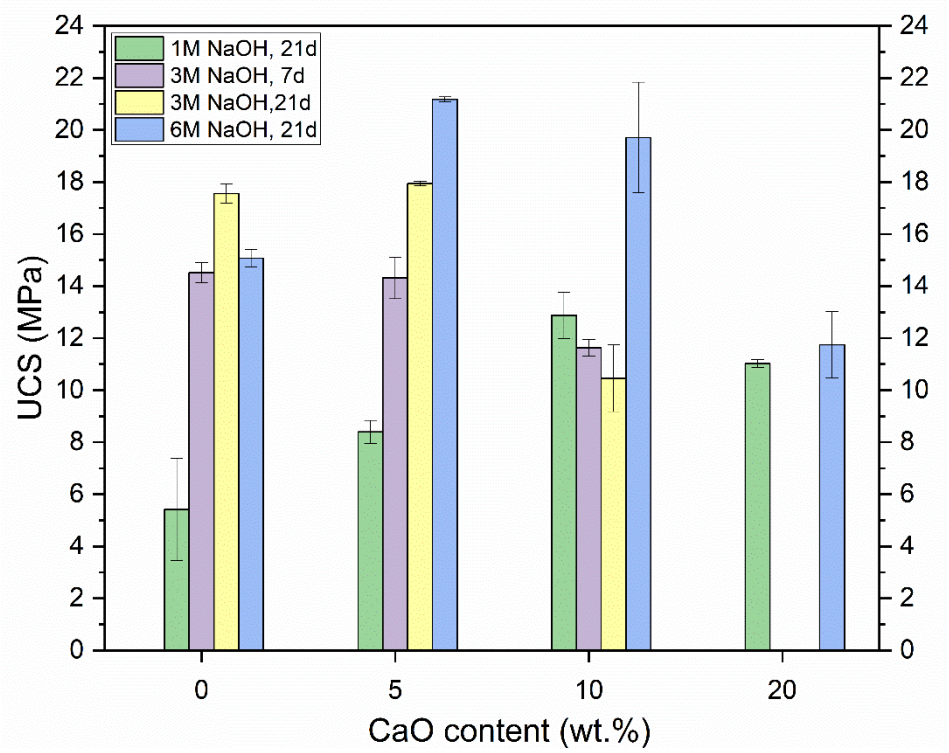

Figure 5. Effect of CaO addition on the UCS of non-ferrous slag activated with 1 M, 3 M, and 6 M NaOH solutions.

When GGBFS and iron tailing mix with CaO addition hydrothermally activated in 5M NaOH solution, the produced AAMs after 28 days showed UCS of 13 and 9.5 MPa with 4.5 and 9 % CaO, respectively[31]. When these results are compared to the results from the present study it is shown that the slag used benefitted more from CaO addition. In this work, UCS values obtained with 6M-5CO and 6M-10CO were 21.2 and 19.7 MPa, respectively. In the present study, the UCS value obtained with 6M-10CO was twofold compared to FA AAMs with 10% CaO addition produced in [32].

Sodium silicate activated kaolin-based AAM with CaO additions of 5, 10, 15, and 20 % were studied[44]. After 7 days of curing the samples reached UCS values of 40, 48, 42, and 35 MPa, respectively. Similar to the present work, the addition of CaO in a content exceeding 15% leads to a more prominent decrease in UCS.

The high contents of CaO led to a decrease in the strength of the produced mortars, depending also on the molarity of the activating solution. For example, the 1 M activated sample had only a small decrease in UCS when the dosage was increased from 10 to 20 wt.%. This might be explained with the lowest initial alkalinity of the solution[44]. Excessive addition of CaO led to a decrease in UCS, by destabilizing Na_2O-CaO-SiO_2-

Al_2O_3-H_2O gel from C-A-S-H gel formation at high alkalinity[44]. Also, an excess in CaO addition may cause carbonation that is linked with loose microstructure[31]. In a study, where volcanic ash was replaced by CaO in sodium silicate activated samples, the low replacement content did not affect UCS and an additional increase in CaO resulted in increased UCS compared to the reference sample by reacting with excess aluminosilicate ions to form C-A-S-H gel connecting the gaps between particles[74].

Also, the addition of CaO below 10 wt.% led to an increase in strength, especially for the low molar solutions. This effect may be connected with the increased total alkalinity of the system due to the presence of Ca^{2+} ions. Also, CaO hydration increases temperature and thus enhances slag hydration[31]. This may lead to the increasing dissolution of silica and aluminium[44], forming C-A-S-H gel. However, as will be seen in the next section, the contribution of katoite, but not C-S-H phases is responsible for the increased compressive strength of the alkali-activated non-ferrous slags.

6.1.4 Magnesium oxide addition

The effect of magnesium oxide addition on the UCS of the mortar is presented in Figure 6. MgO additions of 5, 10, and 20 wt.% were studied with NaOH molarities of 3 and 6. Mortars activated with 3 M solution showed a decrease in UCS after 14 and 28 days of curing compared to the reference sample. A decrease of 40.35 % to 37.26 % at 14 days and 28.73 % to 37.9% at 28 days was observed. Replacement of slag with 5, 10, and 20 wt.% with MgO resulted in similar values of UCS between 10.33 to 11.34 MPa after 28 days of curing. Mortars activated with 6 M solution exhibited a slight increase in UCS. The highest increase was with 10 wt.% replacement after 7 and 28 days of curing, 19.05 %, and 10.95 %, respectively.

UCS of zeolite with 4, 6, and 8 % of MgO activated with NaOH activator and basalt aggregates were studied. UCS values of zeolite binder with NaOH activator and basalt aggregates with 4, 6, and 8 % of MgO were reported to be 12, 13, and 12.5 MPa after 28 days of curing[75]. 5 and 10% MgO addition in the present study showed UCS of 10.5 and 10.3MPa and 18.8 and 16.7 MPa with 3M and 6M NaOH solution, respectively. The 3M NaOH activated behaved similarly as in [75]. GGBFS with 2 to 10% MgO with 2% intervals was activated with 4% equivalent NaOH. Standard sand was used as aggregate with a binder to the sand ratio of 1:2. After 28 days of curing the UCS values obtained

were 37.5, 36, 35, 31, 32, and 28 MPa with 0, 2, 4, 6, 8, and 10 % MgO. Hence, increasing the content of MgO leads to a gradual decrease in the strength of AAM.

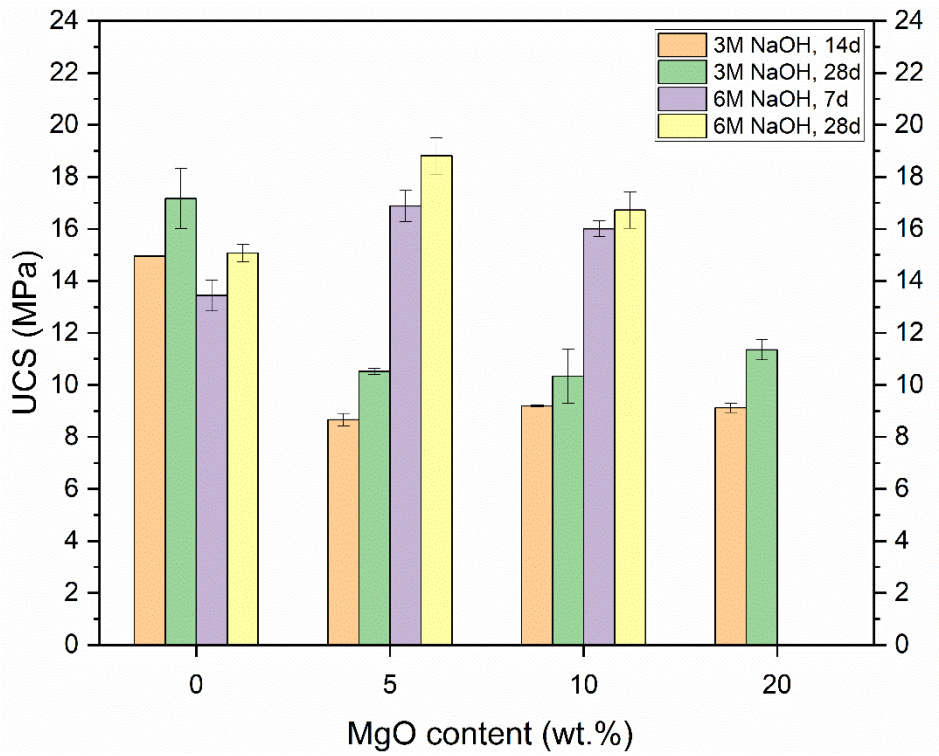

Figure 6. Effect of MgO addition on the UCS of non-ferrous slag activated with 1M, 3M, and 6M NaOH solutions.

As it was shown, magnesium might not take place in the gel structure thus not affecting the UCS of the mortars. The MgO probably acts as a filler and nucleation location leading to slight increases in UCS with a 6 M solution. MgO addition has been shown to increase water demand leading to dilution of starting materials. This in turn leads to decreased UCS.[76]

Despite the poor reactivity of MgO suggested from the results, several publications [77]–[79] concluded that MgO reacts with broken Si-O and Al-O bonds in the AAM. This leads to the formation of magnesium silicate hydrate or hydrotalcite-like phases leading to a decrease of AlO_4^- and SiO_4^- that act as monomers in the AAM[80]. The effect of MgO content was studied in GGBS activated with sodium hydroxide and silicate solutions. The MgO content varied from 8 to 13 wt.%. The study found that the amount of hydrotalcite-like phases increases and aluminum uptake in the C-(N)-A-S-H gel decreases as MgO content increases in the hydroxide-activated system. The silicate-activated samples

correlated with increasing MgO content and total hydrates formed, leading to an increase in UCS. This was confirmed in another study where the UCS of silicate-activated GGBSs tripled when MgO content was doubled. Magnesium is present in AAMs mainly in the hydrotalcite-like phases, where it acts as a network modifier cation together with calcium[24].

6.1.5 Silica fume addition

The effect of silica fume addition on the UCS of the mortar is presented in Figure 7. Due to lower workability, the slag was replaced with 1, 5, and 10 wt. % of silica fume using a higher solution to binder ratio. NaOH solution molarities were 1, 3, and 6 M. The UCS of almost all samples increased significantly. In contrast, the mix 1M-5SF showed a prominent drop in UCS up to 0.65 MPa and 0.57 MPa at 7 and 14 days, respectively, compared to the reference samples 2.86 MPa (77.27 % decrease) and 5.42 (89.48 % decrease) MPa at 7 and 14 days, respectively.

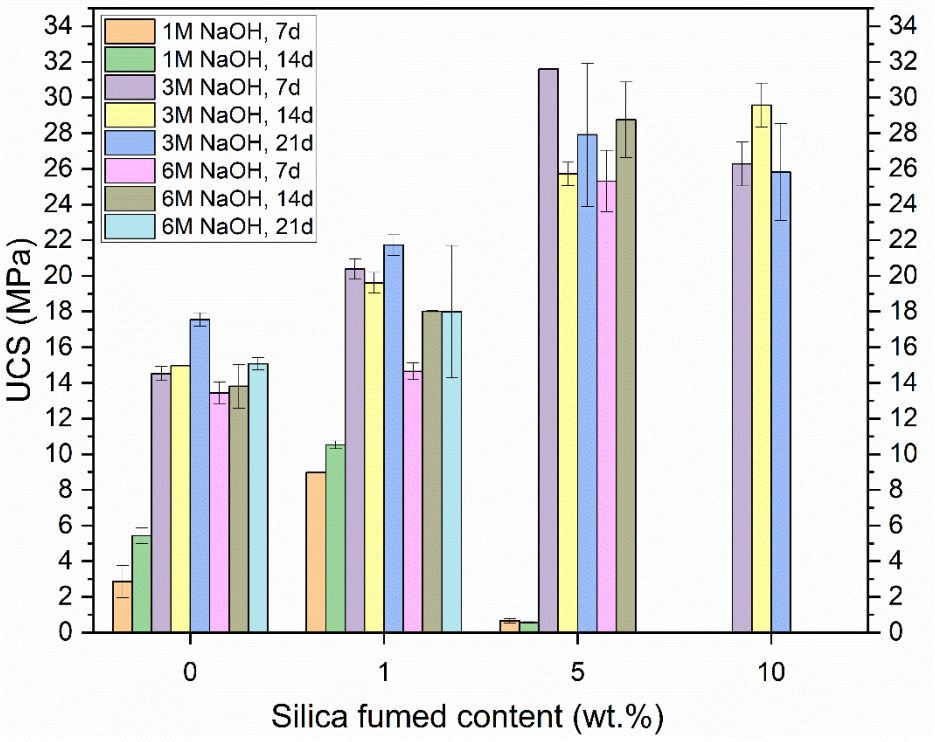

Figure 7. Effect of silica fume addition on the UCS of non-ferrous slag activated with 1M, 3M, and 6M NaOH solutions.

The replacement of slag with 10 % of silica fume lowered the workability significantly, thus focus was moved to 1 and 5 % replacement. 10 % replacement with 3M activation

solution increased the UCS after 7, 14, and 21 days of curing compared to the reference samples by 81.0 %, 97.66%, and 47.12 %, respectively. The 1% replacement exhibited the most significant increase in UCS with 1M activation solution, 214.34 % and 94.10 % increase after 7 and 14 days of curing. The 5 % replacement showed the highest values of UCS. The UCS of the samples activated with 3 M solution increased compared to the reference sample after 7, 14, and 21 days of curing by 117.63 %, 71.93 %, and 59.03 %, respectively. With 6 M NaOH solution, the 1 % replacement of slag with silica fume did not increase the UCS noticeably. The 5 % replacement increased the UCS by 108.18% compared to the reference sample after 14 days of curing.

According to the literature overview, the 28-day UCS of GGBFS activated with 3 wt.% NaOH solution (Na_2O molar composition 0.13) was measured to be 25, 23, 25, and 24.5 MPa with silica fume content of 0, 3, 5, and 8 %, respectively. Similar UCS values have been reported in previous studies[39]. The mix composition is similar to the present study. The minor impact of silica fume on UCS was considered to be due to the lower dissolution rate of silica fume[39]. The similar mortar compositions in the present study 3M-5SF and 3M-10SF exhibited the UCS of 27.9 and 25.8 MPa, respectively, after 21 days of curing. UCS values obtained in [36] showed similar results with silica fume addition of more than 5 % did not increase the UCS significantly.

As can be seen from Figure. 7, the 5% of silica fume addition had a negative effect on the UCS at 1M NaOH. This was measured four times and the UCS values were below 1 MPa. This might be due to the unreacted silica fume or the low stability of the formed hydrated phases. Using a low concentration of alkaline activators has resulted in silica fume agglomeration, resulting in decreased mechanical performance of the mortars [36]. On the other hand, the study [38] showed that excess silica will lead to the unavailability of Na_2O to dissolute the silica fume and aluminosilicate phases of the precursor[38]. The unavailability of alkali in 1M activated mortars and the high content of silica fume might be the reason for the poor UCS of the mortars. The 1M sample activated with 1% silica fume supports the effect of increased Si/Al ratio as the ratio is significantly lower when compared to 5% silica fume with the same molarity.

At 3 and 6M of NaOH, the activated samples possessed the positive effects of silica fume addition, suggesting that silica fume is incorporated in the reaction product. The following

study has suggested that silica fume requires higher molarity of NaOH solution to be hydrated. Although, the study observed that 6M NaOH solution was not sufficient for complete hydration of silica fume[36]. This is supported by a study in which the UCS enhancing properties of silica fume were attributed to pore structure refinements[38]. The role of silica fume as a filler is not as evident in the present study as the increase of silica fume from 5 to 10% did not increase the UCS significantly. The main role of silica fume addition was attributed to the available silica for the polymerization reactions and reduction of permeability of the hardened AAM[23], [37].

To conclude, the UCS enhancing properties of silica fume are attributed to the increased polymerization. The interfacial bond strength between binder and aggregate increases thus increasing the UCS. Excessive addition of silica fume lowers the mechanical properties of the AAM due to an increase in Si/Al(Fe) ratio thus inhibiting the geopolymerization. This also leads to the unavailability of Na_2O to dissolute the silica fume and aluminosilicate phases of the precursor [38].

6.2 Characterization of the reaction products

6.2.1 XRD

To study the effects of selected additives on the reaction product formation XRD analysis was performed. Pastes chosen for XRD analysis were activated with 1 and 6 M NaOH solutions without additives and with CaO and silica fume additives at low and high concentrations i.e., 1 and 10 wt.%. The main crystalline phase for the initial slag and all the alkaline-activated pastes was wüstite (see Appendix 9-18, where the full XRD patterns are present). The ratio between crystalline and amorphous fractions remained unchanged after alkali-activation according to Rietveld refinement. This implies that wüstite was unreactive in alkaline conditions. Similarly in literature, crystalline phases such as hematite in red mud [81] and fayalite in NFMS [82] were shown not to be involved in the binder formation.

A closer look at the XRD pattern between 5 and 35 degrees for initial slag, 1M NaOH activated and 6M NaOH activated pastes shown in appendix 8 Figure A48 (1M and 6M NaOH activated mortars XRD is also presented in figures 8 and 9) revealed the development of diffraction peaks that were not present in the initial slag. With 6M NaOH

activated paste broad peak at 7º and double peak at 34º might indicate the formation of Fe-rich variety of C-S-H gel with a similar structure as tobermorite [83], which is an ordered type of C-S-H (I) gel [84]–[86]. Another explanation for these peaks is the co-existence of strätlingite and C-S-H gel structures that have similar XRD patterns[86], [87]. These peaks were not present in the XRD pattern of 1M NaOH activated paste. The formation of this phase may reflect the increased crystallinity of the C-S-H phase in a higher alkalinity activator solution if the main reaction product is proposed to be related to this phase or the formation of a new silicate hydrated phase at high alkalinity. This supports the higher UCS obtained with a 6M NaOH activator.

XRD patterns of 1 and 6M NaOH activated pastes where the slag was replaced with 1 and 10 wt.% of CaO are presented in Figure 8. The 10 wt.% replacement with both molarities also developed peaks at 2θ of 21.25º that can be attributed to portlandite formation. Replacement of slag with 10 wt.% CaO with both 1 and 6M NaOH activated pastes developed katoite peaks at 20º, 23º, 31º, and 33º. These peaks attributed to katoite formation are supported in the literature[88]. Thus, the formation of katoite could be responsible for the increase in UCS after slag replacement with CaO. Although the diffraction peaks associated with katoite have higher intensity with 6M activator solution, the contribution to UCS development was more evident with lower molarity activator solution. To conclude the katoite phase formation may be one of the phases related to UCS development in the systems activated with low molarity activators.

Katoite is a completely hydrated hyrdogrossular group mineral, which is represented by $Ca_3Al_2(SiO_4)_{3-x}(OH)_{4x}$, where x is 3. The resulting structure has vacancies instead of the SiO_4 like in the hydrogrossular structure[89]. O-H bonds do not have a role in crystal cohesion in katoite, unlike in C-S-H gel. Compared to the grossular, katoite has lower mechanical properites[90]. The formation of katoite and its dissolution leads to the crystallization of tobermorite[88]. It is suggested that katoite formation could improve the concrete's durability due to more heat liberation, thus making the concrete more stable and reducing sulphate content[91]. One study showed the possibility of a solid solution of Fe-katoite formation forming C-A-F-S-H gel[92]. This might indicate that Fe is taking part in the reaction products in the present study. Katoite formation might lead to the porous and weak microstructure of the AAM leading to decreased UCS[93].

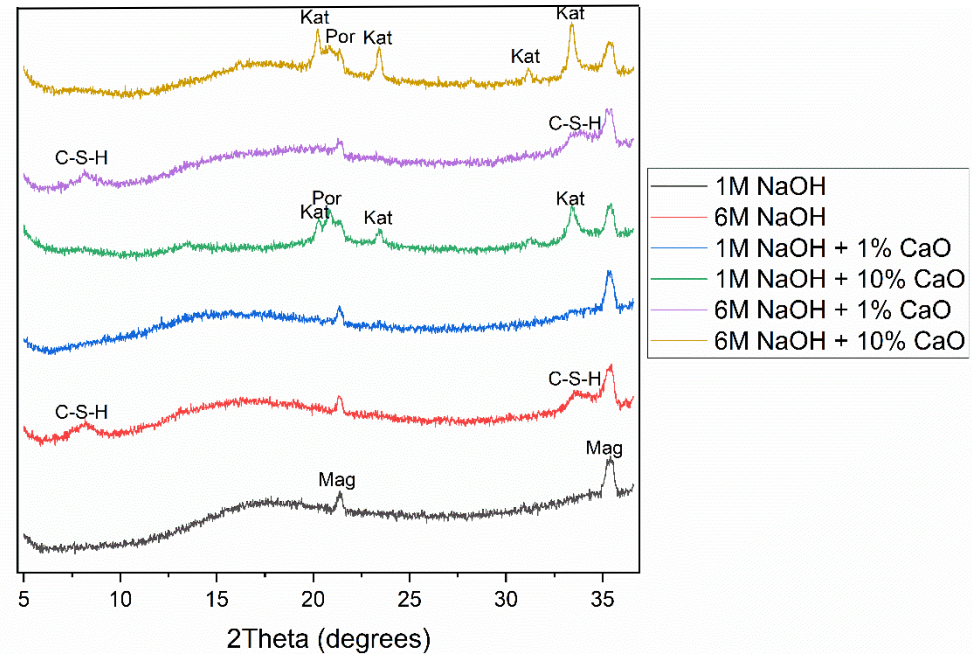

Figure 8. XRD patterns of the pastes of alkali-activated slags after 28 days of curing with slag replaced with 1 and 10 wt.% of CaO activated with 1 and 6 M NaOH solution. The phases are designated as follows: Mag – magnetite, C-S-H – calcium silicate hydrate (or calcium iron silicate hydrate) phase, Por – portlandite, and Kat – katoite.

Figure 9 indicates the effect of silica fume on the diffraction pattern of alkali-activated slag pastes. There was no C-S-H or katoite formation with 1M NaOH-activated pastes. This correlates with the low UCS values obtained with silica fume additions using low a molarity activator solution. This shows that silica fume is not an optimal additive to be used with a low molarity activator solution to obtain higher UCS. The C-S-H phase diffraction peaks were also found in the pastes with slag replaced with silica fume activated with 6M NaOH solution. However, it is interesting to note that higher amounts of silica fume diminished the peaks. This might suggest that the higher content of silica fume may form a more amorphous C-S-H del variety. This is well supported by a study [36] where the formation of a similar phase was observed in the XRD pattern, this was only attributed to samples activated with NaOH, but not with sodium silicate solution activated samples. The UCS values were higher with samples activated with silicate solutions than with pure Na/K hydroxide solutions. This suggests that the high silica content forms a more uniform, amorphous structure[94]. Studies have suggested that silica fume requires higher molarity NaOH solution to be hydrated. Although the study observed that 1M NaOH solution was not sufficient for complete hydration of silica

fume[36]. In the present study, it is observed that 6M NaOH solution hydrated silica fume and results in C-S-H gel formation.

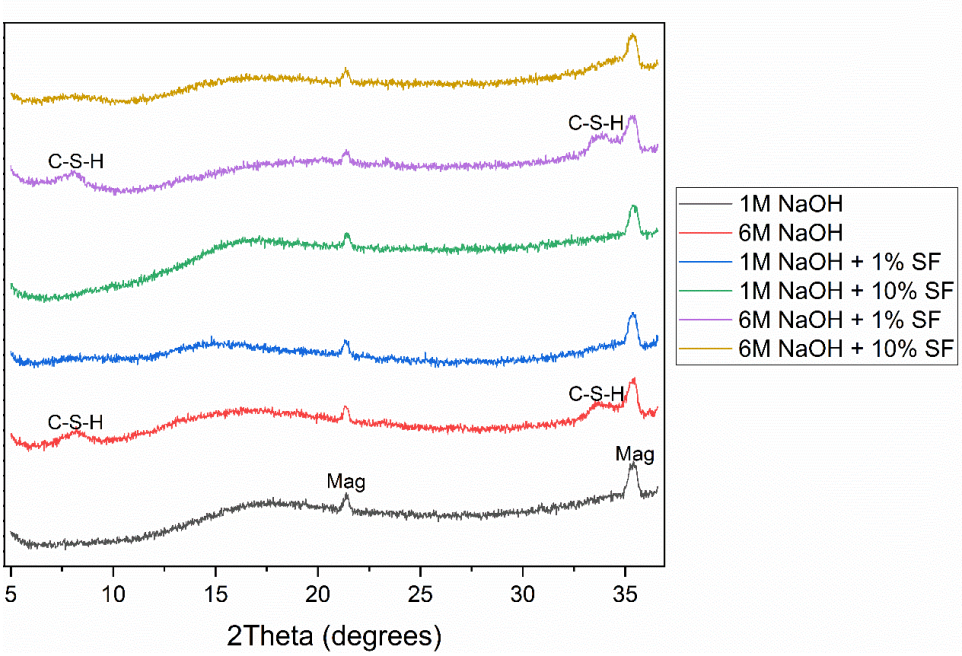

Figure 9. XRD patterns of the pastes of alkali-activated slags after 28 days of curing with slag replaced with 1 and 10 wt.% of silica fume activated with 1 and 6 M NaOH solution. The phases are designated as follows: Mag – magnetite, C-S-H – calcium (iron) silicate hydrate phase.

6.2.2 FT-IR

FT-IR spectra of the initial slag is presented in appendix 8 Figure A49. The FT-IR spectra (shown in Figure 10) of the pastes from slag activated with 1M and 6M NaOH solutions show the development of silicate hydrate reaction products. Bands developed at ~1667 and ~3530 cm^{-1} are associated to the bending vibration of molecular H_2O. The water molecules indicated by these peaks are surface adsorbed or entrapped in the pores of the polymeric matrix[95]. Studies have shown that another type of O-H bond at ~3755 cm^{-1} indicates the minor presence of hydroxyl groups [86], [96], [97]. 6M NaOH activated paste formed more hydrated products than 1M NaOH activated. These are visible in Figure 22 where the broad peaks at ~1667 and ~3530 cm^{-1} are more significant.

The peak at 1504 cm^{-1} suggests the presence of CO_3^{-2} groups[86], [96], [97]. The formation of these groups is due to atmospheric carbonation of the pastes from alkali-activation, paste preparation, and curing[86], [96], [97]. The XRD pattern of 6M and 1M

pastes (Figure 18) supports the hydrate product formation. The enhanced formation of hydrate products explains the higher UCS of the 6M mortar 15.34 MPa compared to 1M 5.42 MPa.

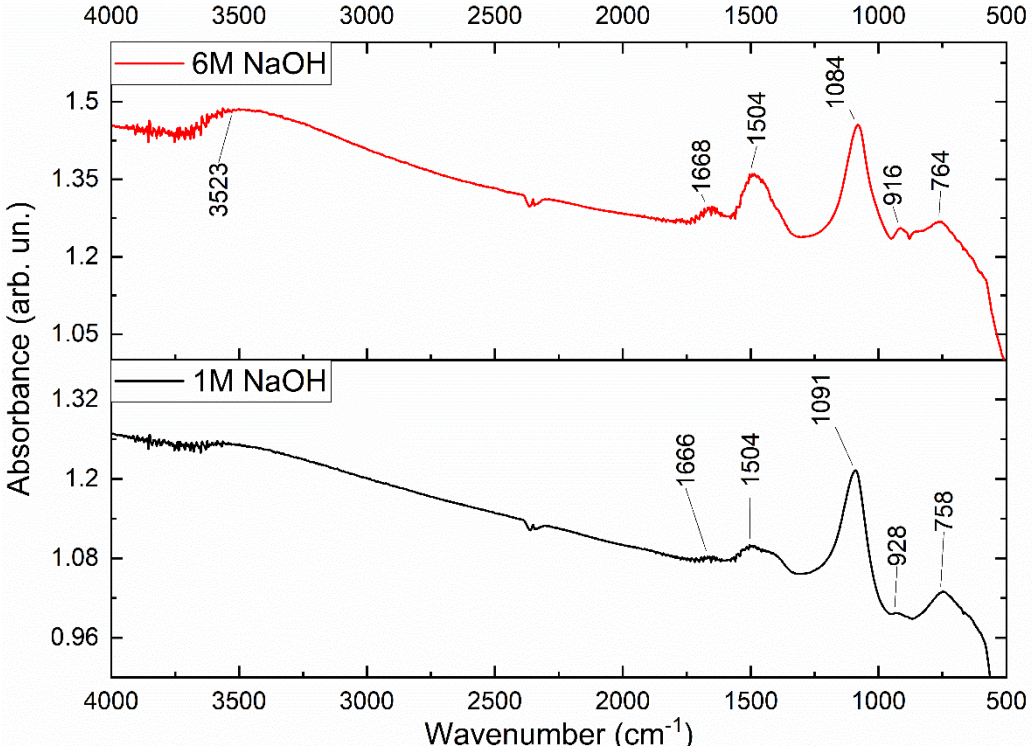

Figure 10. FT-IR spectra of 28 days cured 3M and 6M NaOH activated pastes from wüstite slag.

The main bands related to silica are located at 1084-1091 cm^{-1} they are associated with asymmetrical stretching vibrations of Si–O–Fe, Si–O–Al, and Si-O-Si bonds in SiO_4 tetrahedra[96]The position of this band at high wavenumber and the sharp shape is typical for neither C-S-H gels nor alkali-activated Fe-rich silicate glasses and sands. These bands are characteristic peaks for developing geopolymer networks, characteristic peaks of the inorganic polymer network[95]. For C-S-H gels this band usually appears at ~950 cm^{-1} [85] and for alkali-activated slags and glasses at ~870-970 cm^{-1} [98] [99]. This suggests that the main reaction products are different in the present study from those observed in previous studies with different AAMs. The shifting of Si-O to a higher wavenumber can be attributed to increasing the degree of polymerization[97], [100], [101]. The shift may also be attributed to the oxidation of Fe^{2+} in the slag to Fe^{3+} in the AAM, [82] and nanoscale clustering of Fe that results in more Si-OP-Si and Fe-O-Fe bonds, and fewer Si-O-Fe bonds[99]. Considering the structure of tobermorite, the shift to a higher wavenumber of Si-O stretching vibrations in Q_3 could be explained by increasing cross-

linkage by increasing Mg and Fe substitutions for Si[96], [102]. An increase in the amount of bridging oxygens is expected with the network forming Fe^{3+} content increase. The Fe^{3+} enhances corner-connected tetrahedra[102]. The peak located at 928 cm^{-1} for 1M and 916 cm^{-1} for 6M sample could be attributed to OH^- groups connected to the silicate network. An increased degree of hydration makes this peak more developed. Shoulder in the main silica peak or a separate peak at 930-940 cm^{-1} is usually attributed to Si-OH bending vibration modes located at 950 cm^{-1} [103] and 910 cm^{-1} [104] The peak at ~760 cm^{-1} could be attributed to the silicate glass form unreacted slag particles since the peak did not change in intensity or wavenumber in any samples (see Figures 22-24). For example, in the waste glass, a clear peak at 770 cm^{-1} was observed for Si-O in the silicate tetrahedra[105], [106].

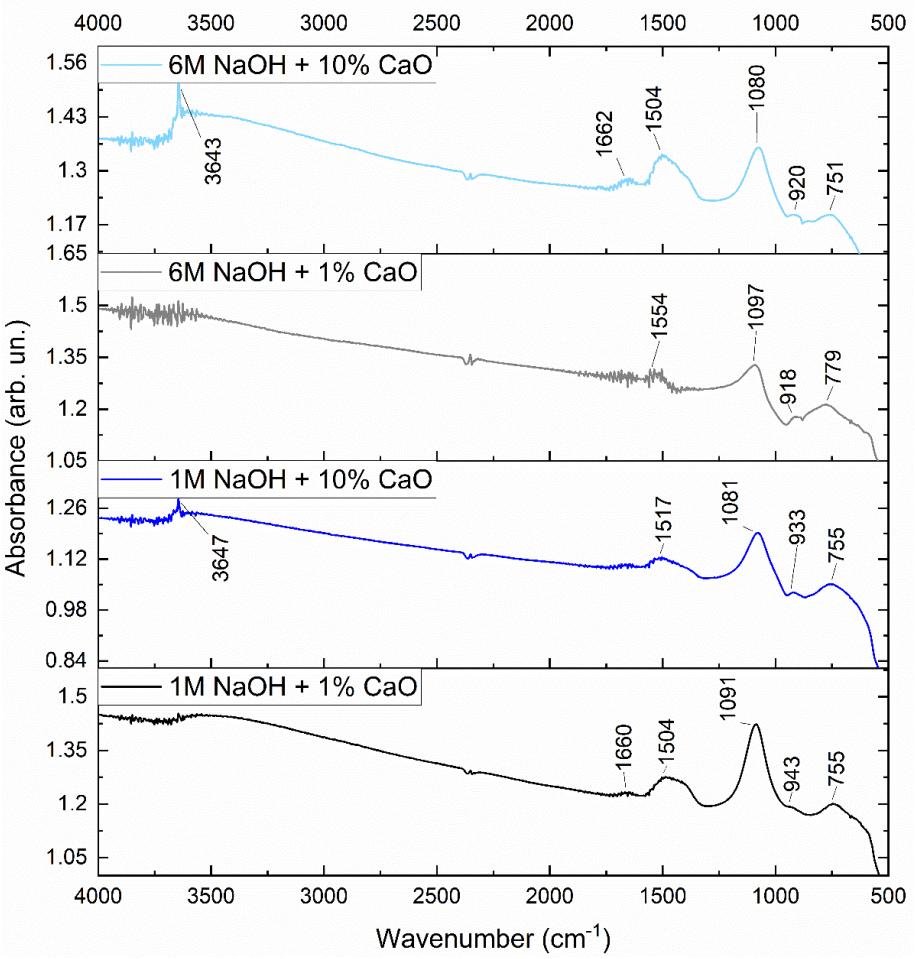

Figure 11. FT-IR spectra of 28 days cured 3M and 6M NaOH activated pastes from wüstite slag with 1 and 10% slag replacement with CaO.

When slag was replaced with 1 wt.% and 10 wt.% of CaO, it imposed a prominent effect on the FT-IR spectra of alkali-activated slag pastes as seen in Figure 11. The 1%

replacement in 1M activated showed some intensity changes. However, the 1% replacement in 6M activated samples led to the disappearance of a peak located in 1504 cm^{-1} connected to CO_3^{-2} groups[86], [96], [97]. This may indicate that the carbonation for these samples is mainly connected with the formation of sodium carbonates, thus depending on the amount of Na in the activating solution.

Increasing the amount of slag replaced with CaO from 1 to 10% with 1M and 6M activator shifted the main silica band to lower wavenumber by about 10 cm^{-1}. This could be explained by the increase in the Ca/Si ratio in the gel. Ca/Si ratio plays a significant role in C-S-H formation. According to a study, low a Ca/Si ratio causes a significant increase in UCS due to C-S-H gel formation[107]. Increasing the Ca/Si ratio causes breaks in the silicate chains leading to a redistribution of aluminum in the tetrahedral sites[108]. A similar shift in the main silica band occurred in FT-IR when the Ca/Si ratio increased from 1 to 1.7[109]. This was attributed to the partial substitution of Si-O-Si by Si-O-Al and terminal bonds $Si-O^-$ forming due to the increased amount of Ca in the system. The peak formed at ~3645 cm^{-1} can be attributed to the minor precipitation of $Ca(OH)_2$[109].

The effect of slag replacement with 1 wt.% and 10 wt.% of silica fume in the alkali-activated slag pastes is presented in Figure 12. A minor shift occurred in the main silicate band to higher wavenumbers could be attributed to a higher degree of polymerization[97], [100], [101]. The replacement with silica fume in all pastes showed less prominent carbonated and hydrated bond development. In general, these samples did not develop high UCS values. This is due to a need for higher molarity for silica fume to be reactive[36]. The 1M activated pastes with 10 wt.% of silica fume showed a double main silica peak cantered at 1151 and 1234 cm^{-1}. This may indicate that silica fume was not reactive, thus relating to the low UCS values of the samples with low molarity and high content of silica fume. This is supported in previous studies [36]. Paste activated with 6M NaOH and 10 wt.% replacement of silica fume caused a shift to higher wavenumbers in the main silicate band. This suggests that silica is incorporated into the reaction product. Thus, the increase from 1 to 10 wt.% of slag replaced with silica fume led to an increase in the peak's wavenumber from 1089 to 1136 cm^{-1}.

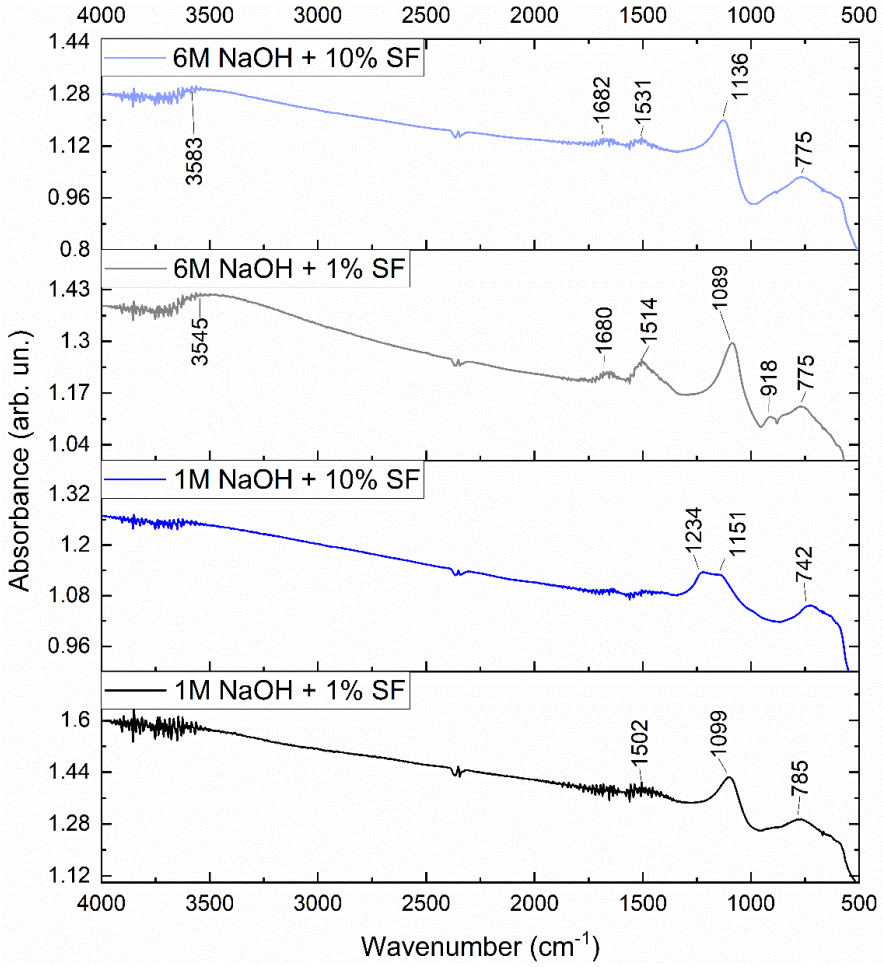

Figure 12. FT-IR spectra of 28 days cured 3M and 6M NaOH activated pastes from wüstite slag with 1 and 10% slag replacement with silica fume.

6.2.3 Microstructure investigation by SEM

The samples selected for SEM analysis were air cured 3M, 6M, 3M-5SF, and 1M-10CO. The microstructure of the mortars is presented in Figure 13, where a) 3M, b) 6M, c) 3M-5SF and d) 1M-10CO. From Figure 13, it can be seen that all samples showed reaction product that is seen as grey or dark grey, unreacted slag seen as light grey, and wüstite seen as white. In all samples, well-shaped, prismatic, light-grey crystals are observed (they are pointed with red arrows in Figure 13a). According to microchemistry analysis, these crystals are rich in Fe and Al: 46% and 13.2%, respectively. These crystals are located within both the initial slag particles and the reaction product. This suggests that the crystals were present in the initial slag and were unreactive under the conditions applied. In Figure 13a, a mica-like phase was observed, pointed with a yellow arrow. According to chemical analysis, this phase is alumino-silicate, with Al_2O_3 29.4% and SiO_2 41.5%. Thus, it could be a result of the alkali-activation since it is located between

slag particles within the formed gel binder. It can be seen from Figure 13 that the microstructure of the gel phase is quite similar in the samples. 1M-10CO sample shows less uniform reaction product formation compared to the other samples. This is supported by the chemical analysis that is presented in Figures 15-17. The points are taken from the gel phase of the sample. The points are significantly more scattered with the 1M-10CO sample. Figures 14-16 also show that 3M and 6M samples reaction products are similar but with the 3M-5SF higher silicon content is observed. This shows that silica fume addition leads to a more uniform microstructure.

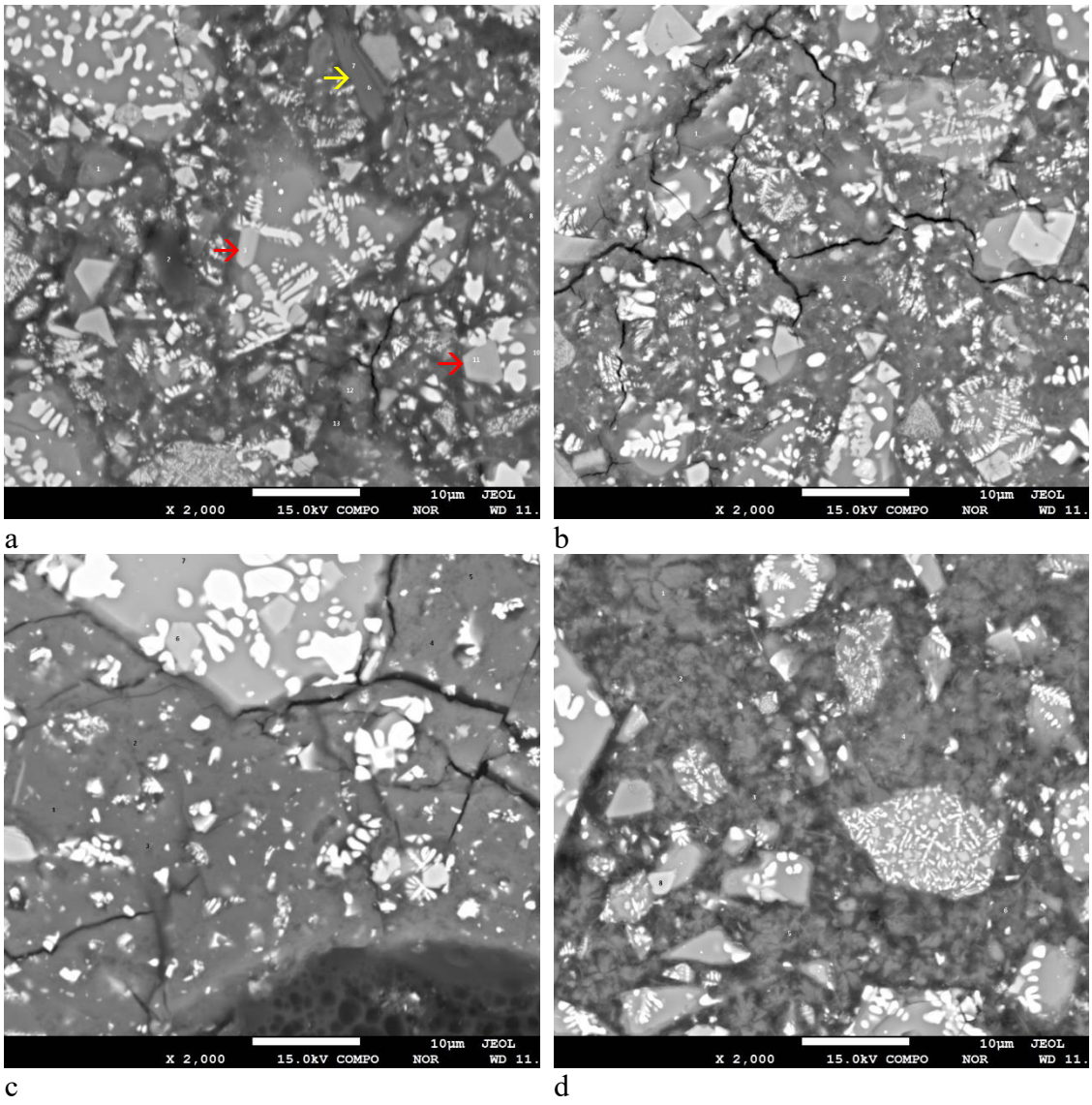

Figure 13. SEM images of a) 3M, b) 6M, c) 3M-5SF and d) 1M-10CO samples.

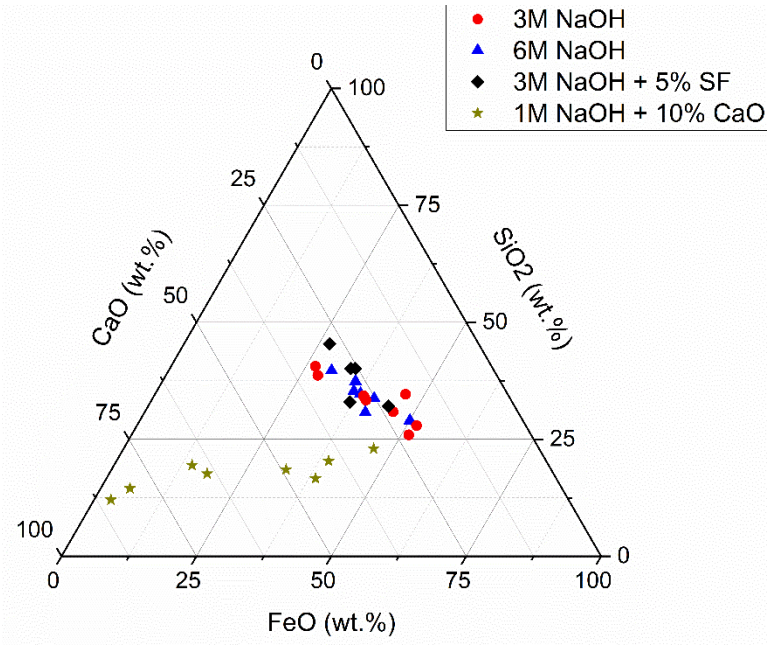

Figure 14. Chemical analysis of the gel phase plotted in a ternary diagram with CaO-SiO_2-FeO.

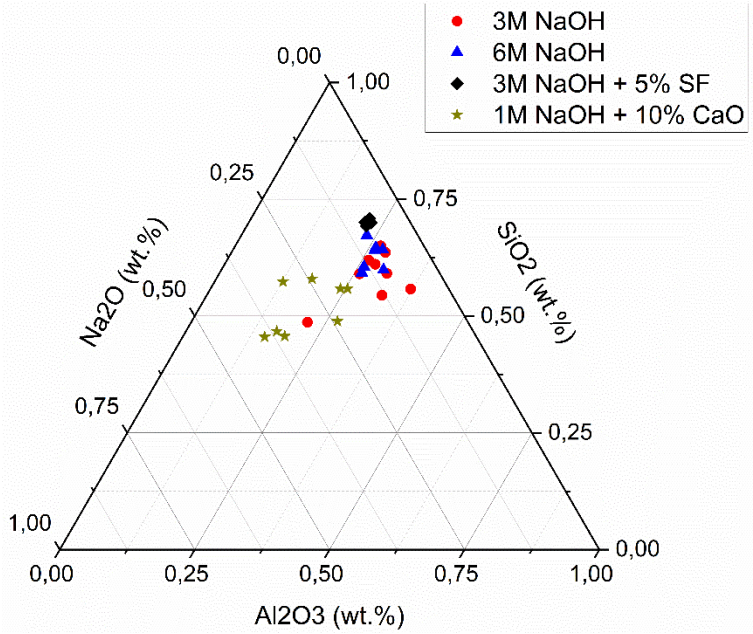

Figure 15. Chemical analysis of the gel phase plotted in a ternary diagram with Al_2O_3-SiO_2- Na_2O.

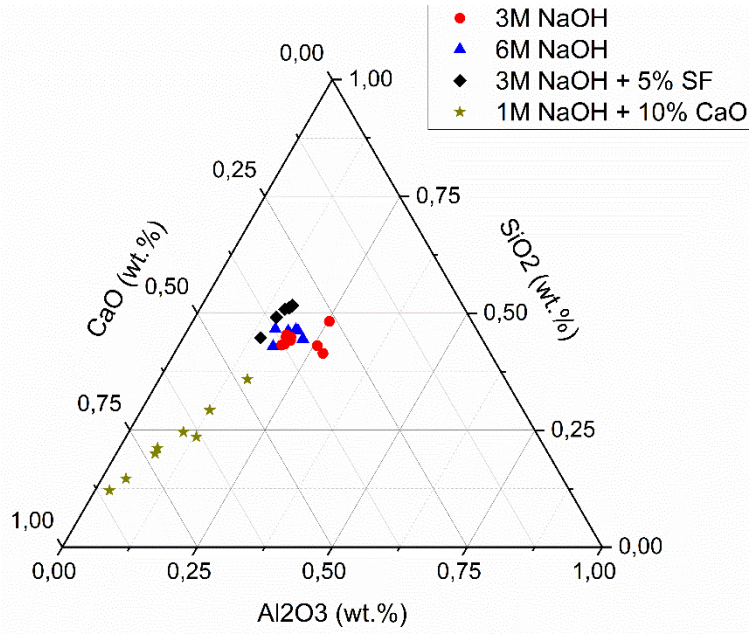

Figure 16. Chemical analysis of the gel phase plotted in ternary a diagram with Al_2O_3-SiO_2- CaO.

6.3Freeze-thaw test

Figures A46 and A47 (Appendix 7) show the effects of 60 and 120 freeze-thaw cycles on the selected mortars (3M, 6M, 3M-5SF, and 1M-10CO). The mortars before the freeze-thaw experiments are presented in Figures A33 b and c, A37 b, and A43 b. (Appendix 6). As seen from the figures, the prepared AAM mortars exhibited very poor freeze-thaw resistance. The only mortar that was still solid after the freeze-thaw was 3M-5SF after 60 cycles. Also, all mortar exhibited significant mass losses. A significant efflorescence occurred in the mortars during the freeze-thaw test. Efflorescence shown in Figure 17 occurred at 22 freeze-thaw cycles. The migration of sodium and the formation of sodium carbonates to the surfaces of the mortars cause formation of micropores[59]. These micropores allow water penetration into the mortar. During the freezing, this absorbed water expands and causes damage to the structure of the mortar.

The pore structure of the AAM matrix plays a significant role in water penetration, and thus amount and size of pores is a significant factor affecting freezing damage. C-S-H gel formation also decreases the porosity of the matrix which consequently decreases water penetration. Even the initial mortars showed a dense structure, the freezing-thawing opened the micropores by efflorescence. Thus, for the durability of alkali-activated

NFMS, the immobilization of Na coming from the solution is the top issue to address in the next research. The next experiments with the same slag activated using silicate solutions exhibited much better performance during freeze-thaw tests.

The best performance of 3M-5SFs in the freeze-thaw cycles is probably due to a higher content of silica. This is supported by a study where increasing the nano-silica content of alkali-activated slag concrete increased the freeze-thaw resistance of the sample. The increased resistance to freeze-thaw was attributed to faster reaction, increased product formation, and more compact structure[110]. As mentioned in the literature review, alkali-activation with hydroxide solution leads to higher permeability and inclination to efflorescence, when compared to silicate-activated AAMs. This is due to the low extent of reaction reached before hardening, leading to an open microstructure with a mobile alkaline pore solution. [4], [6], [8].

Figure 17. Efflorescence of the samples during the freeze-thaw experiments after 22 freeze-thaw cycles.

6.4 Chemical resistance

Figures 18 and 19 show the effect of NaCl, $MgSO_4$, H_2SO_4, and HCl treatment on the compressive strength of the selected mortars 3M, 6M, 3M-5SF, and 1M-10CO after 14 days and 28-days of curing before submerging, respectively. The mortars submerged in water for 14 days are presented in Figure 20. The reference mortars for 28-day treatment are presented in Figures A33 b and c, A37 b, and A43 b. (Appendix 6).

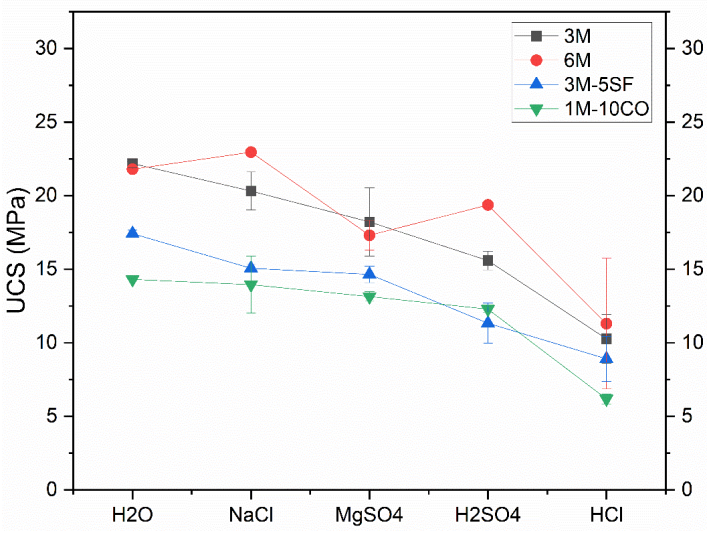

Figure 18. Compressive strength of 3M, 6M, 3M-5SF, and 1M-10CO mortars cured for 14 days and submerged in H_2O, 3 % NaCl, $MgSO_4$, H_2SO_4, and HCl for 14 days.

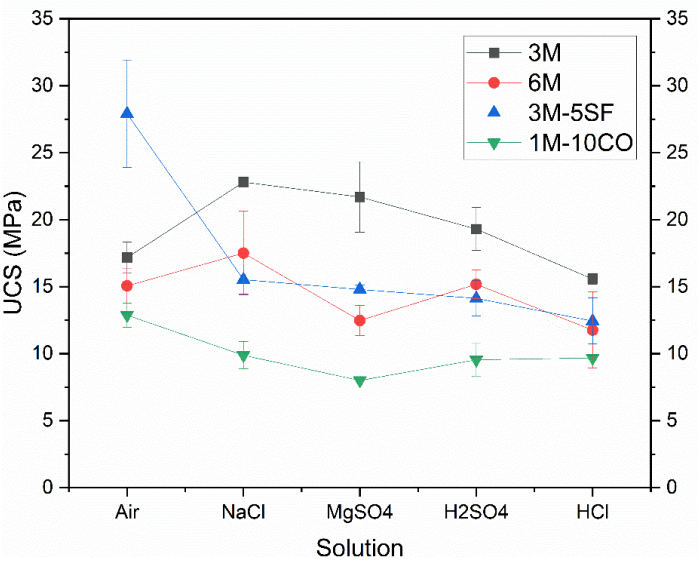

Figure 19. Compressive strength of 3M, 6M, 3M-5SF, and 1M-10CO mortars were cured for 28 days and submerged in 3 % NaCl, $MgSO_4$, H_2SO_4, and HCl for 28 days, where the reference sample was stored in air.

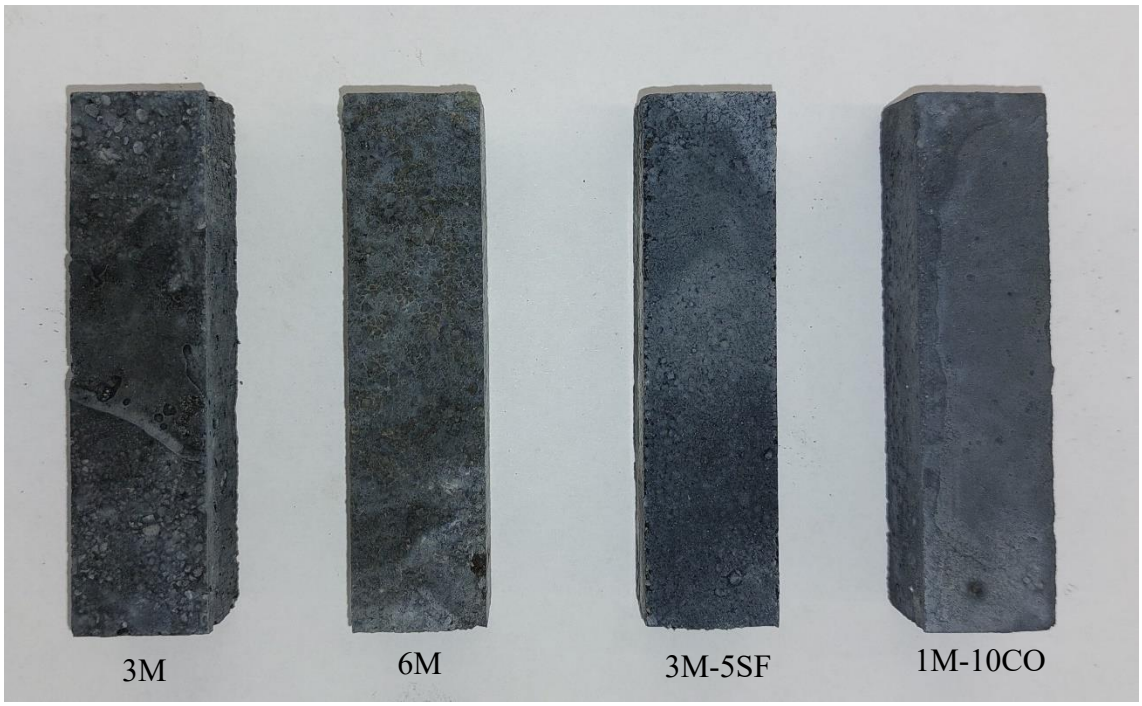

Figure 20. Reference samples submerged in water for 14 days.

6.4.1 NaCl

Figures 21a and 21b show the mortars after treatment in 3% NaCl solution for 14 and 28 days, respectively. No significant visual changes occurred after the applied submersion periods. Compared to the reference sample submerged in pure water, the strength of the samples treated in NaCl did not change significantly. With 3M NaOH-activated mortars, the 14 days submersion decreased slightly the UCS compared to the water submersion. Interestingly, 6M mortar submerged in 3% NaCl for both 14 and 28 days showed a slight increase in UCS. The submersion for 14 days did not affect the UCS of the 1M-10CO mortar compared to the reference mortar.

A more significant increase in the UCS of the 3M sample occurred after the 28-day submersion period compared to the reference mortar that was air cured. The effects were a decrease of 8% and an increase of 33% with 14 and 28 days of treatment, respectively. 28-day submersion led to the increased UCS of the 6M sample, but the increase was not as significant as for the 3M mortar. 6M mortars revealed an increase in UCS by 5% and 16% for 14 and 28 days of the treatment, respectively. The 3M-5SF mortar submerged for 14 and 28 days showed a decrease in UCS. The drop was 13% and 37% with 14 and 28 days, respectively. The decrease was more significant when comparing the 28 days submerged sample and the air-cured reference sample. The UCS was at the same level

after both submersion periods at around 15 MPa. 28-day submersion in NaCl had more a significant decreasing effect compared to the reference mortar. This is probably due to the coarser structure of the mortar. The UCS of 1M-10CO mortars submerged for 14 and 28 days decreased by 2.5% and 23% respectively.

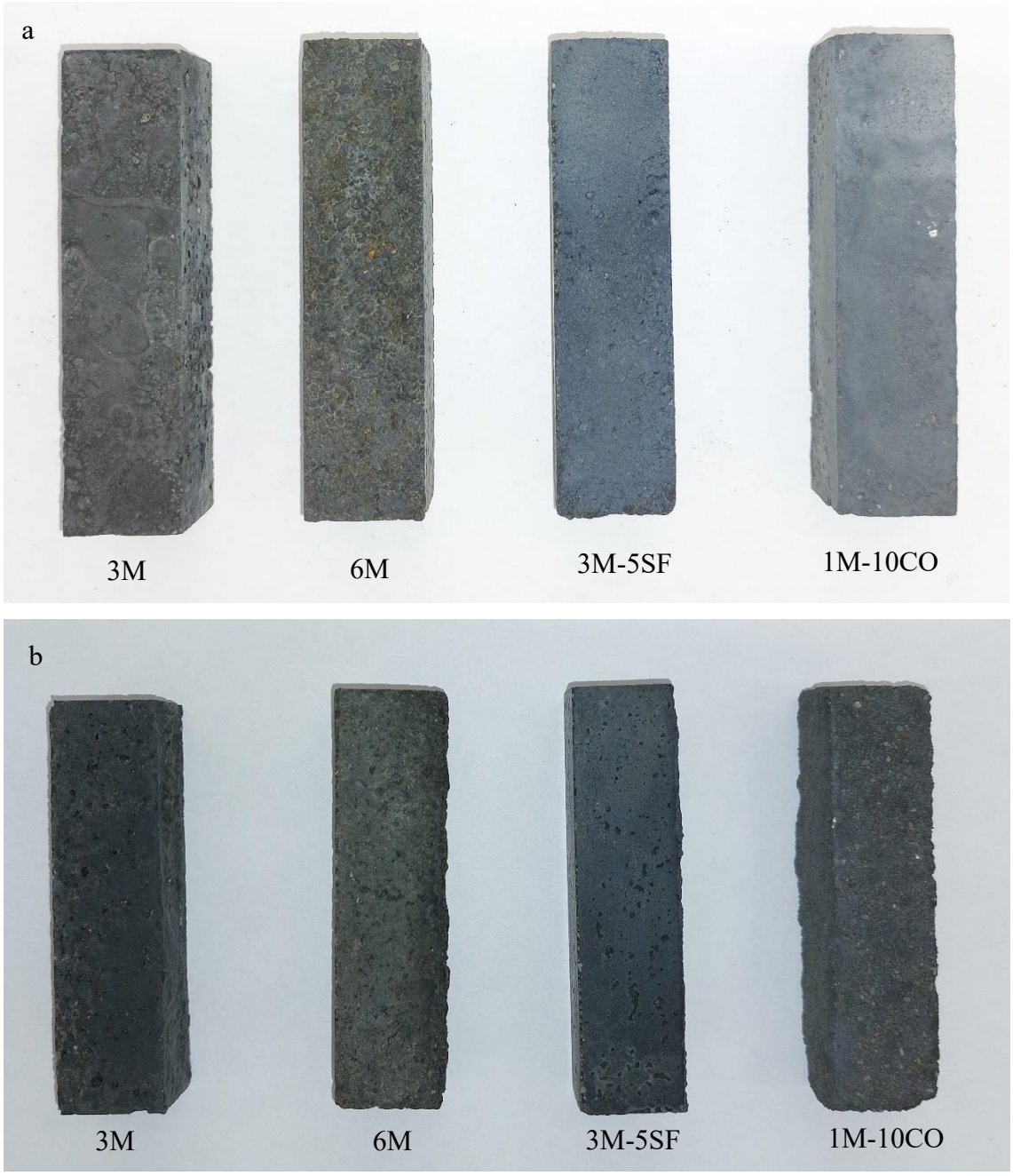

Figure 21. Mortars submerged in NaCl for a) 14 days and b) 28 days.

The UCS of GGBFS mortars activated with sodium silicate solution increased after a 28-day submersion period in the sea water[111]. The similar effects of NaCl treatment on the UCS of the samples of 3M and 6M were observed in the present study. Good

resistance of AAMs to seawater attack was proven by a study where slag and FA/slag mixture AAMs were submerged in seawater for up to 180 days[112]. The resistance of GGBFS mortars to salt water was studied and similar results compared to the present study were obtained. The freshwater submerged sample reached UCS of a 53 MPa and the UCS of the samples submerged in the seawater was 54 MPa[113].

6.4.2 $MgSO_4$

Figures 22a and 22b present the mortars after the submersion in 3% $MgSO_4$ for 14 and 28 days, respectively. All the mortars after both submersion period exhibit significant visual changes that might be explained by efflorescence or metal sulphate formation on a surface, which was most notably visible for the 6M mortars. This is probably due to the highest amount of sodium in the activator solution, thus forming more Na_2SO_4.

The effect of $MgSO_4$ submersion on the UCS of 3M mortars had a small decreasing effect after 14 days of submersion compared to the reference mortar stored in water. A significant increase in the UCS was observed after 28 days of submersion compared to the air-stored reference sample. A decrease of UCS by 18% and an increase of 37% were detected for the samples submerged for 14 and 28 days, respectively. When comparing the UCS of the 28-day samples submerged in $MgSO_4$ and the mortar submerged for 14 days in water, the $MgSO_4$ submersion showed no prominent changes. It appears that the increase in the activator molarity to 6M decreases the $MgSO_4$ resistance of the mortars. With both submersion periods, the UCS decrease was significant for the 6M mortars. The strength of 6M mortars decreased by 20% and 17% for the samples submerged for 14 and 28 days, respectively. 3M-5SF mortar submerged for 14 days showed a slight decrease in UCS. The decrease was similar to when submerged in NaCl for the same duration. As for the submersion period of 28 days, the 3M-5SF showed a significant decrease when compared to the air stored reference sample. The decrease in UCS was 16% and 40% with 14 and 28 days, respectively. The submersion of 1M-10CO mortar for 14 days had no prominent effect on the UCS. For the longer submersion period, the UCS of 1M-10CO decreased. This is probably due to the coarser structure of the mortar. A decrease in UCS by 8% and 38% were observed after 14 and 28 days of the test, respectively.

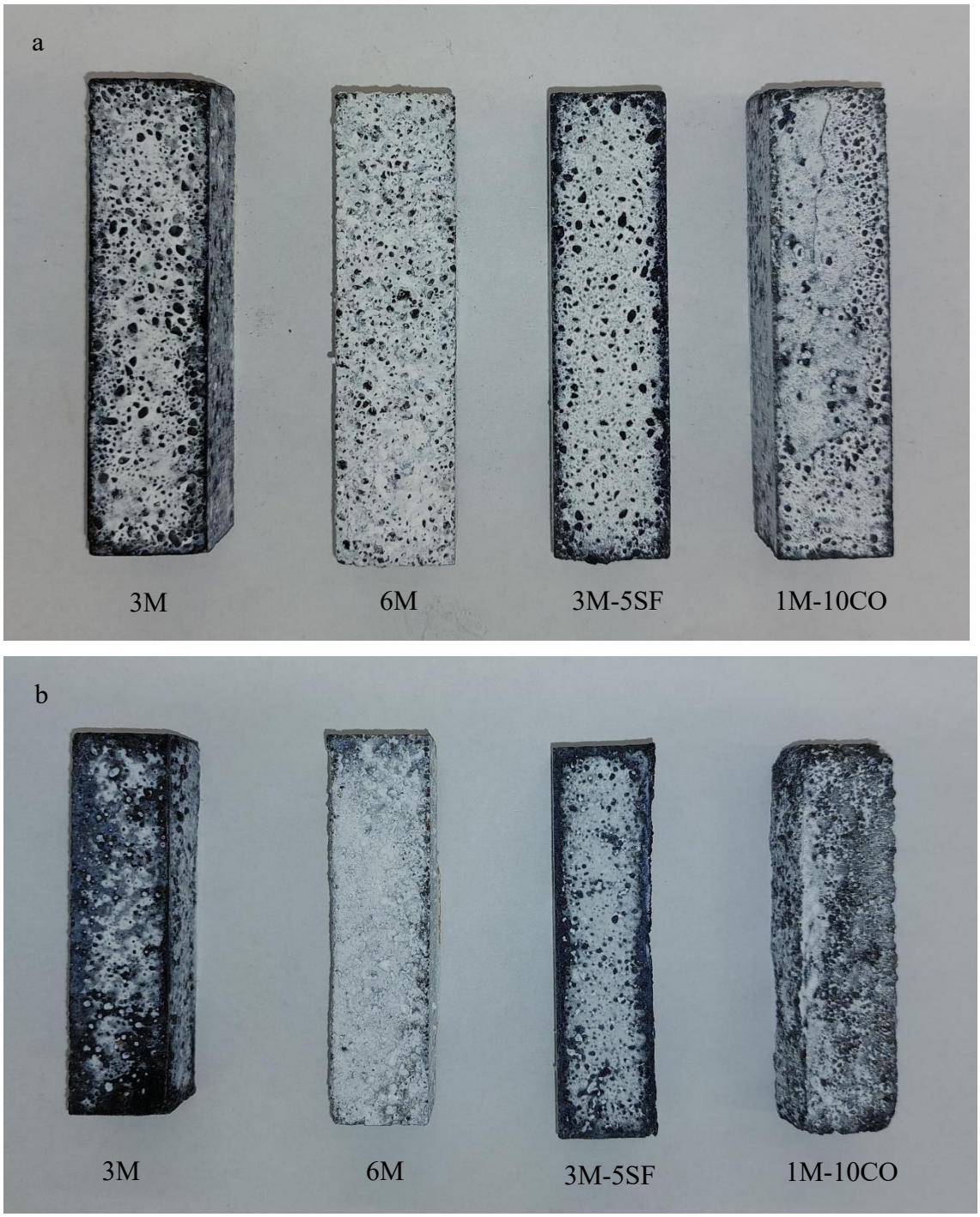

Figure 22. Mortars submerged in $MgSO_4$ for a)14 days and b) 28 days.

GBFS activated with sodium silicate was subjected to a 5% $MgSO_4$ solution for a period of one year [114]. No significant decrease was observed during the first 60 days. The UCS decreased about 10 MPa during the one year. Compared to the OPC reference samples the residual UCS was similar or higher after one year of the exposure. The OPC samples increased in UCS after submersion up to 50 and 120 days. After that, a drastic decrease in strength occurred. After one year the UCS of OPC1, OPC2, and AAM

decreased by 61, 41, and 34%, respectively[114]. In the study, no significant visual changes were observed unlike in the present study. Thus, the $MgSO_4$ causes damage to the AAM structure by diffusion of sulphate ions to the surfaces and thus causes formation and deposition of gypsum or other metal sulphates. This causes expansion and cracking in the structure[66], [114].

6.4.3 H_2SO_4

Figures 23a and 23b present the visual changes of the mortars after immersion in 3% H_2SO_4 for 14 and 28 days. It can be seen from the figures that H_2SO_4 caused some degradation to the mortar surface. During the 28-day submersion period, colour changes occurred on the surface of the mortars. Some losses of UCS occurred for all samples submersed in H_2SO_4 solution for 14 days. However, the longer submersion period slightly increased the UCS of the 3M mortar when compared to the air-stored reference mortar. Consequently, the changes of UCS of 3M sample of air (28 days) and water (14 days) stored references were a decrease by 30% and increase by 12%, respectively. The 6M mortars exhibited better resistance to H_2SO_4 solution than the 3M mortars. The 6M mortars showed a slight decrease in UCS for both submersion periods. The UCS decreased by 11% and increased by 0.8% with a 14- and 28-day submersion period, respectively. H_2SO_4 submersion of the 3M-5SF mortar also decreased the UCS. The 14-day submersion caused a decrease of 35% and the 28-day submersion decreased the strength by 43% compared to the reference mortars. For the 1M-10CO mortar, H_2SO_4 did cause some decrease in UCS after 14 days of submersion. The 28-day submersion, on the other hand, had a more pronounced degradation of the UCS. The decreases in the values were 14% and 26% for the 14- and 28-day submersion periods, respectively.

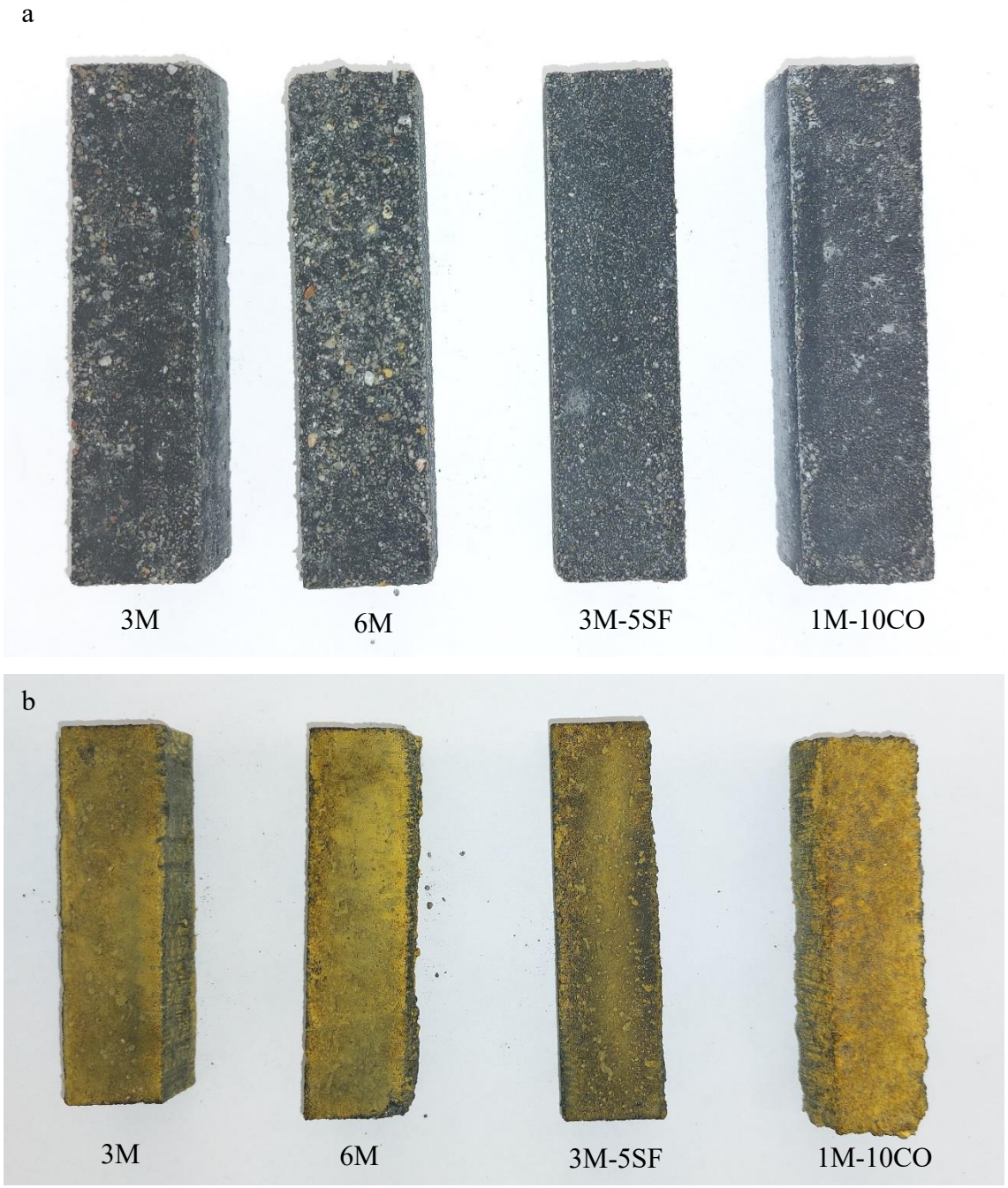

Figure 23. Mortars submerged in H_2SO_4 for a) 14 days and b) 28 days.

The compressive strength of FA-based AAM after the H_2SO_4 submersion of 28, 90, and 365 days decreased by 18, 33, and 52%, respectively[68]. In the present study, the effects of H_2SO_4 on UCS after 28 days of submersion varied, depending on the mortar composition, between an increase of 12% and a decrease of 43%. Note that the use of silica fume and CaO additives showed a decreased resistance of the tested samples to H_2SO_4.

The mixture of GGBFS, FA and glass powder activated with sodium silicate solution with sand as aggregate was exposed to 3% H_2SO_4. FA was replaced with glass powder by 0-40%. The replacement ranging from 10 to 20% performed better compared to the 0% mortar. 30-day submersion led to the decreased UCS of the mortars by 1.25%, 0.75%, and 0.5% with 0, 10, and 20% replacement with glass powder. Increasing glass powder content beyond 20% increased Ca content and decreased resistance to H_2SO_4[115]. Significantly lower resistance was observed in the present study. Similar decreases in UCS were recorded in [115] after 270-365 days. This is probably due to different activator solution.

6.4.4 HCl

Figures 24a and 24b present the visual changes of the mortars after 14 and 28 days of submersion in 3% HCl, respectively. The prominent surface degradation and mass losses were evident for both submersion periods. The surface of the mortars exhibited scaling. The 28-day submersion also caused some colour changes on the surface of the mortar. The effect of HCl submersion on the strength of 3M mortars was significant for both submersion periods. The 14- and 28-day submersion decreased the UCS by 53% and 9% (water-30%), respectively, compared to the water and air reference mortars. A similar trend was shown for 6M mortars with a decrease in UCS of 48% and 22% (water -46%) after 14 and 28 days submerged compared to the reference mortars. UCS of the 3M-5SF mortar decreased by 49% after the submersion of 14 days. 28-day submersion caused a more significant decrease in UCS. The decrease was by 50% compared to the air stored reference mortar and 29% compared to the 14 days water submerged reference mortar. The 1M-10CO showed better resistance to HCl with the longer submersion period. The UCS decreased by 57% and 24% with 14- and 28-day submersion, compared to the reference mortars.

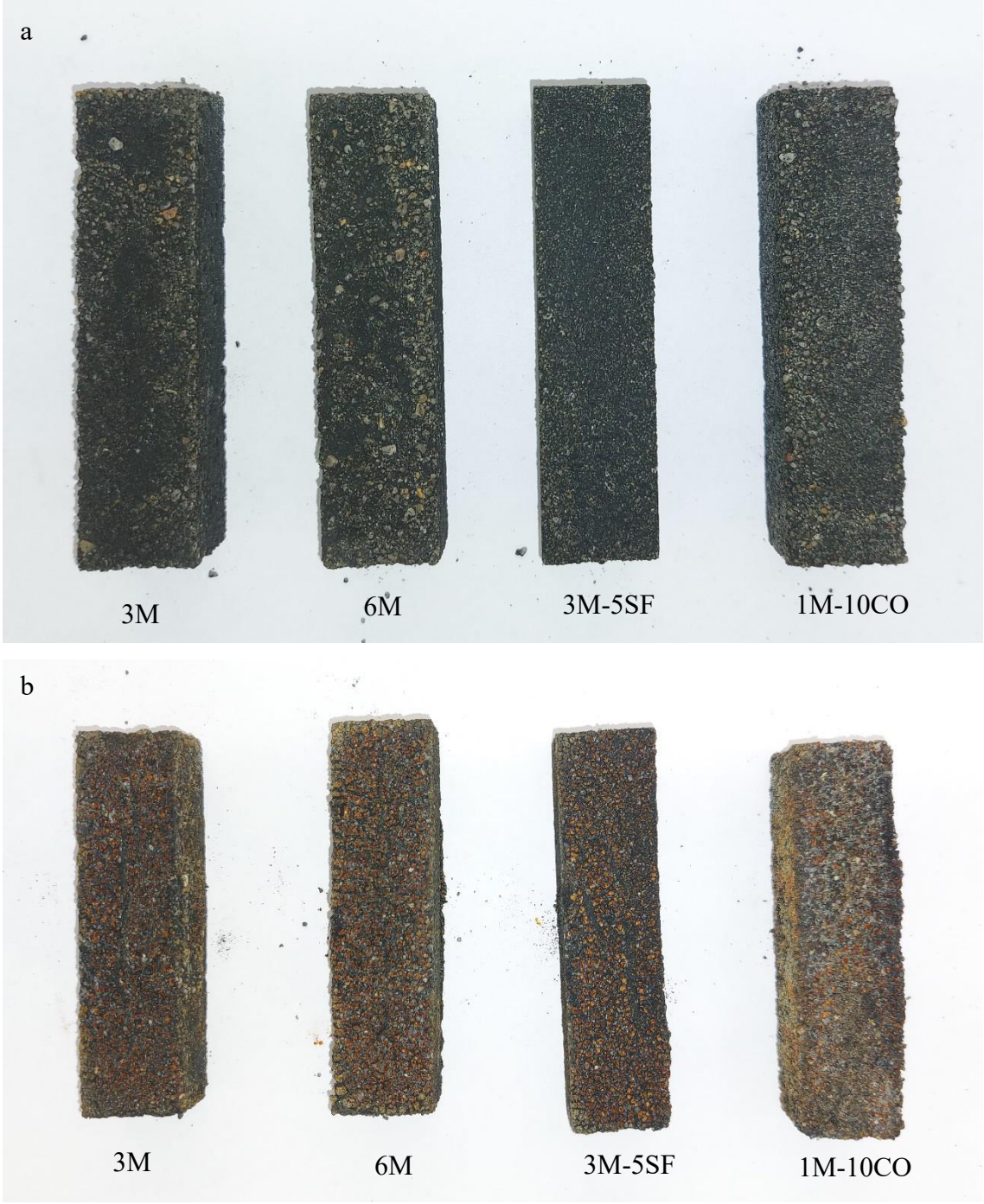

Figure 24. Mortars submerged in HCl for a) 14 days and b) 28 days.

Usually, an HCl attack causes the decomposition of Ca hydration products i.e. C-S-H gel and $Ca(OH)_2$ by forming soluble $CaCl_2$ and water[116]. In the study [115], the authors investigated the resistance of AAM to a 3% HCl solution. The study showed a similar decrease as with H_2SO_4 after 30-day exposure to HCl. The best performing mortar with 20% glass powder lost 12% of its strength after one year of submersion. Decreases in UCS between 1-4.5% has been reported for GGBFS-based AAM activated with NaOH-sodium silicate solution after 28 days exposure to 0.1mol/l HCl[117]. Another study

reported that 28-day submersion in 5% HCl increased the UCS of all mix designs consisting of GGBFS and silica fume activated with sodium silicate-NaOH solution. However, the 90-day submersion caused a decrease in UCS by up to 22%[118]. This shows that including sodium silicate as an activator solution is beneficial to acid resistance of the AAM compared to solely NaOH activation. The use of silicate solution as an activator leads more dense and less porous AAM matrix, thus providing better resistance to acid attacks.

6.4.5 SEM elemental mapping

The samples selected for SEM elemental analysis were air cured 3M, 6M, 3M-5SF, and 1M-10CO; submerged in NaCl 3M, 6M, 3M-5SF, and 1M-10CO; submerged in HCl 3M, 6M, 3M-5SF, and 1M-10CO. Elemental maps for the selected samples are presented in figures 25-28. Elemental levels of Al, Ca, Cl, Fe, Mg, Na, and Si are presented.

Figure 25b shows that the element concentrations in the 3M sample did not change significantly during the NaCl treatment. However, the Cl level was increased only within the gel (reaction product), the Cl penetration did not occur within the initial glassy slag particles. Interestingly to note that NaCl treatment also led to the removal of Na.

The treatment with 3% HCl led to a complete disappearance of Ca and Na, while the Cl level was drastically increased within both the gel and the slag particles. The reduction in the content of Ca and Na, along with Al, led to a relative increase in the Si and Fe contents.

Fe is mainly located in the unreacted slag particles in Figures 25a and 25b. But after the submersion in HCl Fe can be seen in the gel phase, suggesting that HCl dissolved additional Fe from the slag particles and this dissolved Fe was dispersed through the gel phase after submersion in HCl.

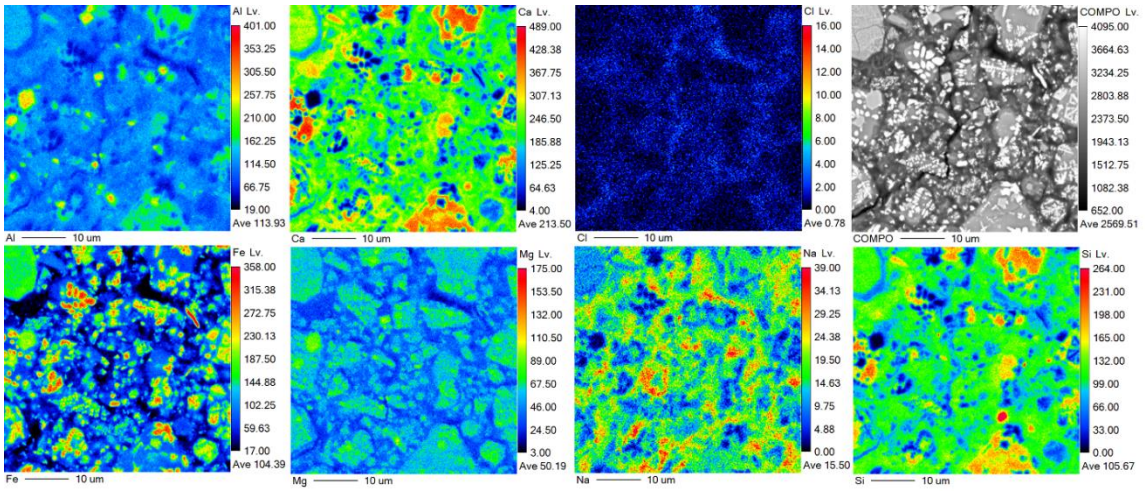

a

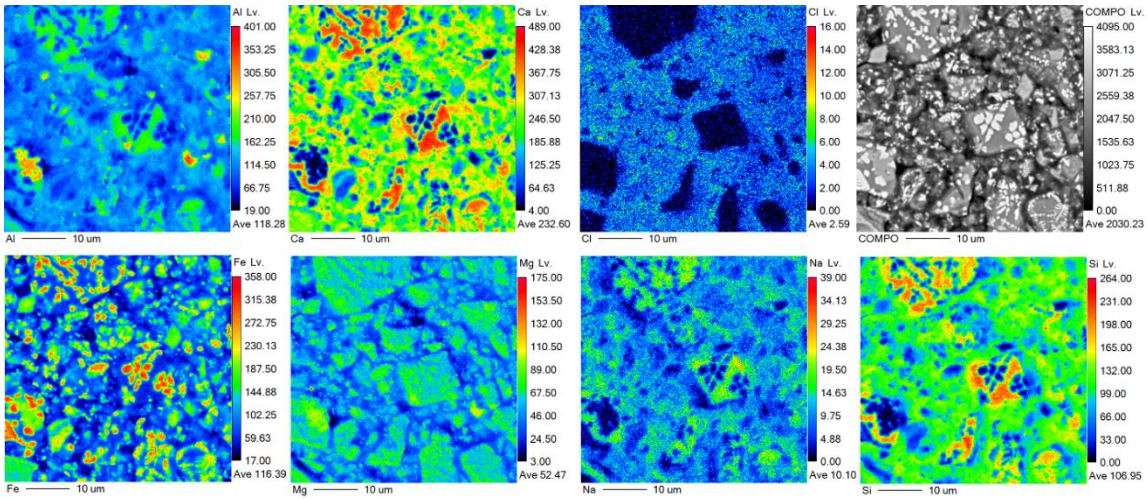

b

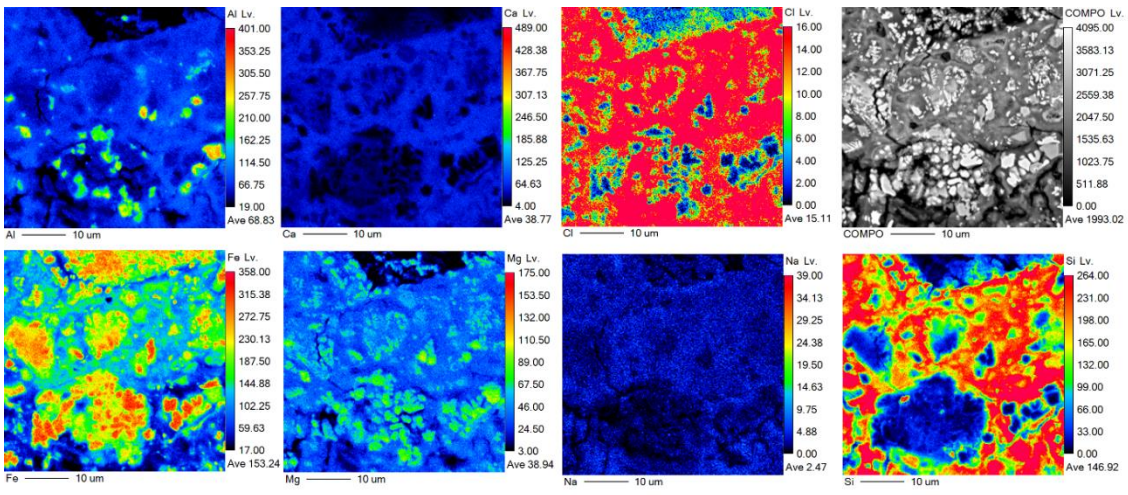

c

Figure 25. Elemental mapping of the alkali-activated slag samples with 3M with a) air cured, b) 3% NaCl and c) 3% HCl solutions.

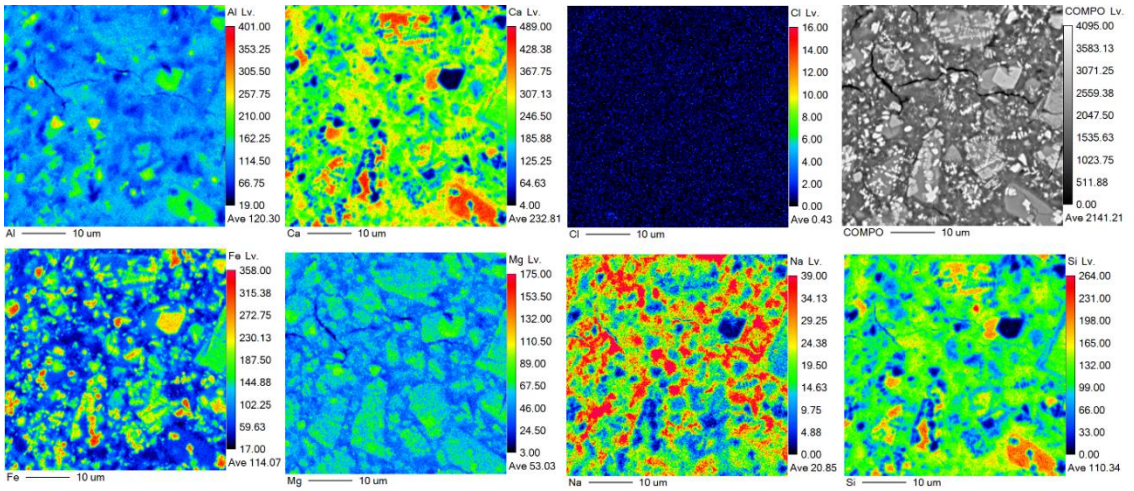

a

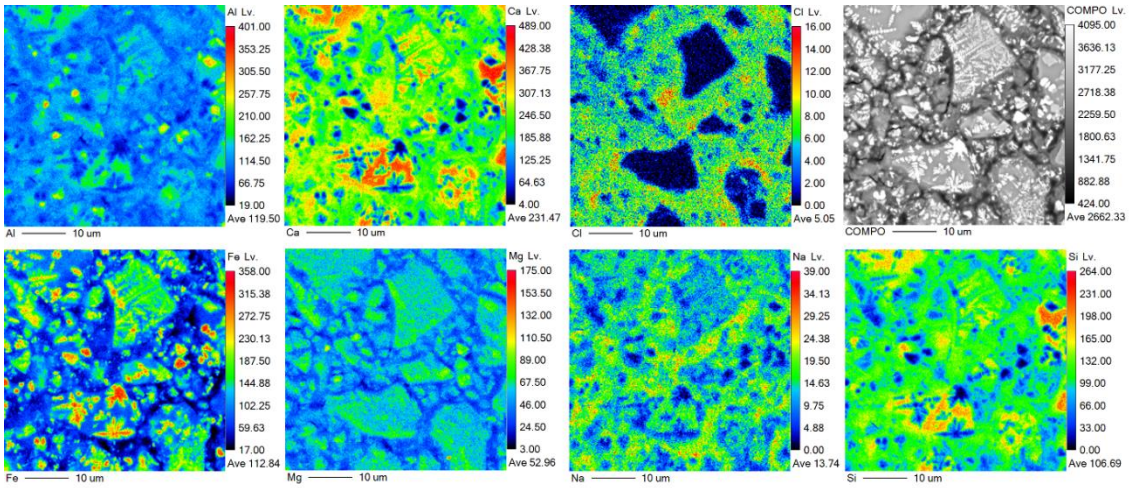

b

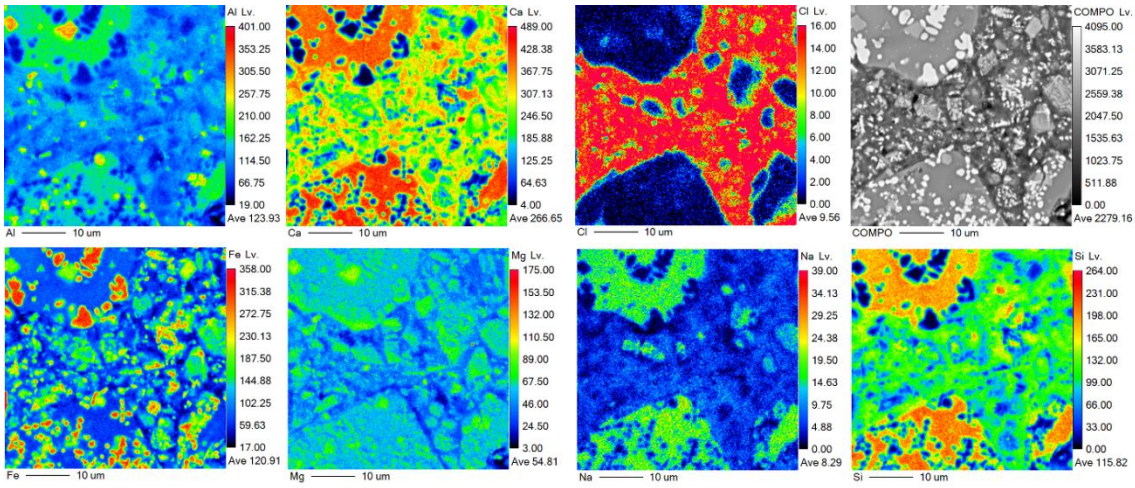

c

Figure 26. Elemental mapping of the alkali-activated slag samples with 6M with a) air cured, b) 3% NaCl and c) 3% HCl solutions.

For the 6M sample, the Al content did not exhibit a decrease after submersion in HCl. Unlike with 3M HCl, the submersion in HCl did not dissolve Ca from the 6M sample. This is probably due to the higher cornet of available Na in the sample that reacts with HCl faster. Similarly, as with the 3M sample, the Cl penetration occurred in the gel phase with NaCl submersion. The HCl submersion caused significantly more vigorous Cl penetration and resulted in some damage to the slag particles like in the case of the 3M sample. As can be seen from Figures 26a-c Fe is mainly located in the unreacted slag particles. The HCl submersion did not cause Fe dissolution from the slag particles like in the case of the 3M sample. NaCl submersion decreased the amount of Na in the gel phase. Interestingly, from Figure 26c, it can be observed that Na is located in the slag particles rather than in the gel phase. Si is observed in the slag particles and the gel phase in the air cured and submerged in NaCl samples.

The sample activated with 3M NaOH and 3% of silica fume and treated in NaCl solution showed a slight decrease in the content of Cl within the gel. This seems to be correlated with the Na content. In the treatment with HCl, the removal of Ca and Na occurred from both the slag and the gel particles. This led to a relative increase in Fe content within the glassy slag particles and Si within the gel.

In particular, Cl penetration occurred after NaCl submersion quite uniformly in the gel phase. Figure 27a shows that Cl penetration is more significant in areas where cracks occur. HCl submersion causes slag particle dissolution and severe Cl penetration of the gel phase. The gel phase of the 3M-5SF sample after NaCl submersion was rich in Na. The opposite was observed with 3M and 6M samples after submersion in NaCl solution. The HCl submersion, on the other hand, dissolved all the Na to the solution. This is supported by the ternary diagram presented in Figure 27b, where the HCl submersion caused a decrease in the Na content compared to the air-cured and NaCl-submerged samples. The Si structure of the gel phase was uniform after NaCl submersion with some areas with higher Si content.

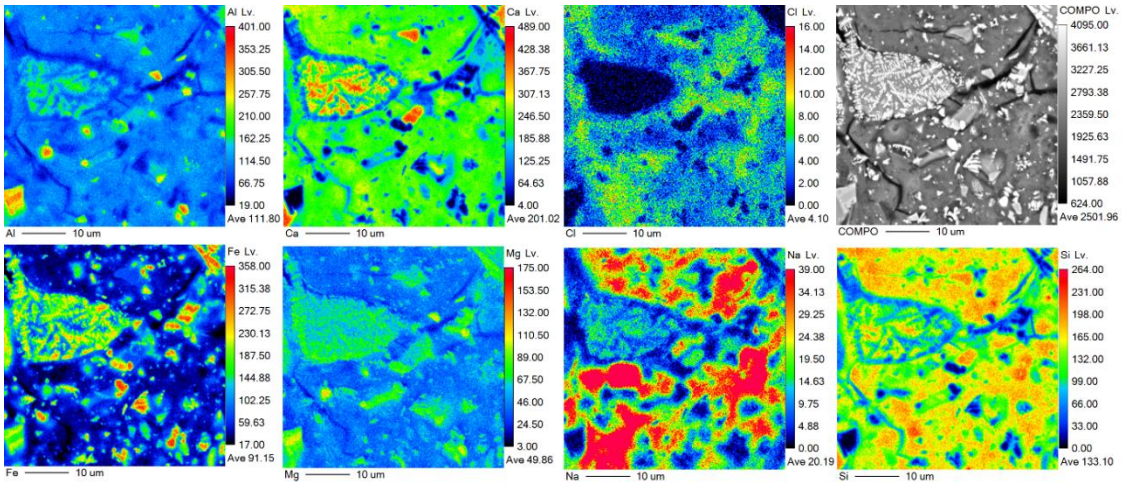

a

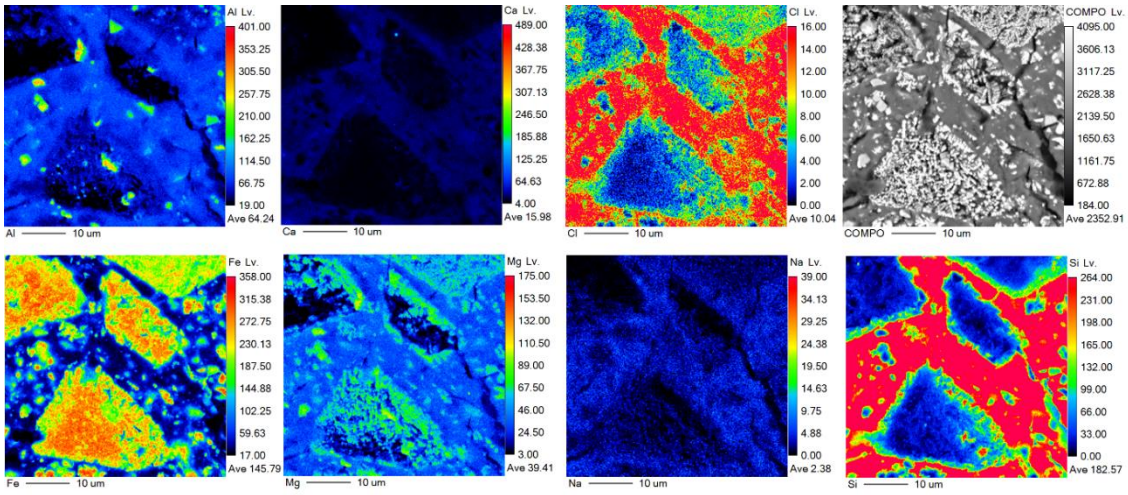

b

Figure 27. Elemental mapping of the alkali-activated slag samples with 3M-5SF with a) 3% NaCl and b) 3% HCl solutions.

The levels of Al in the 1M-10CO after NaCl submersion are uniform and low. In the HCl submerged sample, Al is present in unreacted particles. As for the previous samples, the HCl submersion caused Ca dissolution. In the case of NaCl submersion, Ca is uniformly spread in the sample. For 1M-10CO, the Cl penetration was most significant among the samples after NaCl submersion. HCl submersion caused the particles damage and significant Cl penetration. Fe was dissolved from the slag particles after the HCl submersion. NaCl submersion did not affect Fe. Mg was observed in the slag particles and not in the gel phase after HCl submersion. Na content of the gel phase was low after submersion into NaCl solution. It can be seen from Figure 28a, that Na is located in the slag particles as well. Figure 28b shows that after HCl submersion most of the Na is in the gel phase. Similar to the other samples, the Na content significantly dropped after

submersion in HCl, as seen in Figure 28b. In the case of Si, it can be observed that after NaCl submersion the slag particles are the main locations with Si, suggesting low Si, but high Ca binder composition. After HCl submersion, it can be seen from Figure 28b that Si is unevenly spread in the gel phase and not in the slag particles.

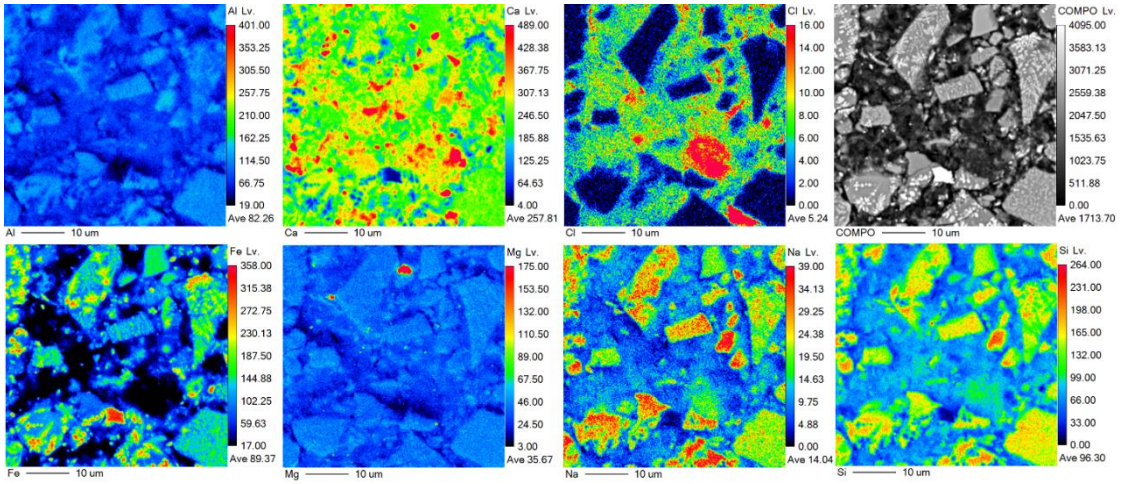

a

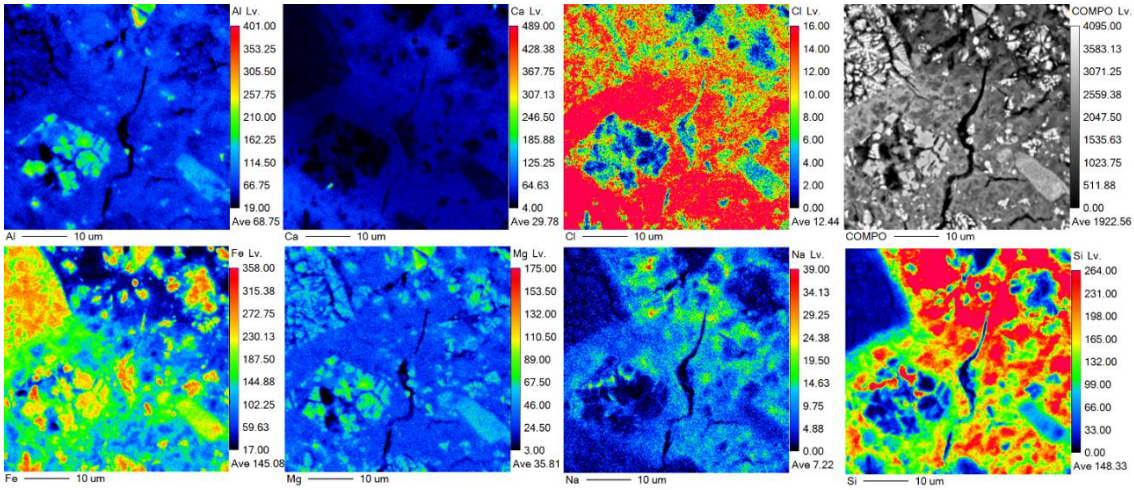

b

Figure 28. Elemental mapping of the alkali-activated slag samples with 1M-10CO with a) 3% NaCl and b) 3% HCl solutions.

Figures 31-34 present a ternary diagram of the samples with different components before and after treatments in NaCl and HCl solutions. The points selected for chemical analysis were mostly from the gel phase with some points in particles that were selected to determine their composition. The gel phase changes are well correlated with the elemental maps in Figures 25-28.

Figure 29a shows that the points only slightly shifted to the area with lower Ca and higher Si contents after treatment with NaCl. When treated with HCl, the points change their position to high Si and low Ca areas. Also, treatment with NaCl slightly increased the content of Cl, while HCl samples exhibited high Fe and Cl, but low Na contents (Figure 29b). From Figure 29d, it can be observed that the treatment of the sample with HCl increased the content of Fe, despite the variable contents of Si and Ca.

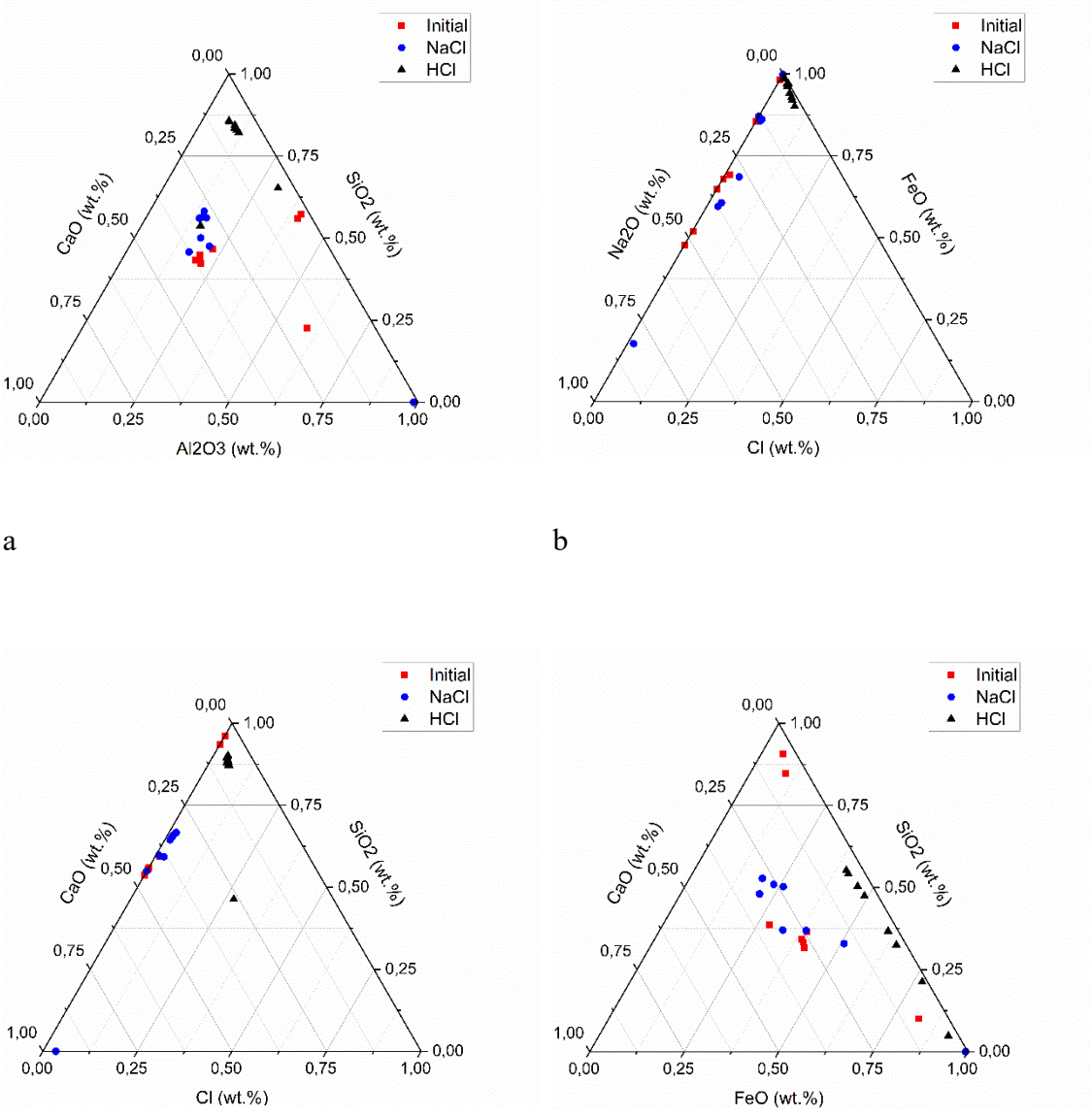

a b

c d

Figure 29. Ternary diagrams of 3M sample with a) Al_2O_3-SiO_3-CaO, b) Cl-FeO-Na_2O, c) Cl-SiO_2-CaO, and b) FeO-SiO_2-CaO.

Figure 30a shows that the ratios between Ca, Si, and Al did not change significantly during the salt and acidic tests. However, Figure 30c indicates that the content of Cl was slightly increased in the row: initial sample → NaCl → HCl. In contrast to other samples, the content of Ca was still high for the HCl-treated samples. This is probably due to the higher content of available Na bonding the Cl. Besides, Figure 30d shows a minor increase in the content of Ca from the initial to HCl-treated samples.

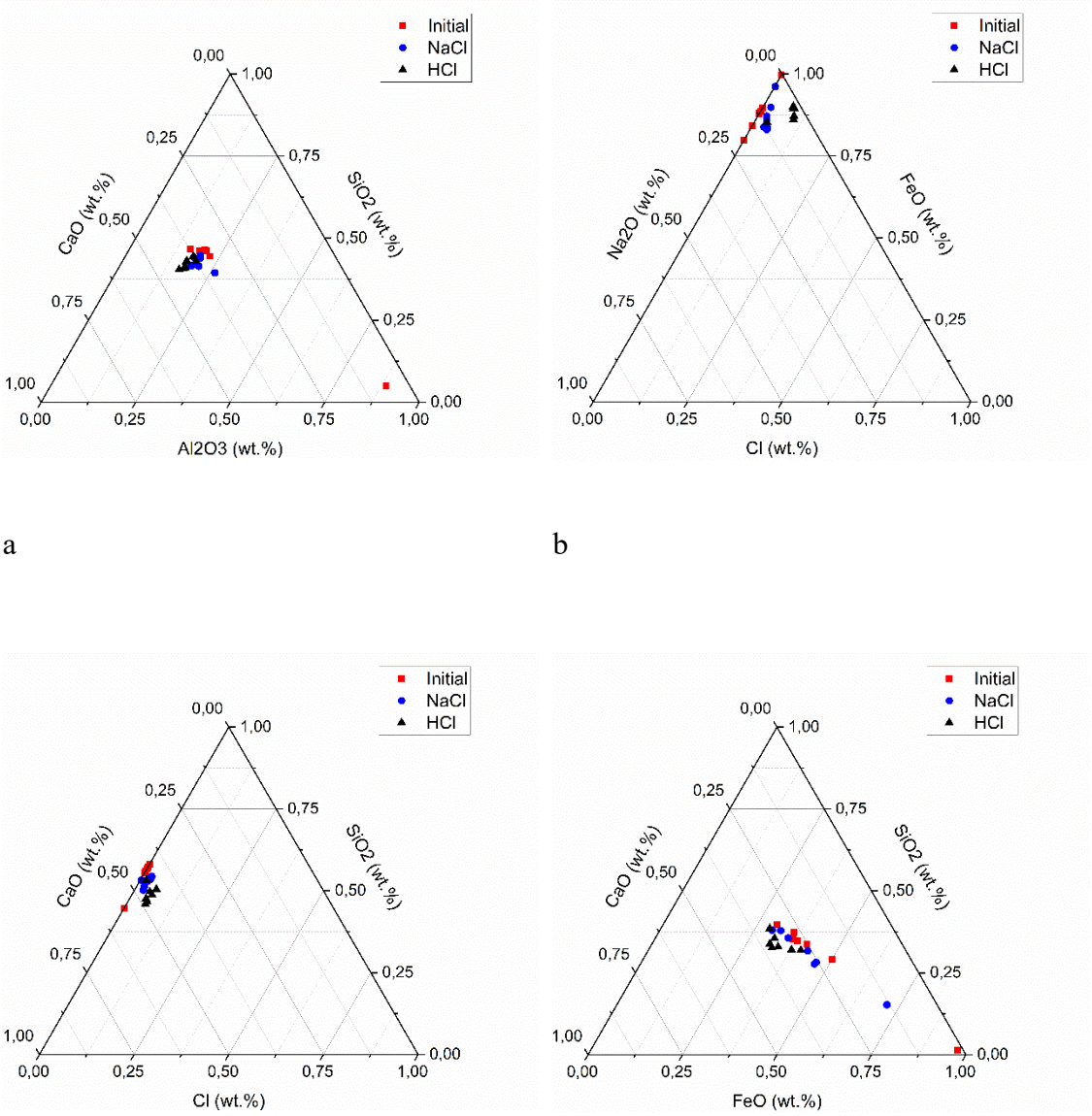

Figure 30. Ternary diagrams of 6M sample with a) Al_2O_3-SiO_3-CaO, b) Cl-FeO-Na_2O, c) Cl-SiO_2-CaO and b) FeO-SiO_2-CaO.

A very similar behaviour can be attributed to the 3M-5SF sample (Figure 31) as it was for the sample 3M (Figure 29). This indicates that the molarity of the solution, but not the silica content, was the main factor affecting the chemistry of the test.

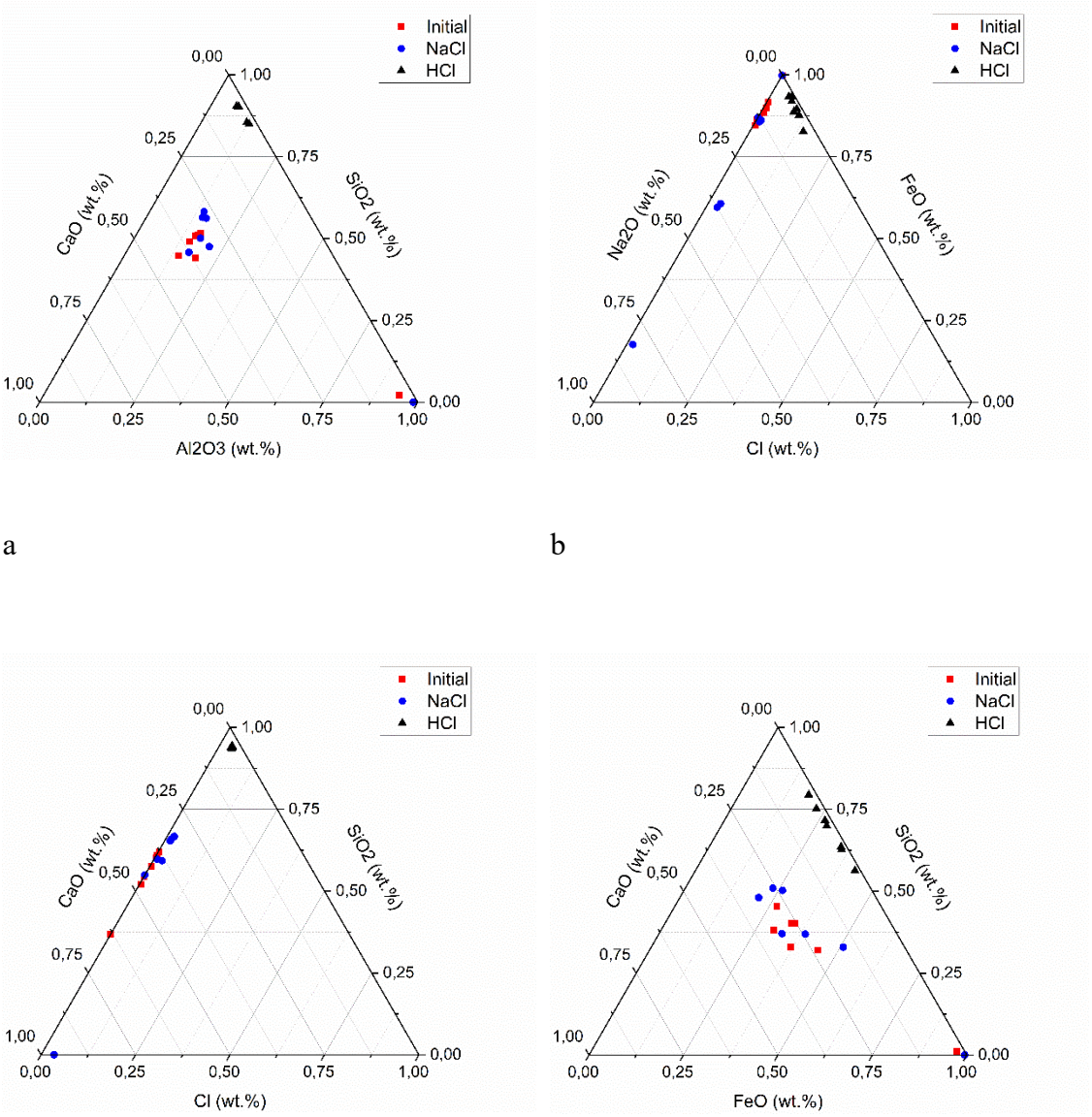

Figure 31. Ternary diagrams of the 3M-5SF sample with a) Al_2O_3-SiO_3-CaO, b) Cl-FeO-Na_2O, c) Cl-SiO_2-CaO and b) FeO-SiO_2-CaO.

The different chemical behaviour is present in Figure 32 for the 1M-10CO sample. The treatment of the sample with HCl led to a prominent shift of the data points to the area with low Ca and high Si contents. The penetration of Cl is more evident for NaCl samples

compared to the initial sample (Figure 32b). An increase in Cl and a decrease in Na contents can be attributed to the HCl-treated samples.

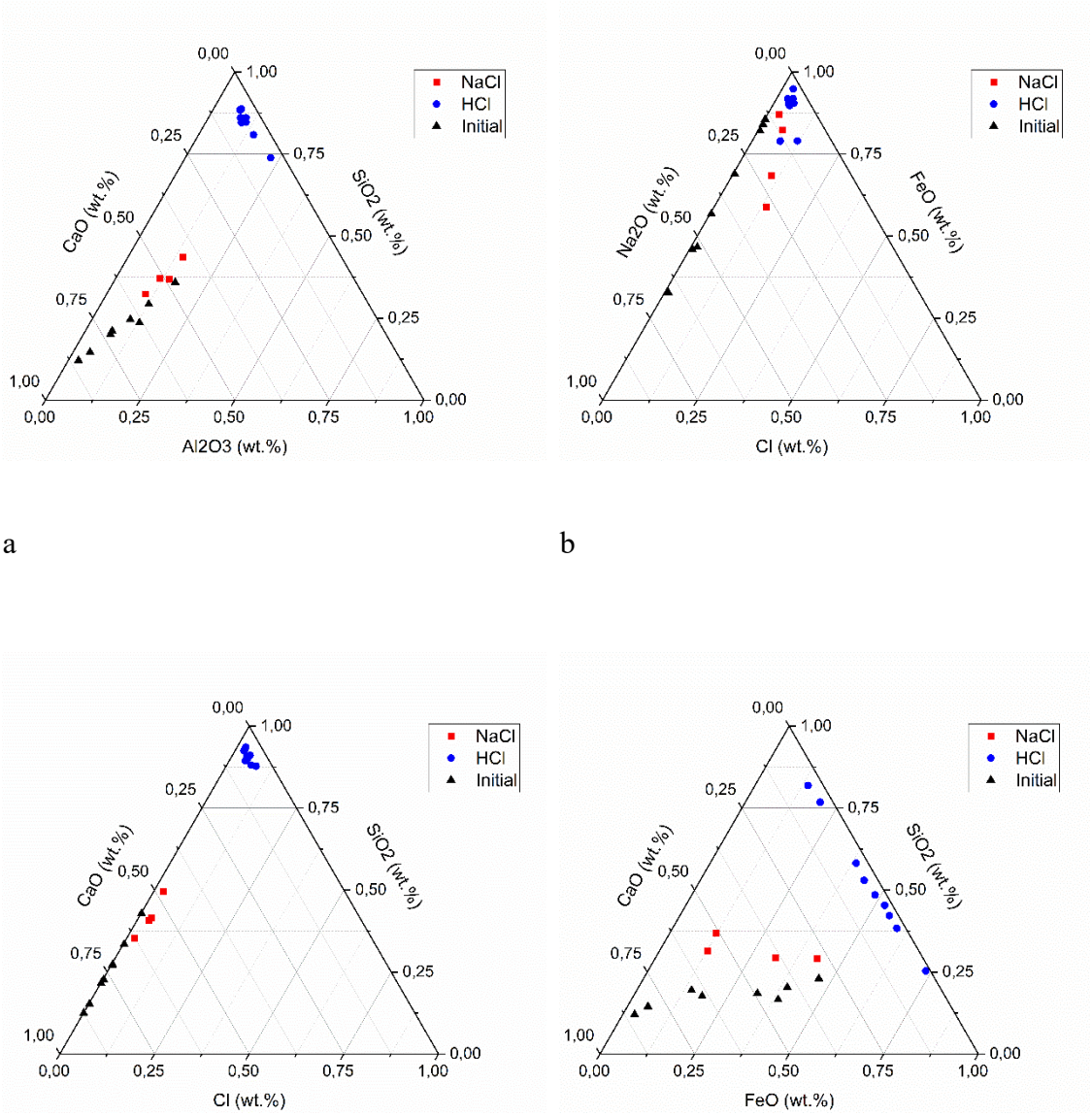

Figure 32. Ternary diagrams of 1M-10CO sample with a) Al_2O_3-SiO_3-CaO, b) Cl-FeO-Na_2O, c) Cl-SiO_2-CaO and b) FeO-SiO_2-CaO.

A quantitative analysis of the penetration of Cl is summarized in Table 2. The penetration was determined by measuring Cl content at various points near the exposed surface. Air-cured reference samples exhibited a low amount of Cl < 0.03 wt.%. The submersion in NaCl solution caused some Cl penetration, but the average Cl content was still below 1 wt.%. The lowest amount of Cl was observed in the 3M sample and the highest in 1M-

10CO. The HCl submersion caused more severe Cl penetration. Similar Cl content was observed with 3M, 6M, and 3M-5SF samples with 1.8 wt.% of Cl. 1M-10CO showed slightly lower Cl content with 1.5 wt.%. The chemical point analysis supports the results obtained from the elemental maps that are presented in Figures 27-30. In another study, NaCl treatment increased the amount of bound Cl increased from 0.004% to 0.059% when comparing the humidity chamber and the sea water submerged samples, respectively[111].

Table 2. SEM-WDS quantification of the Cl penetration for the samples' borders: an average Cl content from the measured points (number of points).

Sample	Air cured avg Cl wt.%	NaCl avg Cl wt.%	HCl avg Cl wt.%
3M	0.028 (13 points)	0.256 (3 points)	1.831 (8 points)
6M	0.007 (8 points)	0.514 (8 points)	1.834 (7 points)
3M-5SF	0.082 (7 points)	0.454 (10 points)	1.849 (8 points)
1M-10CO	0.078 (8 points)	0.755 (4 points)	1.526 (9 points)

Ca disappearing from the samples 3M, 3M-5SF, and 1M-10CO after HCl submersion might be explained with the formation of $CaCl_2$ that is easily soluble. The behaviour is different for the 6M sample. Considering the higher content of available Na, this can be interpreted as consumption of SO_4 with sodium to form sodium sulphate. This suggests that the process of combining Na and SO_4 is much faster than that for Ca and SO_4. The relative increase of Si in the samples is mainly attributed to the Ca content dropping.

In the 1M-10CO sample, the high content of Na in slag particles suggests that 1M NaOH exhibits a low dissolution rate. HCl submersion made Na more mobile, this was observed within the slag particles as well as seen in Figure 30 b. In Figures 27 and 28, the disappearance of Na from 3M and 6M samples after HCl treatment could be due to the dissolution and formation of salts.

When the content of Na is lower, HCl attack causes the decomposition of Ca-bearing hydration products i.e., C-S-H gel and $Ca(OH)_2$ by forming soluble $CaCl_2$ and water[116]. Similarly, the sulphate attack may lead to the conversion of Ca hydrated reaction products into Ca-sulphates and calcium-sulpho-aluminates deposited on the mortar surface, where it is easily dissolved[68].

As can be seen from figures 27-30, the HCl treatment caused damage to the unreacted slag particles. In the case of 1M-10CO, the Fe dissolved from the slag particles increased the Fe content of the gel phase. A similar effect was observed with the 3M sample. It could be explained by the dissolution of Fe by HCl forming $FeCl_2$ or $FeCl_3$ that were absorbed by the gel phase.

6.4.6 Leaching

1M-10CO, 3M-5SF, 3M NaOH, 6M NaOH, 3M-5SF NaCl, 3M-5SF $MgSO_4$, 3M H_2SO_4, 3M-5SF HCl, M-20C (sodium silicate activated mortars), and BJA012 (initial slag sample) were subjected to leaching tests according to SFS-EN 12457-2. One stage batch test at a liquid to solid ratio of 10 l/kg for materials with particle size below 4 mm (without or with size reduction)[119]. Table 3 presents the leaching results of the samples and the of the "Upper limit for roadway waste layer thickness ≤ 1.5 m" according to the Finnish construction act.

Table 3. Leaching of harmful elements from the test samples

Measured elements *[mg/kg]*	**1M-10CO**	**3M-5SF**	**3M-5SF NaCl**	**3M-5SF MgSO4**	**3M-5SF H2SO4**	**3M-5SF HCl**	**3M NaOH**	**6M NaOH**	**initial slag**	**M-20C**	**Upper limit for roadway waste layer thickness ≤ 1.5 m**
pH	12,30	12,14	11,64	11,55	9,72	8,88	12,02	12,32	10,07	12,59	
conductivity [mS/cm]	6,75	5,09	2,888	2,058	3,02	1,908	4,415	8,994	0,11	20,36	
As	<0,01	0,72	0,33	0,30	0,03	0,04	0,46	0,82	0,13	2,25	2,00
Ba	59,00	0,06	<0,06	<0,06	1,50	1,10	0,07	<0,06	1,2	0,339	100,00
Cd	<0,002	<0,002	<0,002	<0,002	<0,002	<0,002	<0,002	<0,002	<0,002	<0,002	0,06
Cr	0,03	0,15	0,04	0,03	<0,01	<0,01	0,11	0,34	<0,01	0,019	10,00
Cu	0,03	0,04	0,04	0,01	<0,01	<0,01	0,02	0,02	0,11	0,267	10,00
Mo	4,0	23,0	3,3	4,4	9,2	6,3	19,0	23,0	0,095	8,1	6,00
Ni	<0,01	<0,01	<0,01	<0,01	<0,01	<0,01	<0,01	<0,01	0,012	0,014	2,00
Pb	0,005	<0,004	<0,004	<0,004	<0,004	<0,004	0,006	<0,004	0,06	<0,004	2,00
Sb	0,04	2,70	2,40	2,00	0,92	1,20	1,60	2,40	0,094	2,44	0,70
Se	<0,04	0,08	<0,04	<0,04	<0,04	<0,04	0,07	0,08	<0,04	0,22	1,00
V	<0,01	11,00	5,70	5,70	0,66	0,44	5,20	8,90	0,065	2,61	3,00
Zn	<0,04	<0,04	<0,04	<0,04	<0,04	<0,04	0,14	<0,04	0,29	0,18	15,00
Hg	<0,004	<0,004	<0,004	<0,004	<0,004	<0,004	<0,004	<0,004	<0,004	<0,005	0,03
DOC	1200	1700	760	680	670	590	1900	1400	<1	1,4	150,00
F	<10	<10	<10	<10	<10	14	<10	<10	89	55	11000,00
Cl	<50	<50	1600	<50	<50	5500	<50	<50	55	439	18000,00
SO4	1300	190	110	960	18000	200	180	150	1900	620	500,00
TDS	15000	16000	13000	8500	25000	11000	14000	25000	2000	13006	

It can be seen from Table 3 that As leaching slightly exceeds the upper limit for roadway waste. This is not observed with NaOH-activated mortars in the present study. The increase of NaOH molarity from 1 to 6 M slightly increases As leaching. Another observation is that acid treatment of the mortars significantly decreases As leaching. Ba leaching is far below the limits, but for 1M-10CO, a significantly higher value compared to the other mortars was observed. Mo leaching for sodium silicate activated mortar is considerably higher than in NaOH activated mortars. The use of lower molarity of NaOH with CaO additives lowers the Mo content in the leachate. Interestingly, the salt solution treatment lowers the Mo leaching levels below the upper limit of roadway waste. The use of 1M NaOH and 10% CaO decreases the Sb leaching. Se leaching levels are drastically lower in NaOH activated mortars than in sodium silicate activated. V leaching values are much lower in 1M-10CO and acid-treated mortars. From 3M and 6M mortars, it can be seen that increase in NaOH molarity increases V leaching.

Leaching of AAM obtained from FA and GGBS activated with NaOH and sodium silicate solution was studied [120]. Two AAMs with different ratios of FA/GGBS and NaOH molarity were produced. Mo leaching reported 28.3 and 1.1 mg/m^3 are similar to lower and higher values obtained for the mortars in the present study. Sb leaching was commonly higher in the present study only the 1M-10CO sample showed significantly lower Sb leaching. Se leaching from the mortars in the present study was significantly lower compared to the FA/GGBS mortars. Also, mortars with more FA showed significantly higher V leaching[120].

7. CONCLUSIONS

In this work, alkali-activation of Fe-rich non-ferrous metallurgical slag with low and high molar NaOH solutions was studied. Previous literature about the topic is scarce and this study was conducted to shed more light on the subject. In addition to alkali solution, the effect of common mineral additives, such as CaO, MgO, $Ca(OH)_2$, and amorphous SiO_2 was evaluated at low and high NaOH molarities. Also, the durability and chemical stability of the produced mortars were studied with a freeze-thaw test and using sulphate, chloride salts, and acids solutions. The main results of the work can be summarized as follows:

1. The effect of different molarity of NaOH activation solution was evident. An increase of the activator molarity from 1 to 3 increased the UCS of the produced mortars significantly. Increasing the activator molarity above 3M did not increase the UCS of the mortars significantly. XRD analysis of pastes explains the better performance of activator molarities of 3 and above with the formation of iron and calcium silicate hydrated products. Also, increasing the activator solution molarity led to a more heterogeneous microstructure of the reaction product formed.

2. Despite the similar nature, the effect of $Ca(OH)_2$, CaO, and MgO on the compressive strength and the reaction products was drastically different. $Ca(OH)_2$ and MgO did not enhance the UCS at low molarities of the NaOH. $Ca(OH)_2$ did not affect UCS with any dosage studied with 1 and 3M solutions. However, mortars with 6M activator solution and $Ca(OH)_2$ revealed a moderately increased UCS for all dosages. The most prominent increase of UCS was observed with 6M-10% $Ca(OH)_2$. MgO had a mainly decreasing effect on UCS with a 3M activation solution for all MgO dosages. A slight increase in UCS was observed with a 6M activation solution. The slag replacement with CaO enhanced the mechanical properties of the produced mortars with 1 and 6 M NaOH activators. The enhancement was more significant with 1M solution due to katoite formation observed by XRD for 10% replacement of slag with CaO.

3. The addition of amorphous SiO_2 (i.e., silica fume) increased the mechanical properties of the produced mortars significantly. The only exception was the addition of 5 wt.% of silica fume to 1 M activated mortars, which led to a complete loss of UCS. 3M and 6M

activated mortars showed almost a double increase of UCS with 5 and 10 % slag replacement with silica fume. From XRD and FT-IR results, it can be suggested that silica fume is not reactive/soluble in low molar NaOH solution (below 3M NaOH). Note that silica fume addition caused some workability issues and thus a higher solution to binder ratio was used.

4. Durability of the produced mortars was studied with freeze-thaw tests and chemical attacks. The freeze-thaw resistance of the mortars carried out for 60 and 120 cycles was observed to be poor, and the best compositions remain solid only up to 60 cycles. The poor performance of the produced mortars against freeze-thaw cycles could be attributed to a high content of Na leading to efflorescence and porosity development. Chemical resistance was studied by treating the mortar samples with 3% solutions of NaCl, $MgSO_4$, H_2SO_4, and HCl for 14 and 28 days. The submersion of the samples in NaCl solution led to a minor increase in the UCS of the mortars without additives. The mortars with CaO and silica fume additives showed a slight decrease in their UCS after NaCl treatment. In contrast, $MgSO_4$ treatment led to a moderate degrading effect on the UCS of all mortars and the deposition of the metal sulphate salts on the mortar's surface. The produced mortars showed weaker resistance to acid treatment. Visual deterioration of the surface was observed in all cases. HCl treatment had a more severe effect on the mortar surface and UCS compared to H_2SO_4. SEM elemental mapping showed that HCl treatment dissolved almost all of the Ca from the AAM matrix.

8. SUMMARY

The worldwide increasing urbanization needs more and more materials to accommodate the increasing demand. One of the most used building materials is concrete. The CO_2 emissions from concrete production is ranging from 5 to 8% of the global CO_2 emissions. In the continuing global warming, more sustainable options for concrete are needed. Alkali-activated materials could be the solution for making concrete materials as a more sustainable alternative. The goal of this study was to produce alkali-activated material from iron-rich slag precursor with different additives without commercial alkali silicate activation solution and asses the mechanical and durability properties of alkali-activated materials.

This thesis is comprised of a literature review and an experimental part on the study of the production and testing of alkali-activated material. In the literature review, circular economy and climate effects in the construction sector are studied. The main principles of alkali-activated materials are reviewed in regard to common precursors, activators, additives, and properties. The experimental part of the present work focused on the production of alkali-activated material from iron-rich slag obtained from zinc production. The activation solution used was NaOH with different molarities. Four different admixtures $Ca(OH)_2$, CaO, MgO, and silica fume were used in different quantities. Compressive strength, XRD and FT-IR analysis, freeze-thaw resistance, chemical resistance, and microstructure of the produced materials were studied.

The results indicate that increasing the molarity of the NaOH activation solution does not necessarily increase the mechanical properties of the material. Increasing the molarity over 3 did not show a significant increase in the compressive strength. It was found that different additives enhanced mechanical properties due to different mechanisms. From the list of additives used, $Ca(OH)_2$ and MgO showed minor decreasing or increasing effects on the material's mechanical performance. Whereas CaO addition increased the mechanical properties, especially with low molarity of activation solution. The most significant enhancement of mechanical properties was observed with silica fume (5-10 wt.%). XRD and FT-IR showed Fe-rich C-S-H gel formation in some samples. Katoite and portlandite were formed when CaO was used as an additive. SEM images revealed that higher molarity and use of silica fume resulted in a more uniform reaction product.

The samples were subjected to 60 and 120 freeze-thaw cycles. The materials produced did not show good freeze-thaw resistance with the best composition lasting for about 60 cycles. Chemical resistance was studied with 3% NaCl, $MgSO_4$, H_2SO_4, and HCl after 14 and 28 days of submersion. The samples showed a better performance in the slats than in acids, but all the samples kept their structural integrities after 28 days. Elemental mapping revealed that HCl submersion removed Ca from the samples. Similar effect was observed with iron.

9. REFERENCES

[1] K. O. Yoro and M. O. Daramola, "CO_2 emission sources, greenhouse gases, and the global warming effect," *Advances in Carbon Capture*, pp. 3–28, Jan. 2020, doi: 10.1016/B978-0-12-819657-1.00001-3.

[2] N. Mohamad, K. Muthusamy, R. Embong, A. Kusbiantoro, and M. H. Hashim, "Environmental impact of cement production and Solutions: A review," *Materials Today Proceedings*, vol. 48, pp. 741–746, Jan. 2022, doi: 10.1016/J.MATPR.2021.02.212.

[3] L. Arnout, G. Beersaerts, M. Liard, D. Lootens, and Y. Pontikes, "Valorising Slags from Non-ferrous Metallurgy into Hybrid Cementitious Binders: Mix Design and Performance," *Waste Biomass Valorization*, vol. 12, no. 8, pp. 4679–4694, Aug. 2021, doi: 10.1007/s12649-020-01322-9.

[4] J. L. Provis, "Alkali-activated materials," *Cement and Concrete Ressearch*, vol. 114, pp. 40–48, Dec. 2018, doi: 10.1016/J.CEMCONRES.2017.02.009.

[5] V. Ponomar, J. Yliniemi, E. Adesanya, K. Ohenoja, and M. Illikainen, "An overview of the utilisation of Fe-rich residues in alkali-activated binders: Mechanical properties and state of iron," *Journal of Cleaner Production*, vol. 330. Elsevier Ltd, Jan. 01, 2022. doi: 10.1016/j.jclepro.2021.129900.

[6] J. L. Provis and S. A. Bernal, "Geopolymers and related alkali-activated materials," *Annual Review of Materials Research*, vol. 44, pp. 299–327, 2014, doi: 10.1146/annurev-matsci-070813-113515.

[7] F. Pacheco-Torgal, J. Castro-Gomes, and S. Jalali, "Alkali-activated binders: A review. Part 1. Historical background, terminology, reaction mechanisms and hydration products," *Construction and Building Materials*, vol. 22, no. 7. pp. 1305–1314, Jul. 2008. doi: 10.1016/j.conbuildmat.2007.10.015.

[8] F. Pacheco-Torgal, J. Castro-Gomes, and S. Jalali, "Alkali-activated binders: A review. Part 2. About materials and binders manufacture," *Construction and*

Building Materials, vol. 22, no. 7. pp. 1315–1322, Jul. 2008. doi: 10.1016/j.conbuildmat.2007.03.019.

[9] M. Carus and L. Dammer, "The 'Circular Bioeconomy'-Concepts, Opportunities and Limitations www.bio-based.eu/nova-papers." [Online]. Available: www.bio-based.eu/nova-papers

[10] J. Kirchherr, D. Reike, and M. Hekkert, "Conceptualizing the circular economy: An analysis of 114 definitions," *Resources, Conservation and Recycling*, vol. 127, pp. 221–232, Dec. 2017, doi: 10.1016/J.RESCONREC.2017.09.005.

[11] Y. Kalmykova, M. Sadagopan, and L. Rosado, "Circular economy – From review of theories and practices to development of implementation tools," *Resources, Conservation and Recycling*, vol. 135, pp. 190–201, Aug. 2018, doi: 10.1016/J.RESCONREC.2017.10.034.

[12] K. T. Adams, M. Osmani, T. Thorpe, and J. Thornback, "Circular economy in construction: Current awareness, challenges and enablers," in *Proceedings of Institution of Civil Engineers: Waste and Resource Management*, Feb. 2017, vol. 170, no. 1, pp. 15–24. doi: 10.1680/jwarm.16.00011.

[13] M. S. Imbabi, C. Carrigan, and S. McKenna, "Trends and developments in green cement and concrete technology," *International Journal of Sustainable Built Environment*, vol. 1, no. 2, pp. 194–216, Dec. 2012, doi: 10.1016/J.IJSBE.2013.05.001.

[14] K. Sakkas, P. Nomikos, A. Sofianos, and D. Panias, "Utilisation of FeNi-Slag for the production of inorganic polymeric materials for construction or for passive fire protection," in *Waste and Biomass Valorization*, 2014, vol. 5, no. 3, pp. 403–410. doi: 10.1007/s12649-013-9278-z.

[15] P. C. Aïtcin, "Portland cement," *Science and Technology of Concrete Admixtures*, pp. 27–51, Jan. 2016, doi: 10.1016/B978-0-08-100693-1.00003-5.

[16] C. Shi, “Strength, pore structure and permeability of alkali-activated slag mortars,” *Cement and Concrete Research*, vol. 26, no. 12, pp. 1789–1799, Dec. 1996, doi: 10.1016/S0008-8846(96)00174-3.

[17] G. F. Huseien *et al.*, “Alkali-activated mortars blended with glass bottle waste nano powder: Environmental benefit and sustainability,” *Journal of Cleaner Production*, vol. 243, p. 118636, Jan. 2020, doi: 10.1016/J.JCLEPRO.2019.118636.

[18] J. Vlček, V. Tomková, P. Babková, M. Vavro, “Alkali-activated composites based on slags from iron and steel metallurgy, *Metalurgija,* Vol. 48, pp. 223-227, Jan. 2009

[19] Y. Pontikes *et al.*, “Slags with a high Al and Fe content as precursors for inorganic polymers,” *Applied Clay Science*, vol. 73, no. 1, pp. 93–102, Mar. 2013, doi: 10.1016/j.clay.2012.09.020.

[20] E. A. Obonyo, E. Kamseu, P. N. Lemougna, A. B. Tchamba, U. C. Melo, and C. Leonelli, “A sustainable approach for the geopolymerization of natural iron-rich aluminosilicate materials,” *Sustainability (Switzerland)*, vol. 6, no. 9, pp. 5535–5553, 2014, doi: 10.3390/su6095535.

[21] I. Maragkos, I. P. Giannopoulou, and D. Panias, “Synthesis of ferronickel slag-based geopolymers,” *Minerals Engineering*, vol. 22, no. 2, pp. 196–203, Jan. 2009, doi: 10.1016/j.mineng.2008.07.003.

[22] A. M. Kalinkin *et al.*, “Geopolymerization behavior of Cu-Ni slag mechanically activated in air and in CO_2 atmosphere,” *International Journal of Mineral Processing*, vol. 112–113, pp. 101–106, Sep. 2012, doi: 10.1016/j.minpro.2012.05.001.

[23] M. Nodehi, & V. M. Taghvaee, “Alkali-Activated Materials and Geopolymer: a Review of Common Precursors and Activators Addressing Circular Economy”, *Circular economy and sustainability*, Vol. 2, pp. 165–196, Mar. 2022, doi: 10.1007/s43615-021-00029-w.

[24] K. Gong and C. E. White, “Impact of chemical variability of ground granulated blast-furnace slag on the phase formation in alkali-activated slag pastes,” *Cement and Concrete Research*, vol. 89, pp. 310–319, Nov. 2016, doi: 10.1016/j.cemconres.2016.09.003.

[25] N. Y. Mostafa, S. A. S. El-Hemaly, E. I. Al-Wakeel, S. A. El-Korashy, and P. W. Brown, “Characterization and evaluation of the hydraulic activity of water-cooled slag and air-cooled slag,” *Cement and Concrete Research*, vol. 31, no. 6, pp. 899–904, May 2001, doi: 10.1016/S0008-8846(01)00497-5.

[26] J. Singh and S. P. Singh, “Geopolymerization of solid waste of non-ferrous metallurgy – A review,” *Journal of Environmental Management*, vol. 251. Academic Press, Dec. 01, 2019. doi: 10.1016/j.jenvman.2019.109571.

[27] M. Ozturk, M. B. Bankir, O. S. Bolukbasi, and U. K. Sevim, “Alkali activation of electric arc furnace slag: Mechanical properties and micro analyzes,” *Journal of Building Engineering*, vol. 21, pp. 97–105, Jan. 2019, doi: 10.1016/j.jobe.2018.10.005.

[28] T. Hertel and Y. Pontikes, “Geopolymers, inorganic polymers, alkali-activated materials and hybrid binders from bauxite residue (red mud) – Putting things in perspective,” *Journal of Cleaner Production*, vol. 258, p. 120610, Jun. 2020, doi: 10.1016/J.JCLEPRO.2020.120610.

[29] R. C. Ropp, “Group 16 (O, S, Se, Te) Alkaline Earth Compounds,” in *Encyclopedia of the Alkaline Earth Compounds*, Elsevier, 2013, pp. 105–197. doi: 10.1016/b978-0-444-59550-8.00003-x.

[30] M. L. Granizo, S. Alonso. M. T. Blanco-Varela, A. Palomo, “Alkaline Activation of Metakaolin Effect of Calcium Hydroxide, *Journal of the American Ceramic Society*, vol. 85, issue 1, pp. 225-231, Dec. 2004, https://doi.org/10.1111/j.1151-2916.2002.tb00070.x.

[31] L. Qing, S. Shaokang, J. Zhen, W. Junxiang, and L. Xianjun, “Effect of CaO on hydration properties of one-part alkali-activated material prepared from tailings

through alkaline hydrothermal activation," *Construction and Building Materials*, vol. 308, Nov. 2021, doi: 10.1016/j.conbuildmat.2021.124931.

[32] P. Prochon, Z. Zhao, L. Courard, T. Piotrowski, F. Michel, and A. Garbacz, "Influence of Activators on Mechanical Properties of Modified Fly Ash Based Geopolymer Mortars", *materials*, vol. 13, issue 5, Feb. 2020, doi: 10.3390/ma13051033.

[33] L. Qing, S. Shaokang, J. Zhen, W. Junxiang, and L. Xianjun, "Effect of CaO on hydration properties of one-part alkali-activated material prepared from tailings through alkaline hydrothermal activation," *Construction and Building Materials*, vol. 308, p. 124931, Nov. 2021, doi: 10.1016/J.CONBUILDMAT.2021.124931.

[34] D. Zhao, "Reactive MgO-modified slag-based binders for cemented paste backfill and potential heavy-metal leaching behavior," *Construction and Building Materials*, vol. 298, p. 123894, Sep. 2021, doi: 10.1016/J.CONBUILDMAT.2021.123894.

[35] M. R. Ahmad, B. Chen, S. Farasat, and A. Shah, "Influence of different admixtures on the mechanical and durability properties of one-part alkali-activated mortars", *Construction and Building Materials*, vol. 265, July 2020, doi: 10.1016/j.conbuildmat.2020.120320.

[36] A. A. Ramezanianpour and M. A. Moeini, "Mechanical and durability properties of alkali activated slag coating mortars containing nanosilica and silica fume," *Construction and Building Materials*, vol. 163, pp. 611–621, Feb. 2018, doi: 10.1016/j.conbuildmat.2017.12.062.

[37] A. M. Boddy, R. D. Hooton, and M. D. A. Thomas, "The effect of the silica content of silica fume on its ability to control alkali–silica reaction," *Cement and Concrete Research*, vol. 33, no. 8, pp. 1263–1268, Aug. 2003, doi: 10.1016/S0008-8846(03)00058-9.

[38] C. B. Cheah, L. E. Tan, and M. Ramli, "The engineering properties and microstructure of sodium carbonate activated fly ash/ slag blended mortars with

silica fume," *Composites Part B: Engineering*, vol. 160, pp. 558–572, Mar. 2019, doi: 10.1016/j.compositesb.2018.12.056.

[39] E. Adesanya, K. Ohenoja, A. di Maria, P. Kinnunen, and M. Illikainen, "Alternative alkali-activator from steel-making waste for one-part alkali-activated slag," *Journal of Cleaner Production*, vol. 274, p. 123020, Nov. 2020, doi: 10.1016/J.JCLEPRO.2020.123020.

[40] S. A. Bernal, E. D. Rodríguez, R. Mejia De Gutiérrez, J. L. Provis, and S. Delvasto, "Activation of Metakaolin/Slag Blends Using Alkaline Solutions Based on Chemically Modified Silica Fume and Rice Husk Ash", *Waste Biomass Valor*, vol. 3, pp. 99-108, Sep. 2011, doi: 10.1007/s12649-011-9093-3.

[41] A. Nmiri, M. Duc, N. Hamdi, O. Yazoghli-Marzouk, and E. Srasra, "Replacement of alkali silicate solution with silica fume in metakaolin-based geopolymers," *International Journal of Minerals, Metallurgy and Materials*, vol. 26, no. 5, 2019, doi: 10.1007/s12613-019-1764-2.

[42] B. S. Gebregziabiher, R. J. Thomas, and S. Peethamparan, "Temperature and activator effect on early-age reaction kinetics of alkali-activated slag binders," *Construction and Building Materials*, vol. 113, pp. 783–793, Jun. 2016, doi: 10.1016/J.CONBUILDMAT.2016.03.098.

[43] M. ben Haha, B. Lothenbach, G. le Saout, and F. Winnefeld, "Influence of slag chemistry on the hydration of alkali-activated blast-furnace slag — Part I: Effect of MgO," *Cement and Concrete Research*, vol. 41, no. 9, pp. 955–963, Sep. 2011, doi: 10.1016/J.CEMCONRES.2011.05.002.

[44] F. Matalkah, R. Aqel, and A. Ababneh, "Enhancement of the Mechanical Properties of Kaolin Geopolymer Using Sodium Hydroxide and Calcium Oxide," *Procedia Manufacturing*, vol. 44, pp. 164–171, Jan. 2020, doi: 10.1016/J.PROMFG.2020.02.218.

[45] K. Gu, F. Jin, A. Al-Tabbaa, B. Shi, and J. Liu, "Mechanical and hydration properties of ground granulated blastfurnace slag pastes activated with MgO–CaO

mixtures," *Construction and Building Materials*, vol. 69, pp. 101–108, Oct. 2014, doi: 10.1016/J.CONBUILDMAT.2014.07.032.

[46] K. M. L. Alventosa and C. E. White, "The effects of calcium hydroxide and activator chemistry on alkali-activated metakaolin pastes," *Cement and Concrete Research*, vol. 145, p. 106453, Jul. 2021, doi: 10.1016/J.CEMCONRES.2021.106453.

[47] Z. Yan, Z. Sun, J. Yang, H. Yang, Y. Ji, and K. Hu, "Mechanical performance and reaction mechanism of copper slag activated with sodium silicate or sodium hydroxide," *Construction and Building Materials*, vol. 266, Jan. 2021, doi: 10.1016/j.conbuildmat.2020.120900.

[48] J. L. Provis and J. S. J. van Deventer, "Alkali Activated Materials, *RILEM State-of-the-Art Reports*, RILEM TC 224-AAM." [Online]. Available: http://www.springer.com/series/8780

[49] J. van de Sande, A. Peys, T. Hertel, H. Rahier, and Y. Pontikes, "Upcycling of non-ferrous metallurgy slags: Identifying the most reactive slag for inorganic polymer construction materials," *Resources, Conservation and Recycling*, vol. 154, Mar. 2020, doi: 10.1016/j.resconrec.2019.104627.

[50] Z. Abdollahnejad, C. Jesus, F. Pacheco-Torqar', and J. B. Aquiar, "One-part geopolymers versus ordinary Portland cement (OPC), Mortars: durability assessment, *WASTES: Solutions, Treatments and Opportunities 2 nd Intemational Conference*, Sep. 2013

[51] A. Peys, L. Arnout, B. Blanpain, H. Rahier, K. van Acker, and Y. Pontikes, "Mix-design Parameters and Real-life Considerations in the Pursuit of Lower Environmental Impact Inorganic Polymers," *Waste Biomass Valor*, vol. 9, pp. 879–889, Feb. 2018, doi: 10.1007/s12649-017-9877-1.

[52] H. T. Türker, M. Balçikanli, I. H. Durmuş, E. Özbay, and M. Erdemir, "Microstructural alteration of alkali activated slag mortars depend on exposed high

temperature level," *Construction and Building Materials*, vol. 104, pp. 169–180, Feb. 2016, doi: 10.1016/J.CONBUILDMAT.2015.12.070.

[53] I. Nikolic *et al.*, "Alkali activated slag cement doped with Zn-rich electric arc furnace dust," *Journal of Materials Research and Technology*, vol. 9, no. 6, pp. 12783–12794, Nov. 2020, doi: 10.1016/j.jmrt.2020.09.024.

[54] I. Nikolić, A. Drinčić, D. Djurović, L. Karanović, V. v. Radmilović, and V. R. Radmilović, "Kinetics of electric arc furnace slag leaching in alkaline solutions," *Construction and Building Materials*, vol. 108, pp. 1–9, Apr. 2016, doi: 10.1016/j.conbuildmat.2016.01.038.

[55] L. Machiels, L. Arnout, P. T. Jones, B. Blanpain, and Y. Pontikes, "Inorganic polymer cement from fe-silicate glasses: Varying the activating solution to glass ratio," *Waste and Biomass Valorization*, 2014, vol. 5, no. 3, pp. 411–428. doi: 10.1007/s12649-014-9296-5.

[56] L. Kriskova, L. Machiels, and Y. Pontikes, "Inorganic Polymers from a Plasma Convertor Slag: Effect of Activating Solution on Microstructure and Properties," *Journal of Sustainable Metallurgy*, vol. 1, no. 3, pp. 240–251, Sep. 2015, doi: 10.1007/s40831-015-0022-8.

[57] P. N. Lemougna, K. J. D. MacKenzie, G. N. L. Jameson, H. Rahier, and U. F. Chinje Melo, "The role of iron in the formation of inorganic polymers (geopolymers) from volcanic ash: A 57Fe Mössbauer spectroscopy study," *Journal of Materials Science*, vol. 48, no. 15, pp. 5280–5286, Aug. 2013, doi: 10.1007/s10853-013-7319-4.

[58] R. I. Iacobescu *et al.*, "The influence of curing conditions on the mechanical properties and leaching of inorganic polymers made of fayalitic slag," *Frontiers of Chemical Science and Engineering*, vol. 11, no. 3, pp. 317–327, Sep. 2017, doi: 10.1007/s11705-017-1622-6.

[59] K. Arbi, M. Nedeljković, Y. Zuo, and G. Ye, "A Review on the Durability of Alkali-Activated Fly Ash/Slag Systems: Advances, Issues, and Perspectives,"

Industrial and Engineering Chemistry Research, vol. 55, no. 19. American Chemical Society, pp. 5439–5453, May 18, 2016. doi: 10.1021/acs.iecr.6b00559.

[60] B. Tailling and P. Krivenko, ”Blast furnace slag – The ultimate binder, *Waste Materials Used in Concrete Manufacturing*, pp. 235-289, 1996, https://doi.org/10.1016/B978-081551393-3.50008-9.

[61] S. Song, N. Zhang, J. Yuan, and Y. Zhang, “New attempt to produce red mud-iron tailing based alkali-activated mortar: Performance and microstructural characteristics,” *Journal of Building Engineering*, vol. 43, Nov. 2021, doi: 10.1016/j.jobe.2021.103222.

[62] K. Komnitsas, A. D. Zaharaki, and A. v Perdikatsis, “Geopolymerisation of low calcium ferronickel slags”, *Advances in geopolymer science and technology*, vol. 42, pp.3073-3082, June 2006, doi: 10.1007/s10853-006-0529-2.

[63] K. Komnitsas, L. Yurramendi, G. Bartzas, V. Karmali, and E. Petrakis, “Factors affecting co-valorization of fayalitic and ferronickel slags for the production of alkali activated materials,” *Science of the Total Environment*, vol. 721, Jun. 2020, doi: 10.1016/j.scitotenv.2020.137753.

[64] R. Wang, Q. Shi, Y. Li, Z. Cao, and Z. Si, “A critical review on the use of copper slag (CS) as a substitute constituent in concrete,” *Construction and Building Materials*, vol. 292. Elsevier Ltd, Jul. 19, 2021. doi: 10.1016/j.conbuildmat.2021.123371.

[65] W. J. Cho and M. J. Kim, “Freeze–Thaw Resistance of Ternary Blended Concrete Using Ferronickel Slag,” *International Journal of Concrete Structures and Materials*, vol. 15, no. 1, Dec. 2021, doi: 10.1186/s40069-020-00447-4.

[66] T. Bakharev, J. G. Sanjayan, and Y.-B. Cheng, “Sulfate attack on alkali-activated slag concrete”, *Cement and Concrete Research*, vol. 32, pp. 211-216, Aug. 2001, https://doi.org/10.1016/S0008-8846(01)00659-7.

[67] J. Kwasny, T. A. Aiken, M. N. Soutsos, J. A. McIntosh, and D. J. Cleland, “Sulfate and acid resistance of lithomarge-based geopolymer mortars,” *Construction and Building Materials*, vol. 166, pp. 537–553, Mar. 2018, doi: 10.1016/j.conbuildmat.2018.01.129.

[68] A. Mehta and R. Siddique, “Sulfuric acid resistance of fly ash based geopolymer concrete,” *Construction and Building Materials*, vol. 146, pp. 136–143, Aug. 2017, doi: 10.1016/J.CONBUILDMAT.2017.04.077.

[69] Z. Abdollahnejad, M. Mastali, B. Woof, and M. Illikainen, “High strength fiber reinforced one-part alkali activated slag/fly ash binders with ceramic aggregates: Microscopic analysis, mechanical properties, drying shrinkage, and freeze-thaw resistance,” *Construction and Building Materials*, vol. 241, p. 118129, Apr. 2020, doi: 10.1016/J.CONBUILDMAT.2020.118129.

[70] S. Siddique and J. G. Jang, “Acid and sulfate resistance of seawater based alkali activated fly ash: A sustainable and durable approach,” *Construction and Building Materials*, vol. 281, p. 122601, Apr. 2021, doi: 10.1016/J.CONBUILDMAT.2021.122601.

[71] T. Sithole, N. Tsotetsi, T. Mashifana, M. L. Ruello, and A. Mobili, “Synthesis of Ambient Cured GGBFS Based Alkali Activated Binder Using a Sole Alkaline Activator: A Feasibility Study,” *applied sciences*, vol. 13, Nov. 2021, doi: 10.3390/app11135887.

[72] S. Boonjaeng, P. Chindaprasirt, and K. Pimraksa, “Lime-calcined clay materials with alkaline activation: Phase development and reaction transition zone,” *Applied Clay Science*, vol. 95, pp. 357–364, Jun. 2014, doi: 10.1016/J.CLAY.2014.05.002.

[73] K. Komnitsas, D. Zaharaki, and V. Perdikatsis, “Effect of synthesis parameters on the compressive strength of low-calcium ferronickel slag inorganic polymers,” *Journal of Hazardous Materials*, vol. 161, no. 2–3, pp. 760–768, Jan. 2009, doi: 10.1016/j.jhazmat.2008.04.055.

[74] T. Hirayama, S. Saiki, S. Kawabata, E. Kusumastuti, F. I. Ariati, and L. Atmaja, "Synthesis of volcanic ash-based geopolymer with calcium oxide (CaO) addition for building material application You may also like Soiling by volcanic ash fall on photovoltaic modules and effects of hydrophilic coating on module cover glass Synthesis of volcanic ash-based geopolymer with calcium oxide (CaO) addition for building material application," *Journal of Physics: Conference Series*, vol. 1567, p. 22030, 2020, doi: 10.1088/1742-6596/1567/2/022030.

[75] M. Kaya, F. Koksal, O. Gencel, M. J. Munir, and S. M. S. Kazmi, "Influence of micro Fe2O3 and MgO on the physical and mechanical properties of the zeolite and kaolin based geopolymer mortar," *Journal of Building Engineering*, vol. 52, p. 104443, Jul. 2022, doi: 10.1016/J.JOBE.2022.104443.

[76] M. A. Hossain, K. M. A. Hossain, T. Manzur, M. J. Hasan, and D. Sood, "Fresh and hardened properties of engineered geopolymer composite with MgO," in *International Conference on Civil, Structural and Transportation Engineering*, 2020, pp. 244-1-244–8. doi: 10.11159/iccste20.244.

[77] S. Abd El-Aleem Mohamed El-Awney, "Effect of reactive magnesium oxide on properties of alkali activated slag geopolymer cement, *Preparation and characterization of Geopolymers and Bio-cement View project Durability of composite cements containing nano-materials (NMs) View project*," Jan. 2015. [Online]. Available: https://www.researchgate.net/publication/320087478

[78] S. N. M. Hairi, G. N. L. Jameson, J. J. Rogers, and K. J. D. MacKenzie, "Synthesis and properties of inorganic polymers (geopolymers) derived from Bayer process residue (red mud) and bauxite," *Journal of Materials Science*, vol. 50, no. 23, pp. 7713–7724, 2015, doi: 10.1007/s10853-015-9338-9.

[79] S. Onisei, K. Lesage, B. Blanpain, and Y. Pontikes, "Early Age Microstructural Transformations of an Inorganic Polymer Made of Fayalite Slag," *Journal of the American Ceramic Society*, vol. 98, no. 7, pp. 2269–2277, 2015, doi: 10.1111/jace.13548.

[80] N. J. Coleman and D. S. Brassington, “Synthesis of Al-substituted 11 Å tobermorite from newsprint recycling residue: A feasibility study,” *Materials Research Bulletin*, vol. 38, no. 3, pp. 485–497, 2003, doi: 10.1016/S0025-5408(02)01056-5.

[81] E. Tajuelo Rodriguez, K. Garbev, D. Merz, L. Black, and I. G. Richardson, “Thermal stability of C-S-H phases and applicability of Richardson and Groves’ and Richardson C-(A)-S-H(I) models to synthetic C-S-H,” *Cement and Concrete Research*, vol. 93, pp. 45–56, 2017, doi: 10.1016/j.cemconres.2016.12.005.

[82] I. Garcia-Lodeiro, A. Palomo, A. Fernández-Jiménez, and D. E. MacPhee, “Compatibility studies between N-A-S-H and C-A-S-H gels. Study in the ternary diagram Na2O-CaO-Al2O3-SiO 2-H2O,” *Cement and Concrete Research*, vol. 41, no. 9, pp. 923–931, 2011, doi: 10.1016/j.cemconres.2011.05.006.

[83] I. García Lodeiro, A. Fernández-Jimenez, A. Palomo, and D. E. Macphee, “Effect on fresh C-S-H gels of the simultaneous addition of alkali and aluminium,” *Cement and Concrete Research*, vol. 40, no. 1, pp. 27–32, 2010, doi: 10.1016/j.cemconres.2009.08.004.

[84] M. U. Okoronkwo and F. P. Glasser, “Stability of strätlingite in the CASH system,” *Materials and Structures/Materiaux et Constructions*, vol. 49, no. 10, pp. 4305–4318, 2016, doi: 10.1617/s11527-015-0789-x.

[85] R. Drochytka and E. Helanová, “Development of Microstructure of the Fly Ash Aerated Concrete in time,” *Procedia Engineering*, vol. 108, pp. 624–631, Jan. 2015, doi: 10.1016/J.PROENG.2015.06.189.

[86] “Katoite: Mineral information, data and localities.” https://www.mindat.org/min-2167.html (accessed Jul. 01, 2022).

[87] P. Adhikari, C. C. Dharmawardhana, and W. Y. Ching, “Structure and properties of hydrogrossular mineral series,” *Journal of the American Ceramic Society*, vol. 100, no. 9, pp. 4317–4330, Sep. 2017, doi: 10.1111/jace.14970.

[88] C. Venkatesh, R. Nerella, M. Sri, and R. Chand, “Role of red mud as a cementing material in concrete: a comprehensive study on durability behavior,” *Innovative Infrastructure Solutions*, vol. 6, p. 13, 2021, doi: 10.1007/s41062-020-00371-2.

[89] S. Goñi, A. Guerrero, M. P. Luxán, and A. Macías, “Activation of the fly ash pozzolanic reaction by hydrothermal conditions,” *Cement and Concrete Research*, vol. 33, no. 9, pp. 1399–1405, Sep. 2003, doi: 10.1016/S0008-8846(03)00085-1.

[90] P. He, B. Zhang, J. X. Lu, and C. S. Poon, “Reaction mechanisms of alkali-activated glass powder-ggbs-CAC composites,” *Cement and Concrete Composites*, vol. 122, p. 104143, Sep. 2021, doi: 10.1016/J.CEMCONCOMP.2021.104143.

[91] V. Ponomar, K. Ohenoja, and M. Illikainen, “Understanding the Role of the Composition of Alkaline Solutions in the Hardening Behaviour of Fe-Rich Binder Based on Jarosite Residue Slag.,” *Available at SSRN: https://ssrn.com/abstract=4028193 or http://dx.doi.org/10.2139/ssrn.4028193*.

[92] C. R. Kaze *et al.*, “Effect of silicate modulus on the setting, mechanical strength and microstructure of iron-rich aluminosilicate (laterite) based-geopolymer cured at room temperature,” *Ceramics International*, vol. 44, no. 17, pp. 21442–21450, Dec. 2018, doi: 10.1016/j.ceramint.2018.08.205.

[93] N. Y. Mostafa, E. A. Kishar, and S. A. Abo-El-Enein, “FTIR study and cation exchange capacity of Fe3+- and Mg2+-substituted calcium silicate hydrates,” *Journal of Alloys and Compounds*, vol. 473, no. 1–2, pp. 538–542, 2009, doi: 10.1016/j.jallcom.2008.06.029.

[94] S. Wang, X. Peng, L. Tang, L. Zeng, and C. Lan, “Influence of inorganic admixtures on the 11 Å-tobermorite formation prepared from steel slags: XRD and FTIR analysis,” *Construction and Building Materials*, vol. 60, pp. 42–47, 2014, doi: 10.1016/j.conbuildmat.2014.03.002.

[95] R. I. Iacobescu *et al.*, “The influence of curing conditions on the mechanical properties and leaching of inorganic polymers made of fayalitic slag,” *Frontiers of*

Chemical Science and Engineering, vol. 11, no. 3, pp. 317–327, 2017, doi: 10.1007/s11705-017-1622-6.

[96] J. Van De Sande, A. Peys, T. Hertel, H. Rahier, and Y. Pontikes, "Upcycling of non-ferrous metallurgy slags: Identifying the most reactive slag for inorganic polymer construction materials," *Resources, Conservation and Recycling*, vol. 154, no. November 2019, p. 104627, 2020, doi: 10.1016/j.resconrec.2019.104627.

[97] A. M. Kalinkin *et al.*, "Geopolymerization behavior of Cu-Ni slag mechanically activated in air and in CO 2 atmosphere," *International Journal of Mineral Processing*, vol. 112–113, pp. 101–106, 2012, doi: 10.1016/j.minpro.2012.05.001.

[98] K. Komnitsas, D. Zaharaki, and V. Perdikatsis, "Effect of synthesis parameters on the compressive strength of low-calcium ferronickel slag inorganic polymers," *Journal of Hazardous Materials*, vol. 161, pp. 760–768, 2009, doi: 10.1016/j.jhazmat.2008.04.055.

[99] M. T. Nayak and J. A. E. Desa, "Roles of iron and lithium in silicate glasses by Raman spectroscopy," *Journal of Raman Spectroscopy*, vol. 49, no. 9, pp. 1507–1513, 2018, doi: 10.1002/jrs.5397.

[100] A. M. Putz and M. V. Putz, "Spectral inverse quantum (Spectral-IQ) method for modeling mesoporous systems: Application on Silica films by FTIR," *International Journal of Molecular Sciences*, vol. 13, no. 12, pp. 15925–15941, 2012, doi: 10.3390/ijms131215925.

[101] S. Puligilla and P. Mondal, "Co-existence of aluminosilicate and calcium silicate gel characterized through selective dissolution and FTIR spectral subtraction," *Cement and Concrete Research*, vol. 70, pp. 39–49, 2015, doi: 10.1016/j.cemconres.2015.01.006.

[102] M. Torres-Carrasco, J. G. Palomo, and F. Puertas, "Sodium silicate solutions from dissolution of glasswastes. Statistical analysis," *Materiales de Construccion*, vol. 64, no. 314, 2014, doi: 10.3989/mc.2014.05213.

[103] J. Ambroise, S. Maximilien, and J. Pera, “Properties of Metakaolin blended cements,” *Advanced Cement Based Materials*, vol. 1, no. 4, pp. 161–168, May 1994, doi: 10.1016/1065-7355(94)90007-8.

[104] W. Kunther, S. Ferreiro, and J. Skibsted, “Influence of the Ca/Si ratio on the compressive strength of cementitious calcium-silicate-hydrate binders”, *Journal of Materials Chemistry A,* vol. 5, July 2017, doi: 10.1039/c7ta06104h.

[105] P. Faucon, A. Delagrave, J. C. Petit, C. Richet, J. M. Marchand, and H. Zanni, “Aluminum Incorporation in Calcium Silicate Hydrates (C-S-H) Depending on Their Ca/Si Ratio”, *Journal of Physical Chemistry B,* vol. 103, pp. 7796-7802, July 1999, doi: 10.1021/jp990609q.

[106] E. Kapeluszna, Ł. Kotwica, A. Różycka, and Ł. Gołek, “Incorporation of Al in C-A-S-H gels with various Ca/Si and Al/Si ratio: Microstructural and structural characteristics with DTA/TG, XRD, FTIR and TEM analysis,” *Construction and Building Materials*, vol. 155, pp. 643–653, Nov. 2017, doi: 10.1016/J.CONBUILDMAT.2017.08.091.

[107] F. Shahrajabian and K. Behfarnia, “The effects of nano particles on freeze and thaw resistance of alkali-activated slag concrete,” *Construction and Building Materials*, vol. 176, pp. 172–178, Jul. 2018, doi: 10.1016/J.CONBUILDMAT.2018.05.033.

[108] Y. Jun Jae Hong Kim Seong Ho Han Taewan Kim, “Influence of seawater on alkali-activated slag concrete”, *Materials and Structures*, vol. 54, May 2021, doi: 10.1617/s11527-021-01719-5.

[109] F. Puertas, R. de Gutiérrez, A. Fernandez-Jimenez, S Delvasto, and J. Maldonado, “Morteros de cementos alcalinos. Resistencia química al ataque por sulfatos y al agua de mar Alkaline cement mortars. Chemical resistance to sulfate and seawater attack”, *Materiales De Construcción*, vol. 52, pp. 55-71, Sep. 2002 Available: http://materconstrucc.revistas.csic.es

[110] L. Mengasini, M. Mavroulidou, and M. J. Gunn, “Alkali-activated concrete mixes with ground granulated blast furnace slag and paper sludge ash in seawater

environments," *Sustainable Chemistry and Pharmacy*, vol. 20, p. 100380, May 2021, doi: 10.1016/J.SCP.2021.100380.

[111] A. Allahvedi and H. Hashemi, "Investigating the resistance of alkali-activated slag mortar exposed to magnesium sulfate attack," *International Journal of Civil Engineering*, vol. 13, no. 4A, 2015, doi: 10.22068/IJCE.13.4.379.

[112] M. N. N. Khan, J. C. Kuri, and P. K. Sarker, "Sustainable use of waste glass in alkali activated materials against H2SO4 and HCl acid attacks," *Cleaner Engineering and Technology*, vol. 6, p. 100354, Feb. 2022, doi: 10.1016/J.CLET.2021.100354.

[113] M. F. Alnahhal, U. J. Alengaram, M. Z. Jumaat, B. Alsubari, M. A. Alqedra, and K. H. Mo, "Effect of aggressive chemicals on durability and microstructure properties of concrete containing crushed new concrete aggregate and non-traditional supplementary cementitious materials," *Construction and Building Materials*, vol. 163, pp. 482–495, Feb. 2018, doi: 10.1016/J.CONBUILDMAT.2017.12.106.

[114] M. Teymouri, K. Behfarnia, A. Shabani, and E. Bastidas-Arteaga, "Mix Design Effects on the Durability of Alkali-Activated Slag Concrete in a Hydrochloric Acid Environment," *sustainability*, vol. 13, July 2021, doi: 10.3390/su13148096.

[115] M. Shariati *et al.*, "Alkali-activated slag (AAS) paste: Correlation between durability and microstructural characteristics," *Construction and Building Materials*, vol. 267, p. 120886, Jan. 2021, doi: 10.1016/J.CONBUILDMAT.2020.120886.

[116] "Translation from Finnish Legally binding only in Finnish and Swedish Ministry of the Environment, Finland Government Decree on the Recovery of Certain Wastes in Earth Construction," 2017.

[117] A. Keulen, A. van Zomeren, and J. J. Dijkstra, "Leaching of monolithic and granular alkali activated slag-fly ash materials, as a function of the mixture

design,” *Waste Management*, vol. 78, pp. 497–508, Aug. 2018, doi: 10.1016/J.WASMAN.2018.06.019.

APPENDIX

APPENDIX 1. Experiment design for reference samples

Table A4. Experiment design for reference samples.

Sample	NaOH (M)	Slag (g)	Sand (g)	Solution (g)	Sand/binder	Solution/binder	Water/binder
KK-1M	1	112.5	225	33.75	0.5	0.3	0.29
KK-1M-s	1	56.25	112.5	22.5	0.5	0.4	0.22
KK-3M	3	112.5	225	28.4	0.5	0.25	0.22
KK-3M-s	3	112.5	225	39.06	0.5	0.35	0.22
KK-6M	6	112.5	225	32.9	0.5	0.29	0.22
KK-9M	9	112.5	225	39.06	0.5	0.35	0.22
KK-1M	1	84.4	168.8	25.32	0.5	0.3	0.29
KK-3M	3	84.4	168.8	25.32	0.5	0.3	0.26
KK-6M	6	84.4	168.8	25.32	0.5	0.3	0.23
KK-3M	3	168.8	337.6	50.64	0.5	0.3	0.26
KK-6M	6	168.8	337.6	50.64	0.5	0.3	0.23

APPENDIX 2. Experiment design for samples with calcium oxide as additive

Table A5. Experiment design for samples with calcium oxide as additive.

Sample	NaOH (M)	Additive (%)	Slag (g)	Sand (g)	Solution (g)	$Ca(OH)_2$ (g)	Solution/binder	Water/binder
KK-1M-1CH	1	1	55.69	112.5	22.5	0.56	0.4	0.35
KK-1M-5CH	1	5	53.44	112.5	22.5	2.81	0.4	0.35
KK-1M-10CH	1	10	50.63	112.5	22.5	5.63	0.4	0.35
KK-1M-20CH	1	20	45	112.5	22.5	11.25	0.4	0.35
KK-3M-5CH	3	5	53.44	112.5	16.45	2.81	0.29	0.26
KK-3M-10CH	3	10	50.63	112.5	16.45	5.63	0.29	0.26
KK-6M-5CH	6	5	53.44	112.5	16.45	2.81	0.29	0.19
KK-6M-10CH	6	10	50.63	112.5	16.45	5.63	0.29	0.19
KK-6M-20CH	6	20	45	112.5	16.45	11.25	0.29	0.19

APPENDIX 3. Experiment design for samples with calcium hydroxide as additive

Table A6. Experiment design for samples with calcium hydroxide as additive.

Sample	NaOH (M)	Additive (%)	Slag (g)	Sand (g)	Solution (g)	CaO (g)	Sand/binder	Solution/binder	Water/binder
KK-1M-5CO	1	5	53.44	112.5	16.88	2.81	0.5	0.3	0.29
KK-1M-5CO-s	1	5	53.44	112.5	22.5	2.81	0.5	0.4	0.38
KK-1M-10CO	1	10	50.63	112.5	16.88	5.63	0.5	0.3	0.29
KK-1M-10CO-s	1	10	50.63	112.5	22.5	5.53	0.5	0.4	0.38
KK-1M-10CO	1	10	151.92	337.6	50.64	16.88	0.5	0.3	0.29
KK-1M-20CO	1	20	45	112.5	16.88	11.25	0.5	0.3	0.29
KK-1M-20CO-s	1	20	45	112.5	22.5	11.25	0.5	0.4	0.38
KK-3M-5CO	3	5	53.44	112.5	16.45	2.81	0.5	0.29	0.26
KK-3M-10CO	3	10	50.63	112.5	16.45	5.63	0.5	0.29	0.26
KK-6M-5CO	6	5	53.44	112.5	16.88	2.81	0.5	0.3	0.23
KK-6M-10CO	6	10	50.63	112.5	16.88	5.63	0.5	0.3	0.23
KK-6M-20CO	6	20	45	112.5	16.88	11.25	0.5	0.3	0.23

APPENDIX 4. Experiment design for samples with magnesium oxide as additive

Table A7. Experiment design for samples with magnesium oxide as additive.

Sample	NaOH (M)	Additive (%)	Slag (g)	Sand (g)	Solution (g)	MgO (g)	Sand/binder	Solution/binder	Water/binder
KK-3M-5MG	3	5	53.44	112.5	22.5	2.81	0.5	0.4	0.35
KK-3M-10MG	3	10	50.63	112.5	22.5	5.63	0.5	0.4	0.35
KK-3M-20MG	3	20	45	112.5	22.5	11.25	0.5	0.4	0.35
KK-6M-1MG	6	1	55.69	112.5	16.88	0.56	0.5	0.3	0.23
KK-6M-5MG	6	5	53.44	112.5	16.88	2.81	0.5	0.3	0.23
KK-6M-10MG	6	10	50.63	112.5	16.88	5.63	0.5	0.3	0.23

APPENDIX 5. Experiment design for samples with magnesium oxide as additive

Table A8. Experiment design for samples with silica fume as additive.

Sample	NaOH (M)	Additive (%)	Slag (g)	Sand (g)	Solution (g)	Silica fume (g)	Sand/binder	Solution/binder	Water/binder
KK-1M-1SF-s	1	1	55.69	112.5	22.5	0.56	0.5	0.4	0.38
KK-1M-1SF	1	1	55.69	112.5	22.5	0.56	0.5	0.4	0,38
KK-1M-5SF	1	5	55.44	112.5	22.5	2.81	0.5	0.4	0.38
KK-3M-1SF	3	1	55.69	112.5	22.5	0.56	0.5	0.4	0.35
KK-3M-5SF	3	5	53.44	112.5	22.5	2.81	0.5	0.4	0.35
KK-3M-5SF-s	3	5	53.44	112.5	32.06	2.81	0.5	0.57	0.5
KK-3M-5SF	3	5	160.36	337.6	67.52	8,44	0.5	0.4	0.35
KK-3M-10SF	3	10	50.63	112.5	0.4	5.63	0.5	0.4	0.35
KK-6M-1SF	6	1	56.25	112.5	16.45	1.85	0.5	0.29	0.22
KK-6M-SF	6	1	28.15	56.25	16.45	4.625	0.5	0.35	0.57
KK-6M-1SF	6	1	53.44	112.5	22.5	0.56	0.5	0.4	0.304
KK-6M-5SF	6	5	47.81	112.5	22.5	2.81	0.5	0.4	0.304
KK-1M-10CO-5SF	1	10 and 5	47.81	112.5	22.5	CaO 5.63 SF 2.81	0.5	0.4	0.38

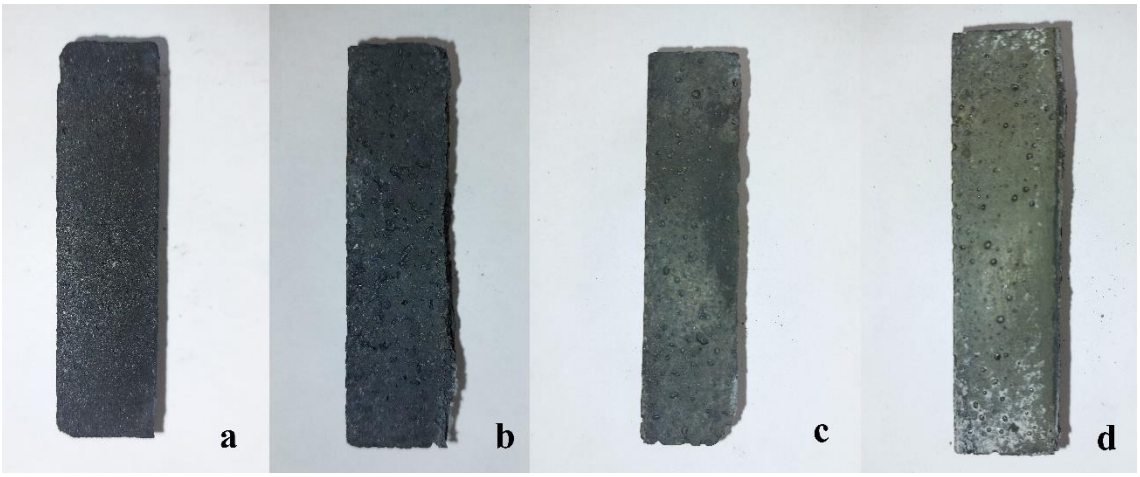

Figure A33. Reference samples with different activation solution molarities: a) 1M b) 3M c) 6 M d) 9M.

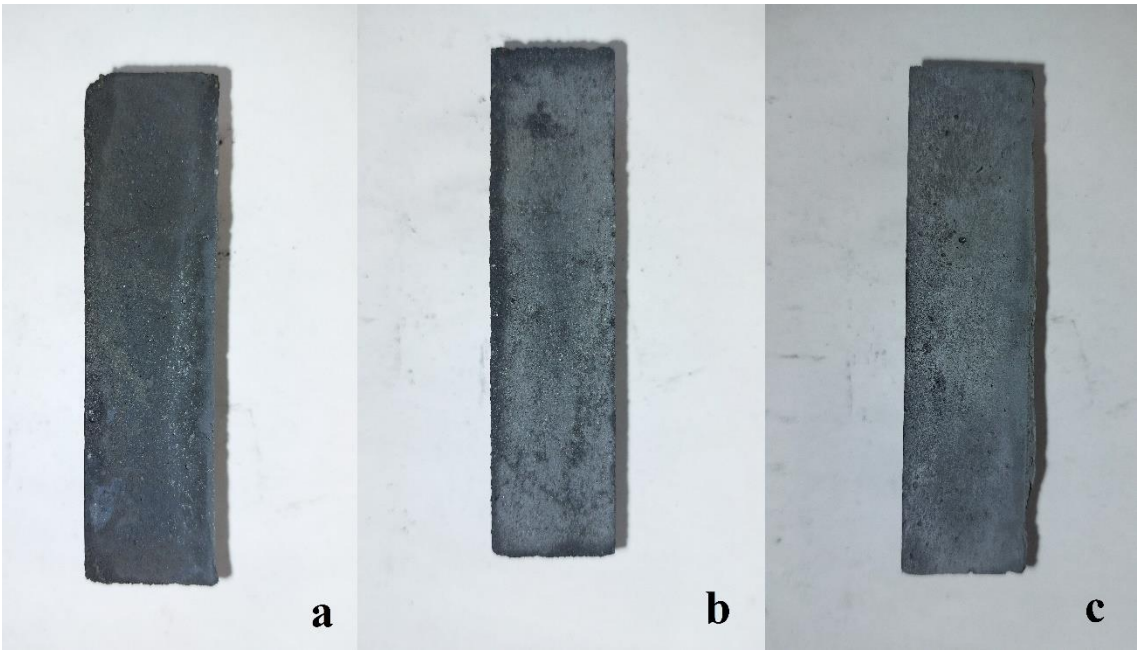

Figure A34. Samples with calcium hydroxide addition: 1 M a) 5 % b) 10 % c) 20 %.

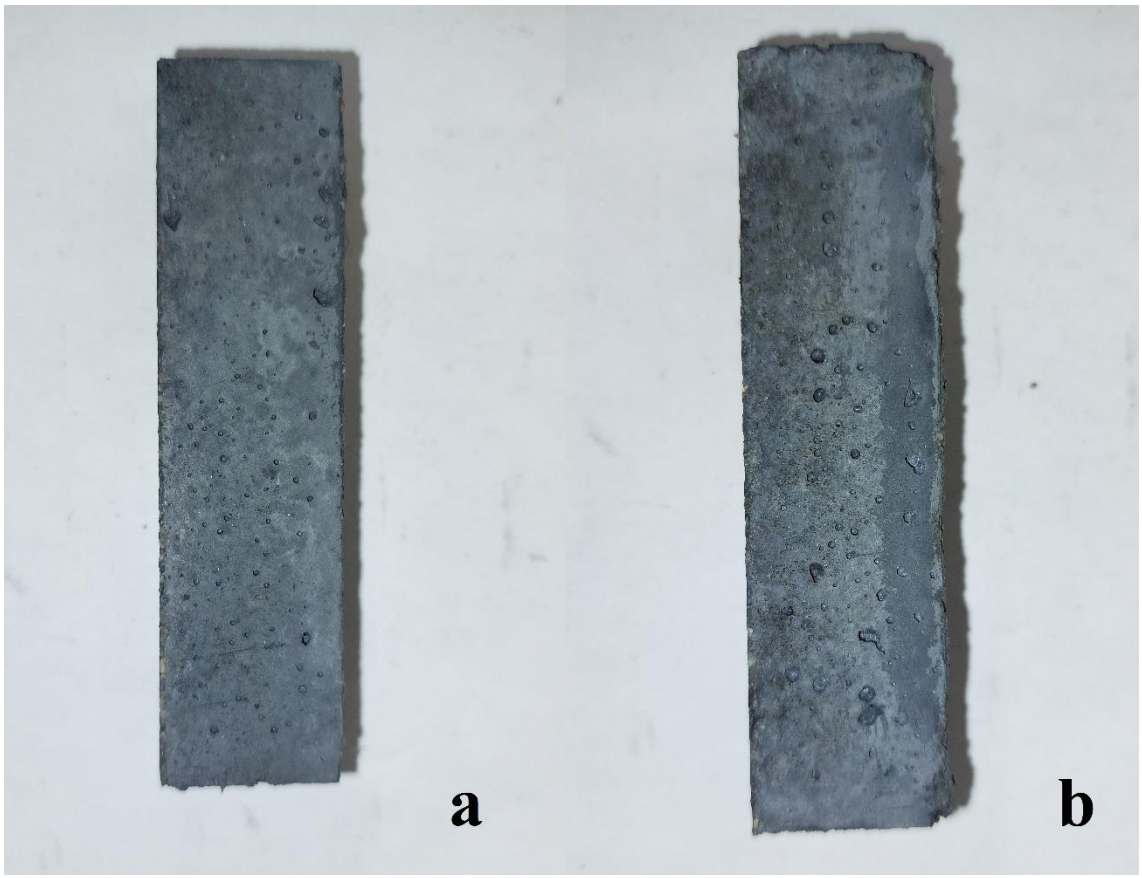

Figure A35. Samples with calcium hydroxide addition: 3 M a) 5 % b) 10 %.

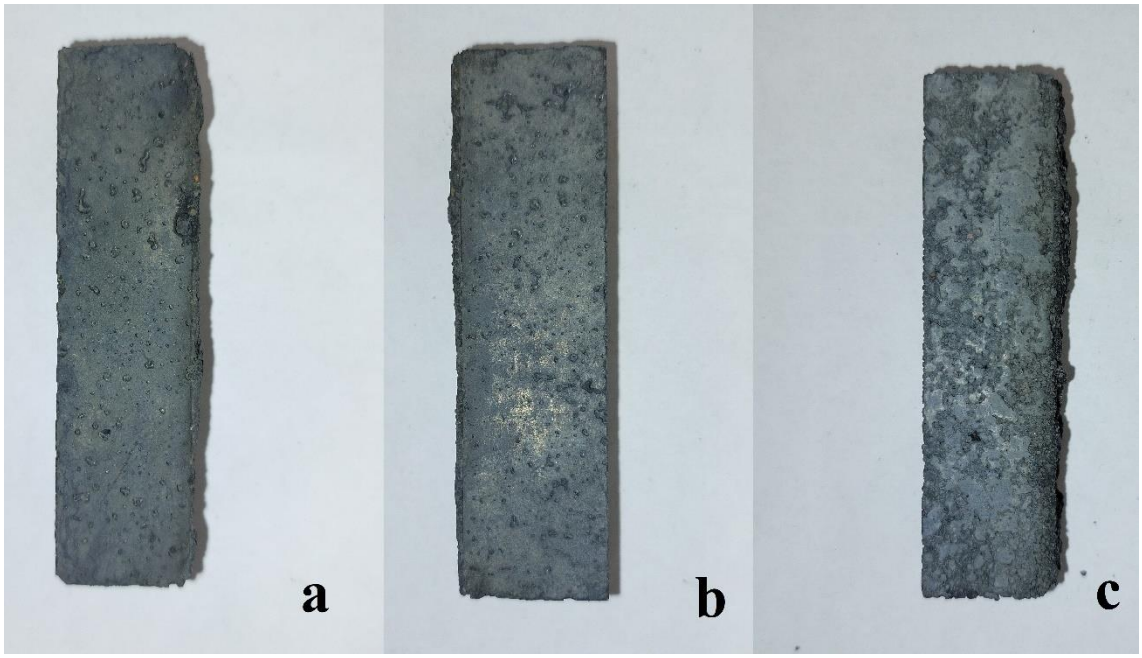

Figure A36. Samples with calcium hydroxide addition: 6 M a) 5 % b) 10 % c) 20 %.

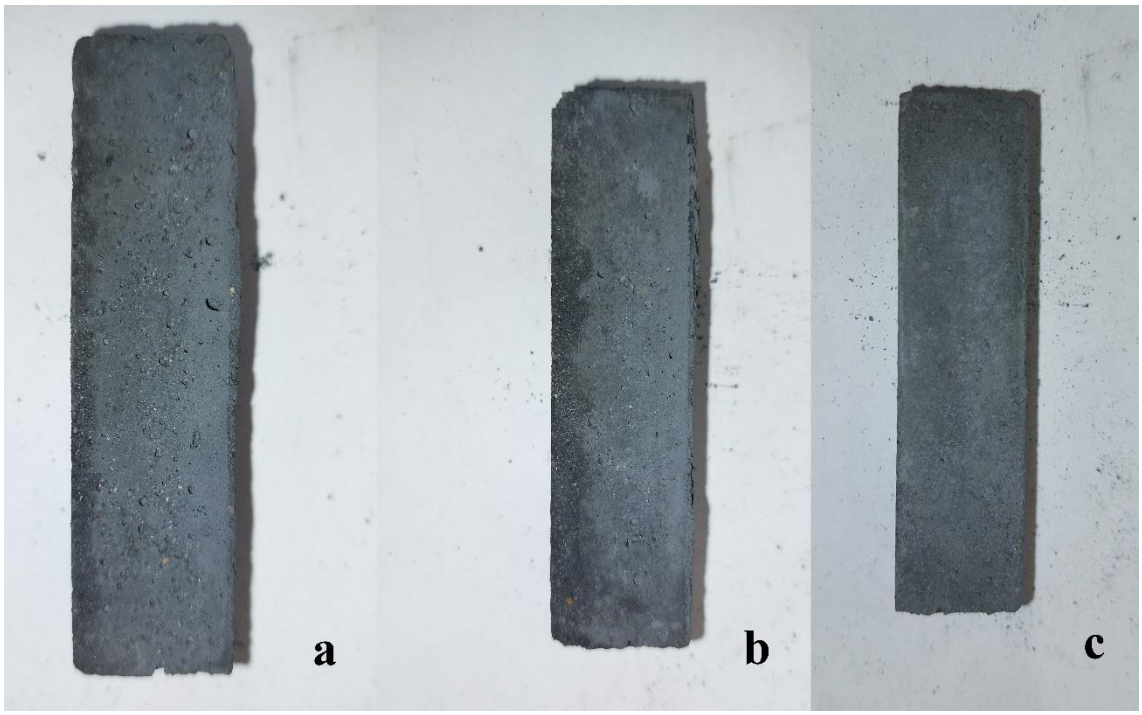

Figure A37. Samples with calcium oxide addition 1M a) 5 % b) 10 % c) 20 %.

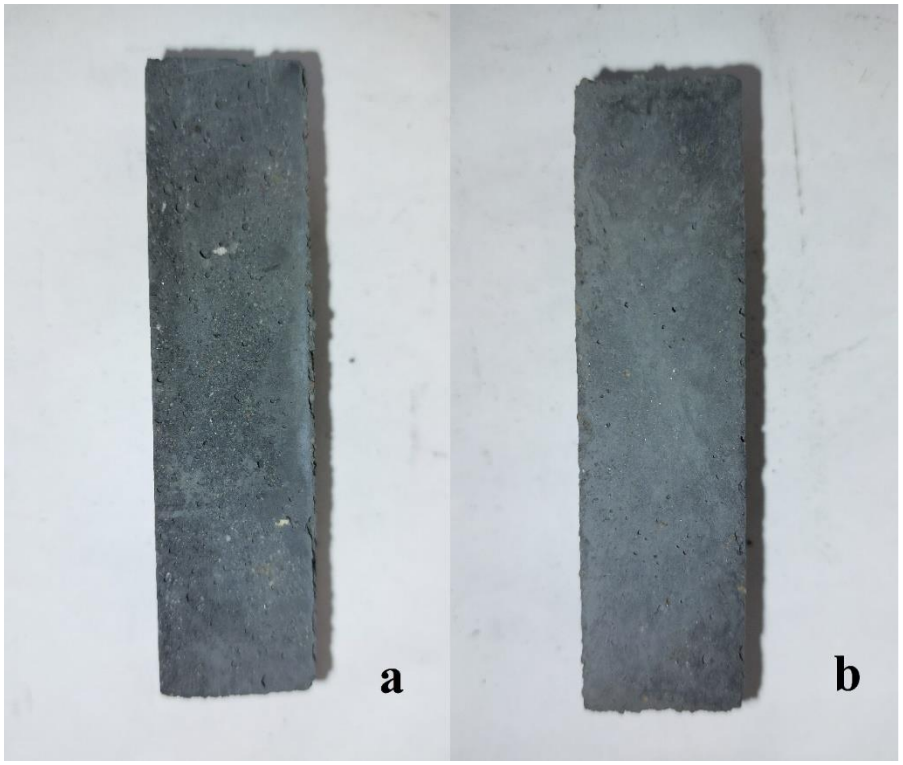

Figure A38. Samples with calcium oxide addition 1M a) 5 % b) 10 %.

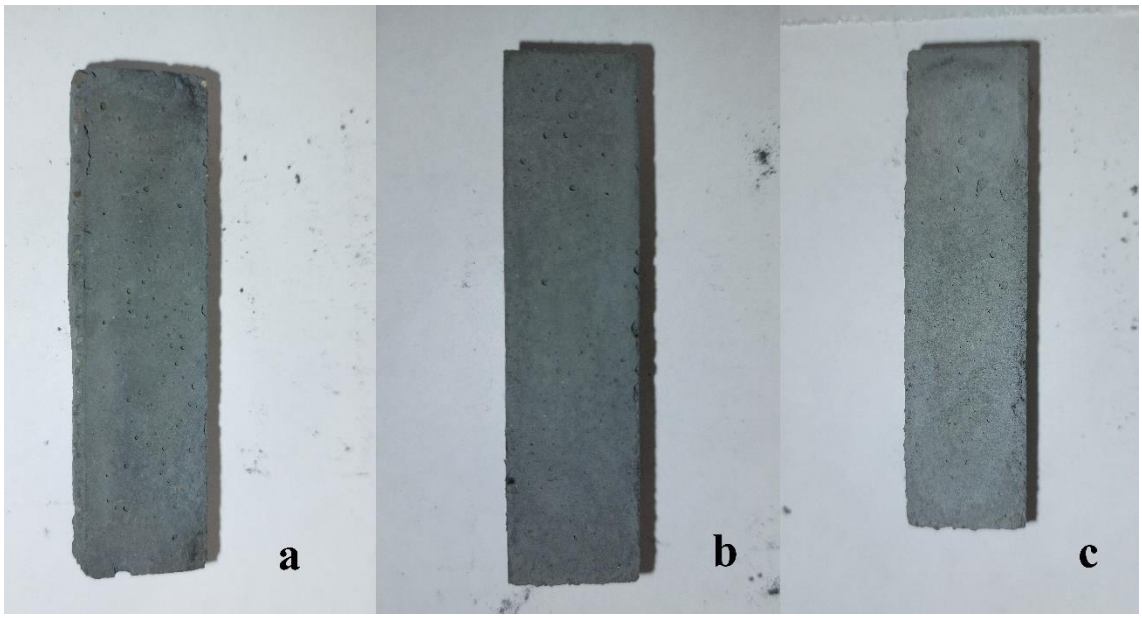

Figure A39. Samples with calcium oxide addition 1M a) 5 % b) 10 % c) 20 %.

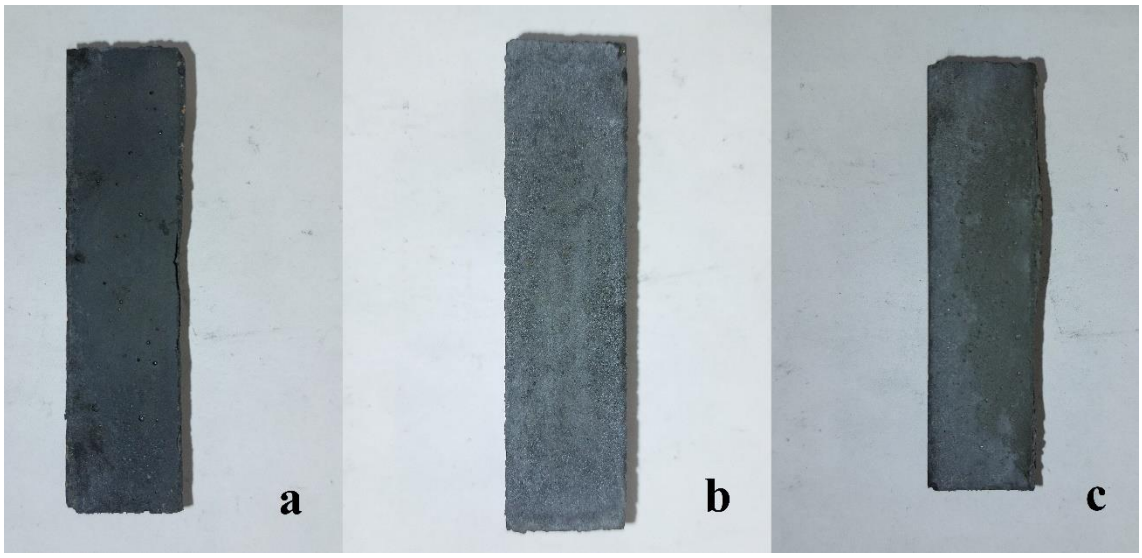

Figure A40. Samples with magnesium oxide addition 3 M: a) 5 % b) 10 % c) 20 %.

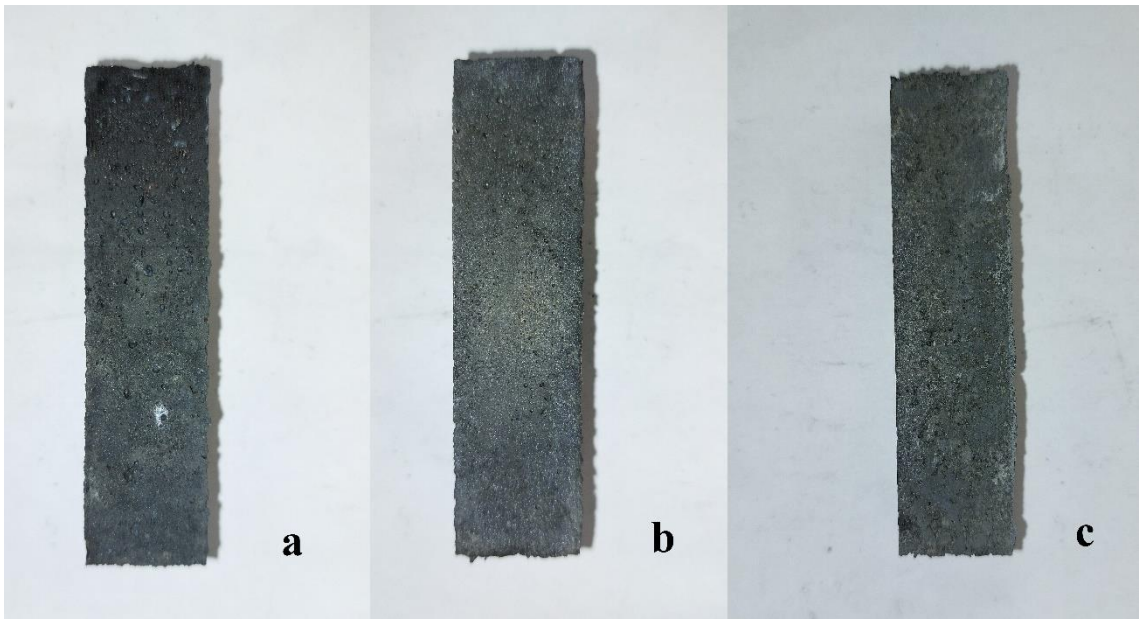

Figure A41. Samples with magnesium oxide addition 6 M: a) 1 % b) 5 % c) 10 %.

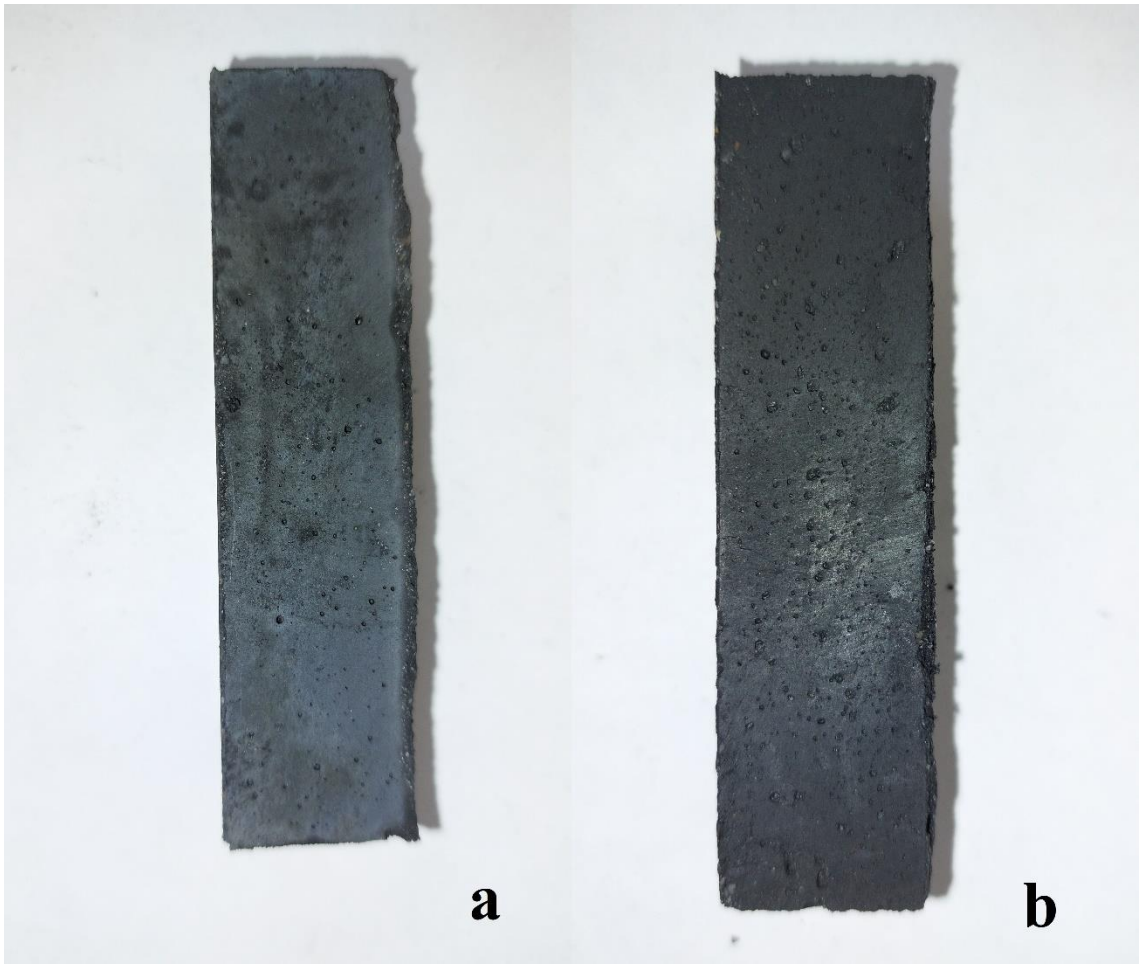

Figure A42. Samples with silica fume addition 1 M: a) 1 % b) 5 %.

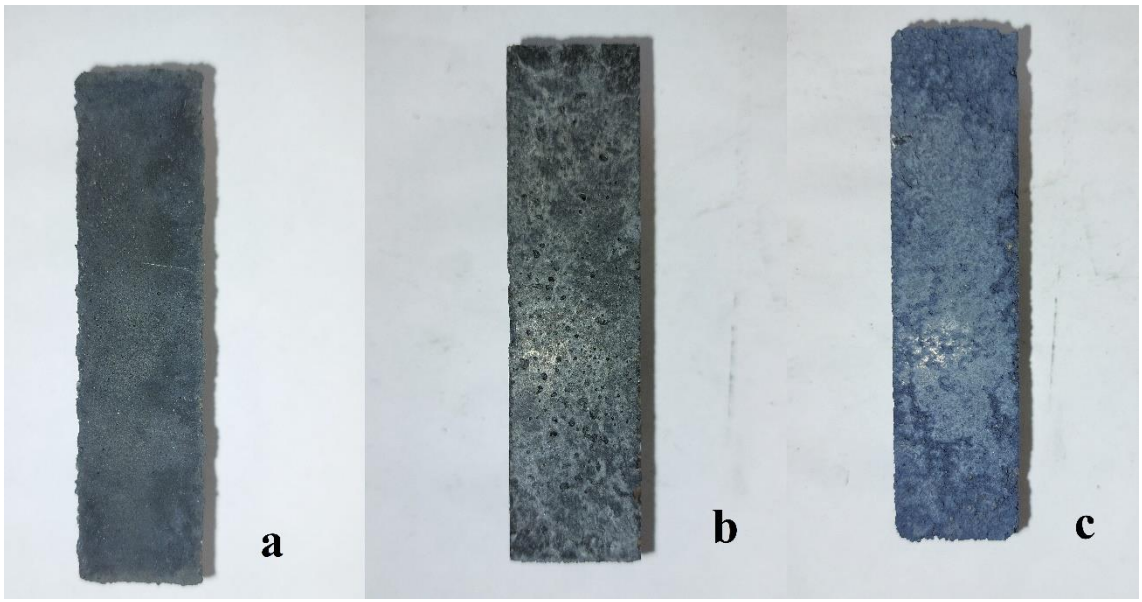

Figure A43. Samples with silica fume addition 3 M: a) 1 % b) 5% c) 10 %.

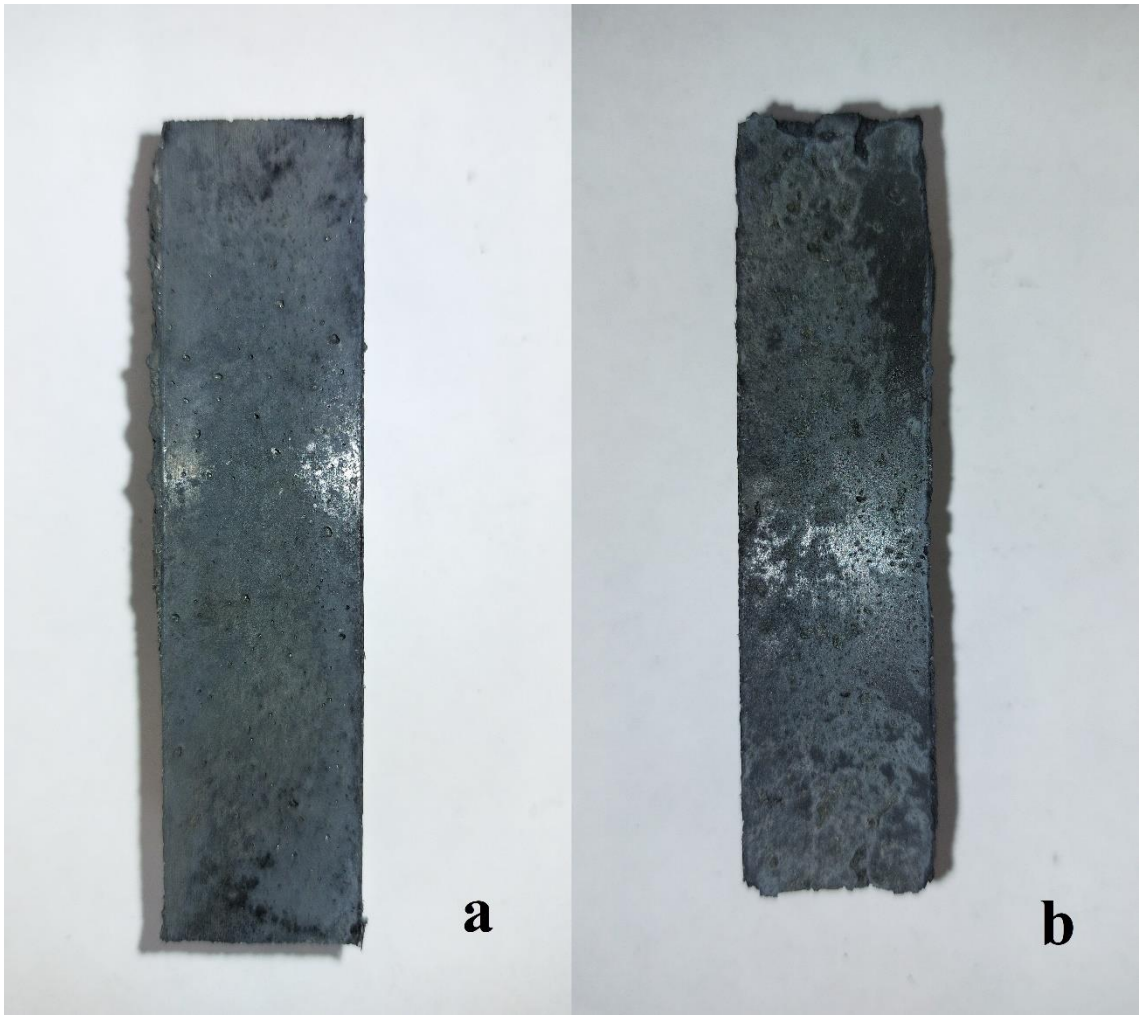

Figure A44. Samples with silica fume addition 6 M: a) 1 % b) 5 %.

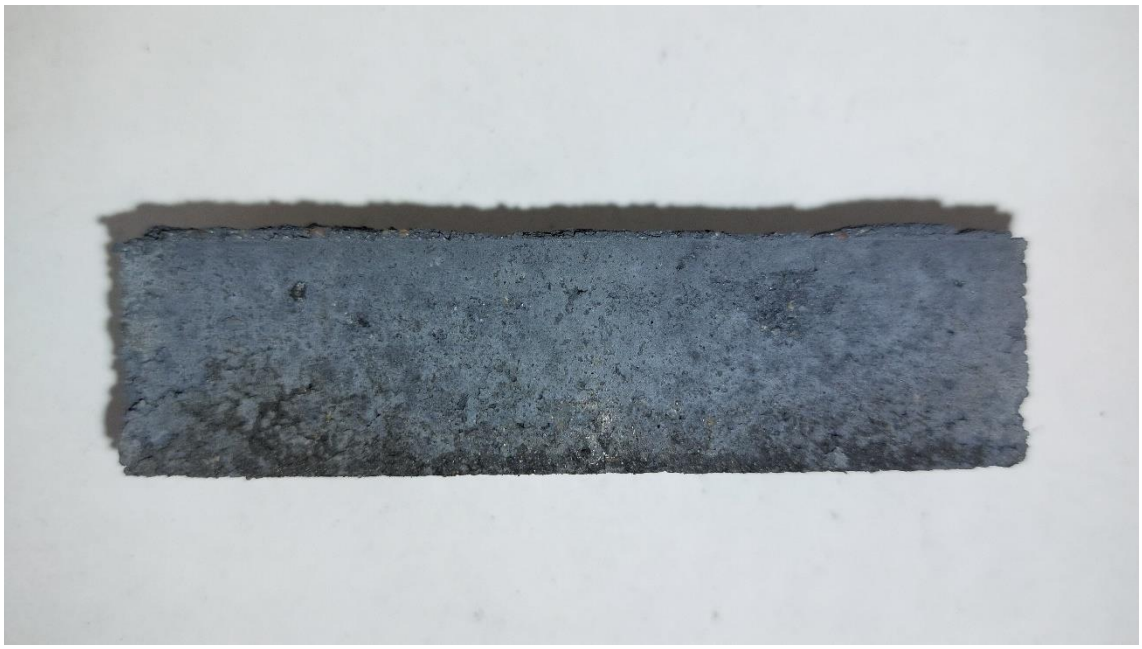

Figure A45. Sample with 10 % CaO and 5 % silica fume addition.

Figure A46. 3M, 6M, 3M-5SF and 1M-10CO mortars after 60 freeze-thaw cycles.

Figure A47. 3M, 6M, 3M-5SF and 1M-10CO mortars after 120 freeze-thaw cycles

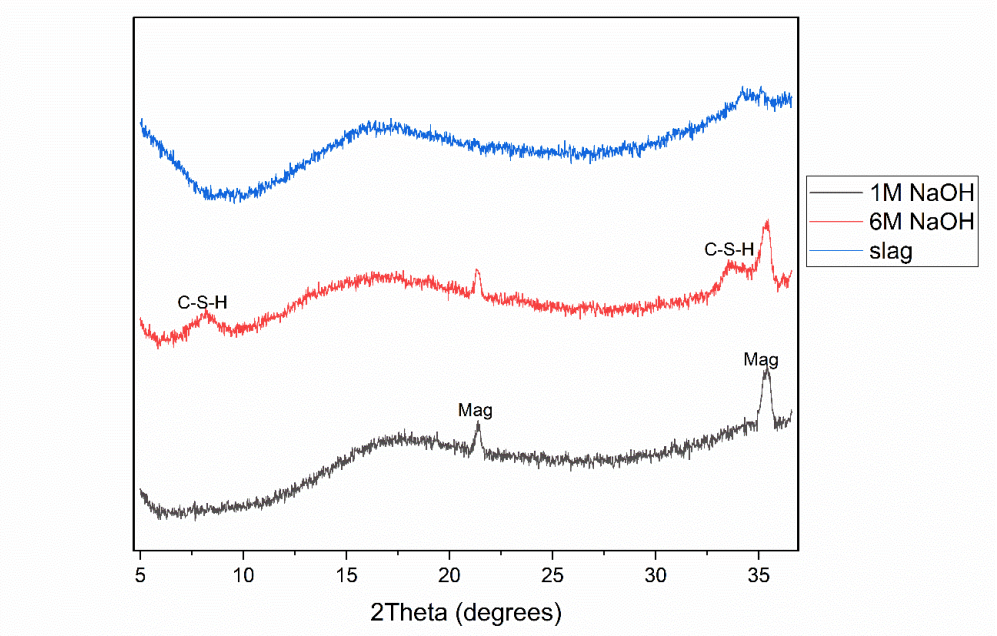

Figure A48. XRD pattern between 3 and 35 degrees of the original slag and 28 days cured pastes activated with 1M and 6M NaOH solution. The phases are designated as follows: Mag – magnetite, C-S-H – calcium silicate hydrate phase

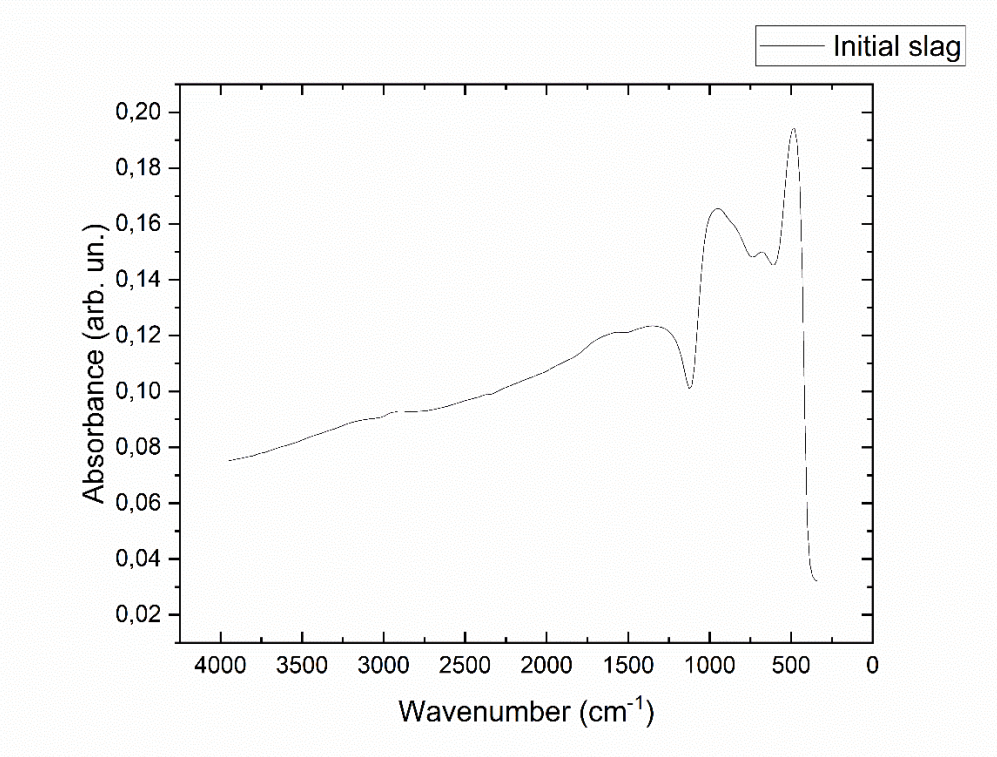

Figure A49. FT-IR spectra of the initial slag

QUANTITATIVE ANALYSIS RESULTS (WPPF)

General information

Analysis date	2022/06/02 15:42:15		
Sample name	1M	Measurement date	2022/05/19 14:29:45
File name	1M.ras	Operator	administrator
Comment			

Qualitative analysis results

Phase name	Formula	Figure of merit	Phase reg. detail	DB card number
Zinc Oxide	Zn O	0.192	ICDD (PDF-4+ 2022)	01-080-3004
Iron Oxide	Fe0.925 O	0.328	ICDD (PDF-4+ 2022)	04-012-3656
hercynite/spinel	Mg0.5 Fe1.5 Al O4	1.017	ICDD (PDF-4+ 2022)	04-021-0464

Weight ratio(Content %)

	Phase name	1M
-	Zinc Oxide	10.00(4)
-	Iron Oxide	20.58(10)
-	hercynite/spinel	8.8(2)
-	Unknown	60.61(18)

Phase data pattern

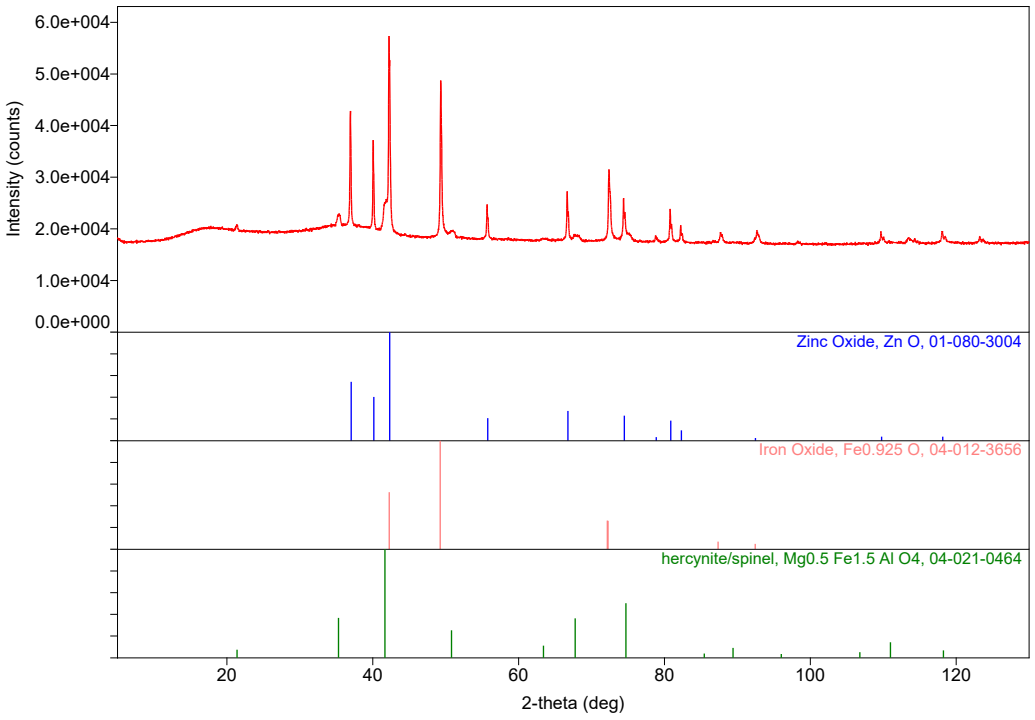

QUANTITATIVE ANALYSIS RESULTS (WPPF)

General information

Analysis date	2022/06/02 16:09:15		
Sample name	6M	Measurement date	2022/05/20 09:02:14
File name	6M.ras	Operator	administrator
Comment			

Qualitative analysis results

Phase name	Formula	Figure of merit	Phase reg. detail	DB card number
Zinc Oxide	Zn O	0.155	ICDD (PDF-4+ 2022)	01-080-3004
Iron Oxide	Fe0.925 O	0.308	ICDD (PDF-4+ 2022)	04-012-3656
magnetite, syn	Fe3 O4	0.792	ICDD (PDF-4+ 2022)	04-018-0091
tobermorite 12.5 A,	Ca7.76 Si6.76	0.978	ICDD (PDF-4+ 2022)	01-081-9792

Weight ratio

	Phase name	Content(%)
-	Zinc Oxide	10.00(3)
-	Iron Oxide	19.11(8)
-	magnetite, syn	8.11(11)
-	tobermorite 12.5 A,	0.70(4)
-	Unknown	62.08(12)

Phase data pattern

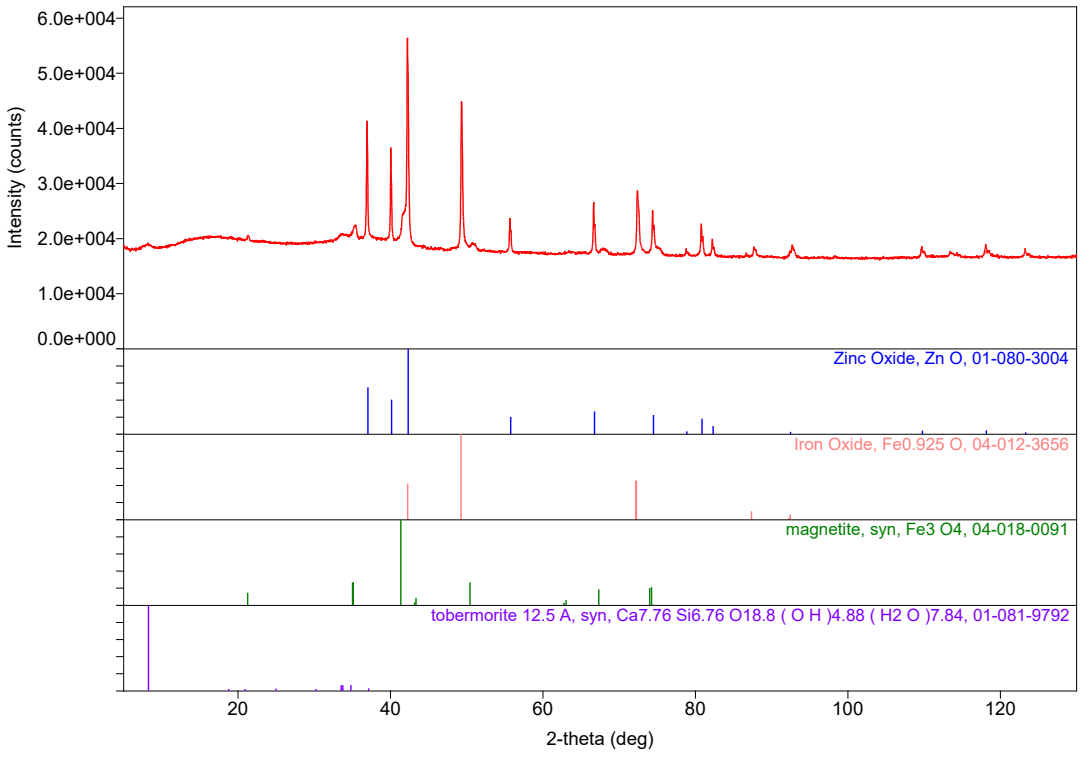

QUANTITATIVE ANALYSIS RESULTS (WPPF)

General Information

Analysis date	2022/06/09 20:05:38		
Sample name	1M_1Co	Measurement date	2022/05/20 08:27:07
File name	1M_1Co.ras	Operator	administrator
Comment			

Qualitative analysis results

Phase name	Formula	Figure of merit	Phase reg. detail	DB card number
Zinc Oxide	Zn O	0.136	ICDD (PDF-4+ 2022)	01-080-3004
Iron Oxide	Fe0.925 O	0.201	ICDD (PDF-4+ 2022)	04-012-3656
Magnesioferrite, Al+3-bearing, syn	Mg Fe1.21 Al0.79 O4	0.635	ICDD (PDF-4+ 2022)	04-014-3054

Weight ratio

Phase name	Content(%)
Zinc Oxide	10.00(4)
Iron Oxide	20.58(10)
Magnesioferrite, Al+3-bearing, syn	9.3(2)
Unknown	60.12(19)

Phase data pattern

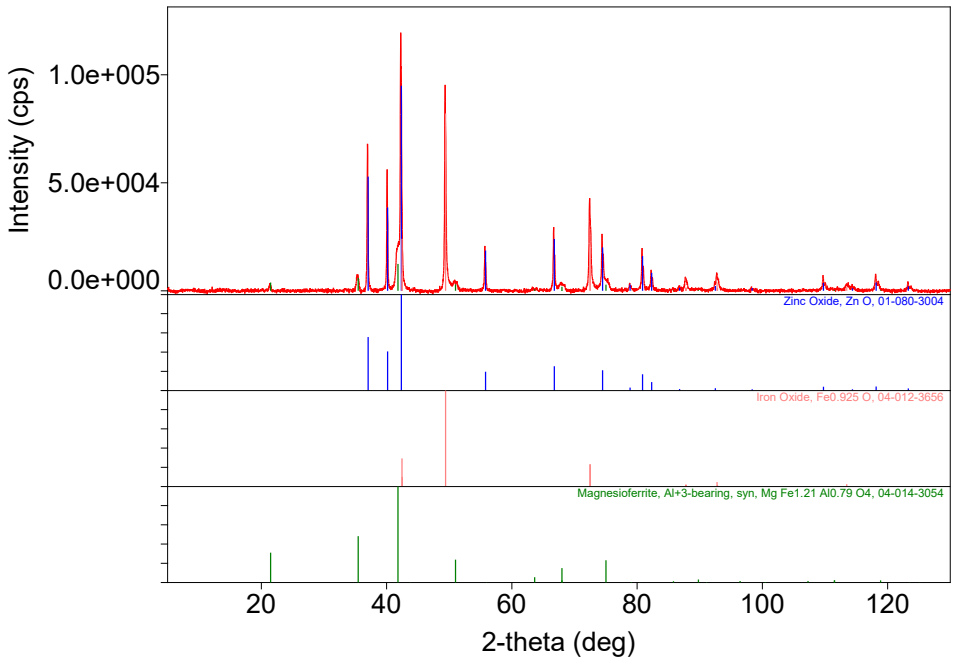

Quantitative Analysis Results (WPPF)

General information

Analysis date	2022/06/02 15:58:30		
Sample name	1M 10CO	Measurement date	2022/05/19 13:06:04
File name	1M 10CO.ras	Operator	administrator
Comment			

Qualitative analysis results

Phase name	Formula	Figure of merit	Phase reg. detail	DB card number
Zinc Oxide	Zn O	0.254	ICDD (PDF-4+ 2022)	01-080-3002
magnesium ferrous oxide	(Mg O)0.432 (Fe O)0.568	0.426	ICDD (PDF-4+ 2022)	01-077-2368
Magnesioferrite,	Mg Fe2 O4	1.212	ICDD (PDF-4+ 2022)	04-001-9288
Katoite	Ca2.93 Al1.97 (Si0.64 O2.56) (O H)9.44	1.218	ICDD (PDF-4+ 2022)	01-077-1713
Portlandite, syn	Ca (O H)2	1.731	ICDD (PDF-4+ 2022)	01-070-5492

Weight ratio

	Phase name	Content(%)
-	Zinc Oxide	10.00(10)
-	magnesium ferrous	11.68(18)
-	Magnesioferrite, syn	6.00(13)
-	Katoite	8.5(4)
-	Portlandite, syn	2.3(2)
-	Unknown	61.5(5)

Phase data pattern

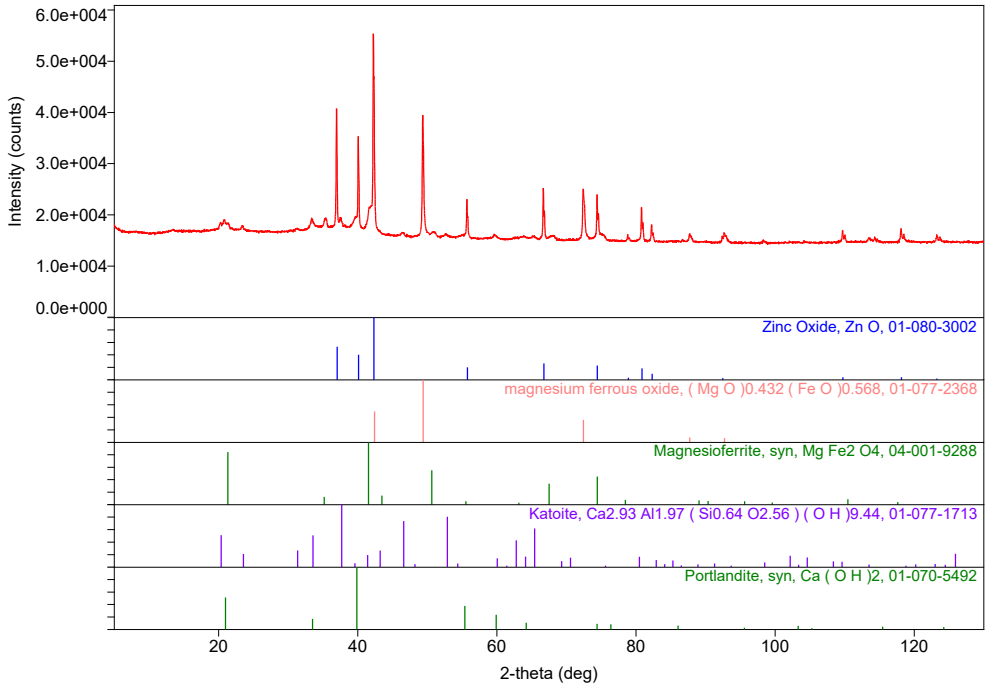

Quantitative Analysis Results (WPPF)

General Information

Analysis date	2022/06/09 20:25:30		
Sample name	6M 1CO	Measurement date	2022/05/19 12:28:32
File name	6M 1CO.ras	Operator	administrator
Comment			

Qualitative analysis results

Phase name	Formula	Figure of merit	Phase reg. detail	DB card number
Zinc Oxide	Zn O	0.252	ICDD (PDF-4+ 2022)	01-080-3002
Iron Oxide	Fe0.925 O	0.345	ICDD (PDF-4+ 2022)	04-012-3656
iron(II) diiron tetraoxide, magnetite	Fe (Fe2 O4)	0.899	ICDD (PDF-4+ 2022)	01-084-6687
tobermorite, syn, tricalcium dihydroxodisilicate hydrate	Ca3 (Si2 O6 (O H)2) (H2 O)	1.695	ICDD (PDF-4+ 2022)	01-081-9794
portlandite	Ca (O H)2	2.430	ICDD (PDF-4+ 2022)	04-014-7723

Weight ratio

	Phase name	Content(%)
-	Zinc Oxide	10.00(12)
-	Iron Oxide	14.89(19)
-	iron(II) diiron tetraoxide, magnetite	3.40(14)
-	tobermorite, syn, tricalcium dihydroxodisilicate hydrate	5.8(5)
-	portlandite	0.3(3)
-	Unknown	65.7(6)

Phase data pattern

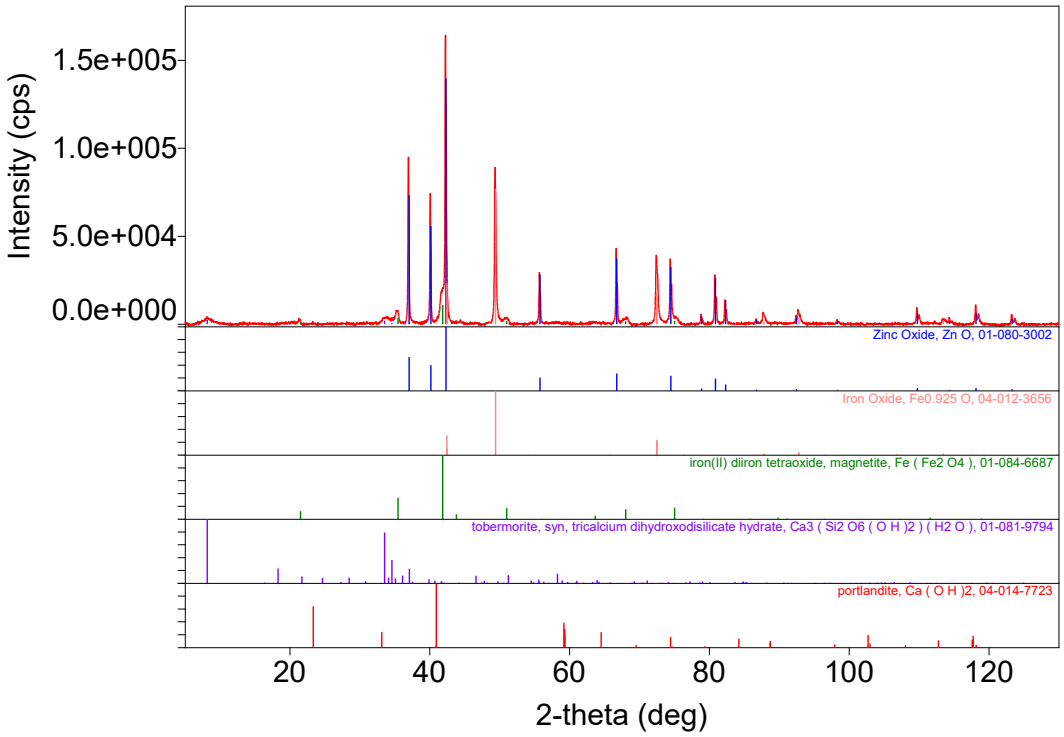

Quantitative Analysis Results (WPPF)

General Information

Analysis date	2022/06/09 20:35:53		
Sample name	6M 10CO	Measurement date	2022/05/19 13:44:53
File name	6M 10CO.ras	Operator	administrator
Comment			

Qualitative analysis results

Phase name	Formula	Figure of merit	Phase reg. detail	DB card number
Zinc Oxide	Zn O	0.193	ICDD (PDF-4+ 2022)	01-080-3002
Iron Oxide	Fe0.925 O	0.459	ICDD (PDF-4+ 2022)	04-012-3656
Katoite, syn	(Ca O)3 (Al2 O3)1.425 (H2 O)4.8	0.891	ICDD (PDF-4+ 2022)	01-076-2505
sodium tecto-alumosilicate hydrate *	Na92.71 (Si96.96 Al95.04 O384) (H2 O)44.5	1.228	ICDD (PDF-4+ 2022)	01-089-5422
Magnetite, Mg-bearing, syn	(Mg0.44 Fe0.56) (Mg0.56 Fe1.44) O4	0.992	ICDD (PDF-4+ 2022)	01-083-7246

Weight ratio

	Phase name	Content(%)
-	Zinc Oxide	10.00(18)
-	Iron Oxide	16.0(3)
-	Katoite, syn	9.6(3)
-	sodium tecto-alumosilicate hydrate *	4.0(7)
-	Magnetite, Mg-bearing, syn	8.2(4)
-	Unknown	52.2(9)

Phase data pattern

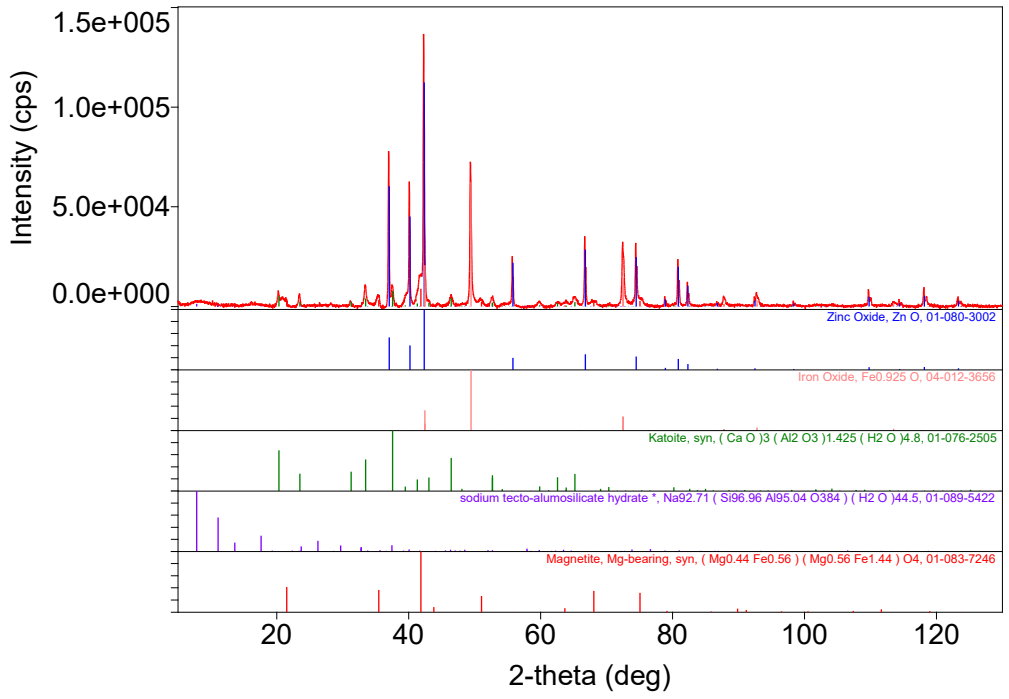

Quantitative Analysis Results (WPPF)

General Information

Analysis date	2022/06/09 20:10:43		
Sample name	1M1SF	Measurement date	2022/05/20 09:37:34
File name	1M1SF.ras	Operator	administrator
Comment			

Qualitative analysis results

Phase name	Formula	Figure of merit	Phase reg. detail	DB card number
Zinc Oxide	Zn O	0.248	ICDD (PDF-4+ 2022)	01-080-3004
Iron Oxide	Fe0.925 O	0.284	ICDD (PDF-4+ 2022)	04-012-3656
magnetite, syn	Fe3 O4	1.196	ICDD (PDF-4+ 2022)	04-018-0091

Weight ratio

	Phase name	Content(%)
-	Zinc Oxide	10.00(3)
-	Iron Oxide	19.68(8)
-	magnetite, syn	7.00(13)
-	Unknown	63.32(12)

Phase data pattern

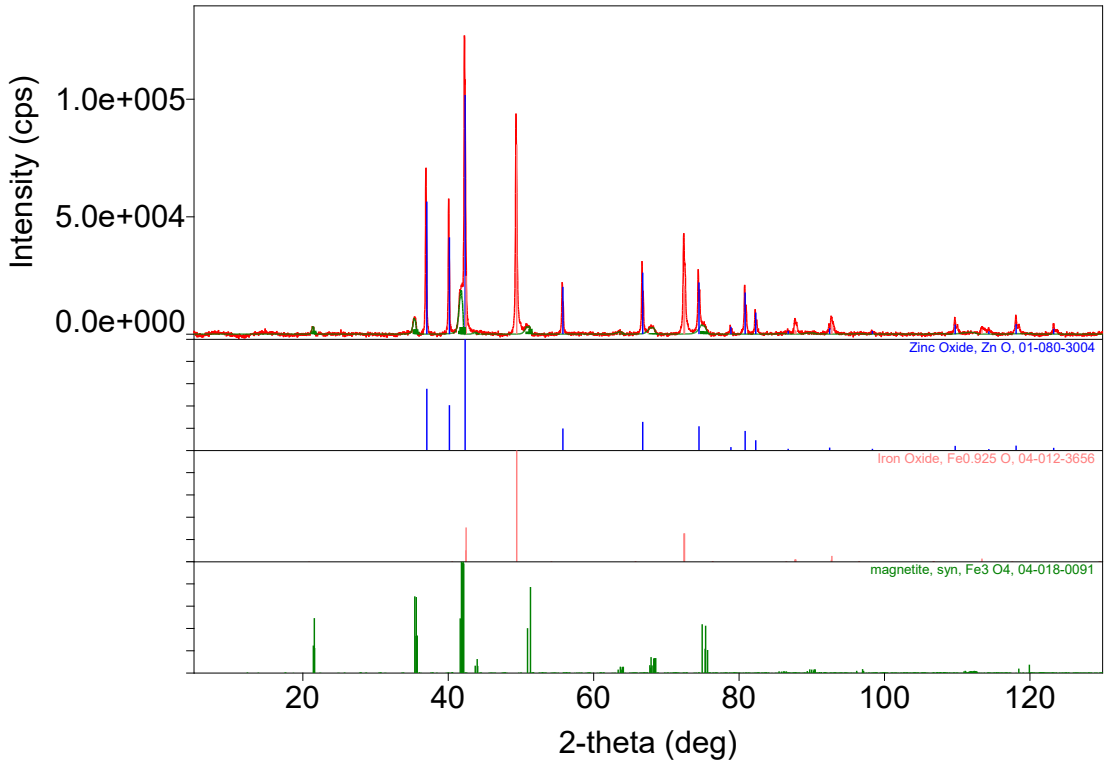

Quantitative Analysis Results (WPPF)

General Information

Analysis date	2022/06/09 20:13:56		
Sample name	1M10SF	Measurement date	2022/05/19 11:39:40
File name	1M10SF.ras	Operator	administrator
Comment			

Qualitative analysis results

Phase name	Formula	Figure of merit	Phase reg. detail	DB card number
Zinc Oxide	Zn O	0.191	ICDD (PDF-4+ 2022)	01-080-3004
Iron Oxide	Fe0.925 O	0.317	ICDD (PDF-4+ 2022)	04-012-3656
iron(II) diiron tetraoxide, magnetite	Fe (Fe2 O4)	0.832	ICDD (PDF-4+ 2022)	01-084-6687

Weight ratio

	Phase name	Content(%)
-	Zinc Oxide	10.00(3)
-	Iron Oxide	17.29(8)
-	iron(II) diiron tetraoxide, magnetite	4.03(14)
-	Unknown	68.68(13)

Phase data pattern

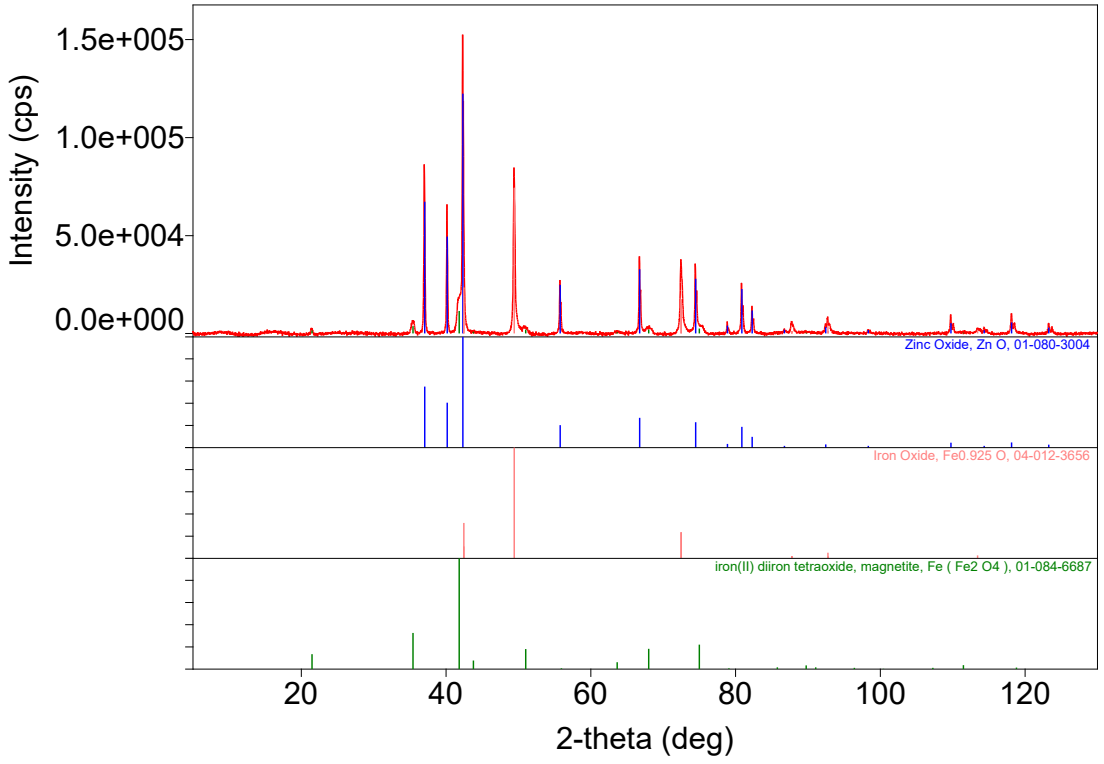

Quantitative Analysis Results (WPPF)

General Information

Analysis date	2022/06/09 20:40:04		
Sample name	6M1SF	Measurement date	2022/05/20 11:11:15
File name	6M1SF.ras	Operator	administrator
Comment			

Qualitative analysis results

Phase name	Formula	Figure of merit	Phase reg. detail	DB card number
Zinc Oxide	Zn O	0.154	ICDD (PDF-4+ 2022)	01-080-3004
Iron Oxide	Fe0.925 O	0.353	ICDD (PDF-4+ 2022)	04-012-3656
tobermorite 12.5 A, syn	Ca7.76 Si6.76 O18.8 (O H)4.88 (H2 O)7.84	1.176	ICDD (PDF-4+ 2022)	01-081-9792
iron(II) diiron tetraoxide, magnetite	Fe (Fe2 O4)	1.466	ICDD (PDF-4+ 2022)	01-084-6687

Weight ratio

	Phase name	Content(%)
-	Zinc Oxide	10.00(4)
-	Iron Oxide	17.12(10)
-	tobermorite 12.5 A, syn	1.13(3)
-	iron(II) diiron tetraoxide, magnetite	5.6(2)
-	Unknown	66.1(2)

Phase data pattern

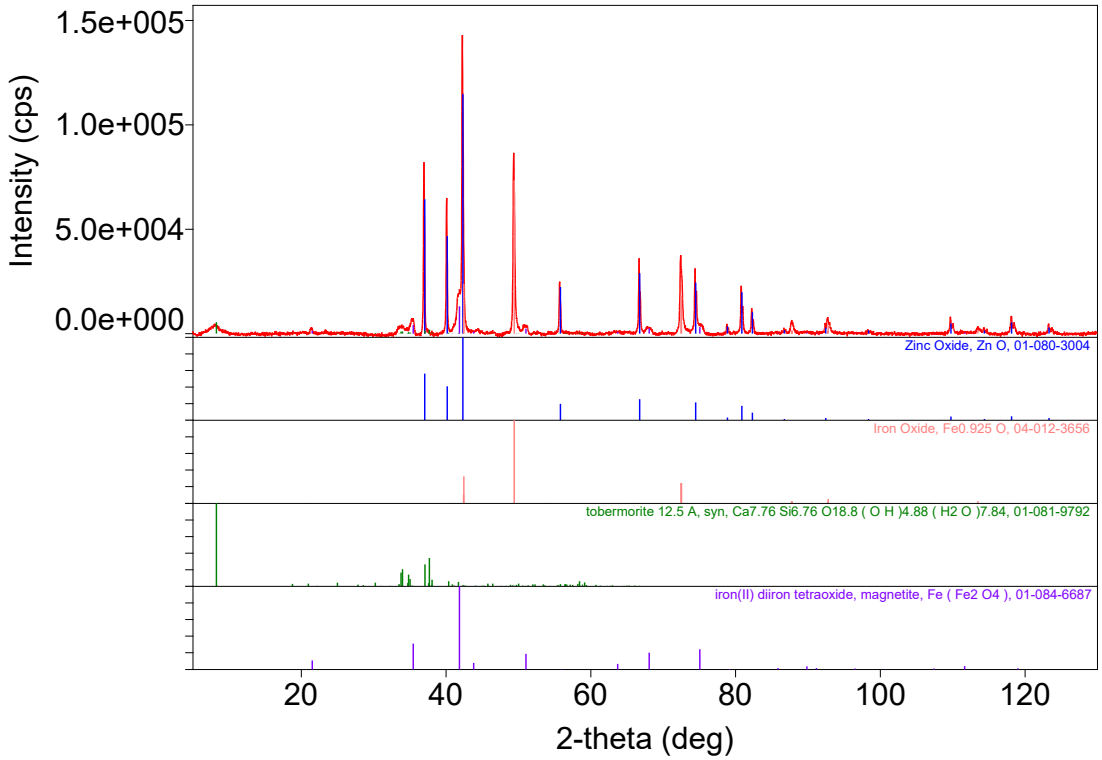

Quantitative Analysis Results (WPPF)

General Information

Analysis date	2022/06/09 20:45:37		
Sample name	6M10SF	Measurement date	2022/05/20 10:14:54
File name	6M10SF.ras	Operator	administrator
Comment			

Qualitative analysis results

Phase name	Formula	Figure of merit	Phase reg. detail	DB card number
Zinc Oxide	Zn O	0.231	ICDD (PDF-4+ 2022)	01-080-3002
Iron Oxide	Fe0.925 O	0.311	ICDD (PDF-4+ 2022)	04-012-3656
magnetite, syn	Fe3 O4	0.701	ICDD (PDF-4+ 2022)	04-018-0091
tobermorite, syn, tricalcium dihydroxodisilicate hydrate	Ca3 (Si2 O6 (O H)2) (H2 O)	1.116	ICDD (PDF-4+ 2022)	01-081-9794

Weight ratio

	Phase name	Content(%)
-	Zinc Oxide	10.00(9)
-	Iron Oxide	16.67(16)
-	magnetite, syn	6.11(10)
-	tobermorite, syn, tricalcium dihydroxodisilicate hydrate	1.8(5)
-	Unknown	65.4(4)

Phase data pattern